REMOVAL OF ORGANIC CONTAMINANTS FROM WATER BY POLYMERIC RESINS: PREDICTIVE MODELING AND DEVELOPMENT OF RESIN-PD COMPOSITES

A Dissertation Submitted

To the Temple University Graduate Board

In Partial Fulfillment

Of the Requirements of the Degree of

Doctor of Philosophy

By

Nastaran Jadbabaei

May, 2016

Examining Committee Members:

Dr. Huichun (Judy) Zhang, Thesis Advisory Committee Chair, Civil and Environmental Engineering, Temple University
Dr. Rominder Suri, Civil and Environmental Engineering, Temple University
Dr. Svetlana Neretina, Mechanical Engineering, Temple University
Dr. Danmeng Shuai, Civil and Environmental Engineering, The George Washington University
Dr. Shenqiang Ren, External Committee Member, Mechanical Engineering, Temple University

SUMMARY

Discharge of many organic contaminants (OCs) to the environment is one of the major concerns to human health and the environment due to their high toxicity. Existing water and wastewater treatment techniques were not specifically designed to remove OCs, and the elimination rate can vary from negligible to over 90%. Developing effective water treatment technologies requires the development of new technologies. Custom-synthesized polymeric resins can selectively target certain OCs by including desired functional groups. Thus, greater efficiency is expected for cation exchange resins (CXRs) than conventional neutral adsorbents in removing cationic OCs, such as aromatic amines and quaternary ammoniums. Moreover, palladium based catalysts supported on polymeric resins are promising in overcoming regeneration problems and convert contaminants to less toxic chemicals. The main goals of this research were to (1) develop predictive models for the sorption of a range of cationic OCs on two CXRs and (2) synthesize novel resin-based Pd catalysts to selectively remove two toxic contaminants, i.e., 4-chlorophenol (4-CP) and 4-nitrophenol (4-NP), and evaluate the possibility of *in situ* regeneration of the spent resins.

To develop predictive models, sorption isotherms were obtained for a diverse set of cationic and neutral compounds, including aromatic and aliphatic quaternary ammoniums, phenols, anilines, and nitrobenzene by two strong CXRs Amberlite 200 and MN500. Among the cations, aromatic or halogenated cations that can undergo stronger nonelectrostatic interactions such as π-π or dipole-dipole interactions showed higher adsorption affinity. Despite the importance of nonelectrostatic interactions, neutral solutes were sorbed much less, indicating electrostatic and nonelectrostatic interactions have synergistic effects on sorption. MN500 had a greater removal capacity than Amberlite 200 due to its microporous structure that enhanced sorption energy. Using poly-parameter linear free energy relationships for a training set of 20 compounds, polarity/polarizability, H-bond acidity, induced dipole, and electrostatic interactions were found to be the dominant interactions. The developed predictive models accurately estimated sorption capacity of a number of OCs by the two resins.

Three neutral resins (MN200, MN100, and XAD4) and two anion exchange resins (IRA910 and IRA96) were then used as supports to develop resin-Pd catalysts. Hydrogenation of 4-CP and 4-NP was examined to evaluate reactivity of the catalysts. Our results show that adsorption and reduction followed similar kinetics, i.e. faster adsorption and reduction at acidic pHs for the neutral resins but faster at basic pHs for the anionic resins. During the catalytic reaction, both 4-NP and 4-CP were not significantly adsorbed by 1 wt% Pd-resin catalysts except for IRA910 when their initial concentrations were < 1 and 1.5 mM, respectively. This suggests that adsorption is likely rate-determining for low initial concentrations. With increasing initial concentration to > 1.5 mM, the adsorbed amount of 4-CP or 4-NP onto the catalysts during reaction also increased, indicating that the rate determining step has switched to surface reaction. The above observation was confirmed by good fitting of the reaction kinetics to two kinetic models developed based on the Langmuir−Hinshelwood model, with the assumption that adsorption and surface reaction are the rate determining step for lower and higher contaminant concentrations, respectively. For the neutral resins, higher 4-NP reduction activity was observed at pH < pK_a =7.15 when the neutral form of 4-NP has a higher adsorption capacity. Neutral pH was more favorable for hydrodechlorination of 4-CP by

the neutral resins when the adsorption capacity of the resins was constant at $pH < pK_a$, this is because higher pH mitigates the adverse impacts of the dehalogenation products (i.e., H^+ and Cl^-) on the catalytic reaction. Anion exchange resin IRA910 showed the highest catalytic activity for both 4-NP and 4-CP at $pH > pK_a$ when the ionic form of the reactants has the highest adsorption capacity.

IRA910 was more sensitive to the poisoning effect of Cl^- on catalytic activity than MN200, because its anion exchange functional groups facilitate Cl^- adsorption and promote the production of $PdCl_3^-$ and $PdCl_4^{2-}$ species. These species tend to form at low pHs and high concentration of Cl^- and are inactive for catalytic reduction. The accumulation of the major reduction products (phenol and 4-aminophenol, respectively, for 4-CP and 4-NP) and the reactants on the resins resulted in catalytic activity loss over eight cycles; catalytic activity was largely restored after resin regeneration. Although a fraction of the reduction products were adsorbed by the catalysts, more than 96% of the formed 4-AP by all the catalysts and the formed phenol by AXRs, and 70% of the formed phenol by MN200 remained in solution phase. Therefore, integration of adsorption and reduction is a promising method for *in situ* regeneration, which can be optimized by selecting a resin that has low adsorption affinity toward reduction products.

In conclusion, this study provided a mechanistic understanding of the sorption of a wide range of organic cations by the cation exchange resins. The developed predictive modeling can estimate sorption capacity of a target contaminant by a specific sorbent at any environmentally relevant pH, which can help select the best treatment scenario without conducting trial experiments. The developed resin-based palladium catalysts can convert priority contaminants to less toxic and more desirable compounds and enable in situ regeneration of the resins. The products can be further subjected to biodegradation or recovered for other usages. This new knowledge is believed to be applicable to developing new sustainable water treatment technologies, and to processes involving separation and purification of materials.

AKNOWLEDGMENTS

I would like to thank my advisor and mentor Dr. Huichun (Judy) Zhang for the constant guidance and support I have received from her throughout my studies. She is always there for help and encouragement, giving comments and suggestions for my research and future plans. I really appreciate the patience and commitment she has had towards my learning process.

I would also like to thank my committee members Dr. Rominder Suri, Dr. Svetlana Neretina, Dr. Danmeng Shuai and Dr. Shenqiang Ren for their support, advice, and willingness to serve on my dissertation advisory committee.

I truly appreciate the help of Dr. Zdilla and Dr. Grandstaff for their help with analysis using the XRD and ICP-OES instruments. Thanks to Ian McKendry for his help in XRD analysis. Also, I am very grateful to Dr. Strongin's graduate students Samantha and Kristin for helping me in TEM analysis. I am thankful to Dr. Bingjun Pan for his help with data analysis and lab work. Also, I would like to thank to Drs. Rouzbeh Tehrani and Gangadhar Andaluri for their help in labs in times of need. I also like to thank Ryan Slobodjian and Quiana for helping me in the lab.

I would also like to thank my lab members Saru, Yiling, Jianzhi, Kowsalya, Anthony Shields, and Shubo for always being so helpful and kind. I also wish to express my thanks to my fellow graduate students Sibia, Asad, Rashid, Ela and Srishty for their company and encouragements.

I dedicate this dissertation work to my dearest parents Salman Jadbabaei and Asiyeh Vahabi for giving me life, love, and support. I am very grateful for the love and support of my husband Amin Vakilipour who never stopped encouraging me. I would like to thank my siblings for their love, support, and companionship.

This work was partly supported by Grants from the U.S. Geological Survey, the Pennsylvania Water Resource Research Center and the Pennsylvania Sea Grant. Dissertation completion grant was provided by the Temple University's Graduate School. Support was also provided by the Department of Civil and Environmental Engineering at Temple University.

TABLE OF CONTENTS

LIST OF FIGURES

LIST OF TABLES

LIST OF ACRONYMS

4-AP	4-aminophenol
4-CP	4-chlorophenol
4-NP	4-nitrophenol
AXRs	Anion exchange resins
COCs	cationic organic contaminants
CPs	Chlorophenols
CXRs	cation exchange resins
D-A	Dubinin-Astakhov
HDC	Hydrodechlorination
IOCs	ionic organic compounds
L-H	Langmuir-Hinshelwood
NPM	nonpolar moieties
NPs	Nitrophenols
OCs	organic contaminants
pp-LFERs	Poly-Parameter linear free-energy relationships

CHAPTER 1

INTRODUCTION

1.1 Background

Discharge of toxic compounds to the environment has been of increasing concern over the past a few decades. Organic contaminants (OCs) such as halogenated compounds, nitroaromatics, aromatic amines, and quaternary ammonium cations are common contaminants in water and wastewater effluents that have toxic effects on human health and the environment. They can be discharged to the environment from the wastewater effluents of pharmaceutical, personal care product, pesticide, and dyestuff industries.[1-4] For example, phenolic compounds such as chlorophenols and nitrophenols are widely used in manufacturing of pesticides and dyestuffs.[3, 5] There are more than 100,000 commercially available dyes and over 7×10^5 tons of dye-stuff produced annually.[6] It has been estimated that 10 to 15% of dyes are lost in the waste effluents.[7] The total pesticide consumption by U.S. was 516 million pounds in 2008[8] and average pesticide consumption of various types of pesticides was estimated to be 2.2 Kg/ha in European Environment Agency member countries.[9]

High concentrations of OCs have been detected in wastewater effluents and sewage sludge. For example, many antibiotics and analgesic and anti-inflammatory pharmaceuticals were detected up to 7900 ng/l in the effluents of Wastewater Treatment Plants (WWTPs) in north America.[10] OCs such as phthalic acid esters and nitroaromatics occurred in sewage sludge from wastewater treatment plants in China with total concentrations ranging from 10 to 114 mg kg^{-1}.[11] During 1999 and 2000, the U.S. Geological Survey (USGS) studied the occurrence of 95 organic wastewater contaminants in 139 streams throughout the U. S. These contaminants were detected in 80% of the stream samples at concentrations less than 1.0 μg/L.[12] In 2008, USGS found the occurrence of a wide variety of organic compounds in more than 50 percent of the water and sediment samples in the streams of northeast Ohio.[13] In another study by USGS, thirty organic compounds were detected in groundwater with concentrations less than 0.1μg/L.[14] In addition, there are a large number of other studies reporting the occurrence of OCs in different environments throughout the world.[15-17] Concerns over some of these OCs include serious effects on human health over long period of time such as carcinogenic effects,[18] negative hormonal and toxic effects on various organisms at concentrations as low as μg/kg.[12]

Existing water and wastewater treatment technologies used to treat OCs include adsorption on conventional adsorbents (e.g., activated carbon),[19] catalytic and chemical oxidation,[20] and UV photolysis.[21] The removal efficiency of different contaminants varies with the physicochemical properties of the pollutants and the types of wastewater treatment technology used. For example, removal efficiency of many endocrine disrupting chemical (EDCs) by activated carbon was reported >90%, while some EDCs such as ibuprofen and sulfamethoxazole had lower removals (40-60%).[22] Removal efficiency of many pharmaceuticals and personal care products (PPCPs) by activated carbon has been reported to vary from 70% to 90%, while it was lower than 20% by lime softening and coagulation methods.[23, 24] Among the conventional technologies, adsorption on activated carbon is a common method for treatment of water and wastewater effluents;[19, 25] however, it has shown poor removal for polar and hydrophilic contaminants such as 6-aminopenicillanic acid under typical treatment pHs.[26] Advanced oxidation processes are energy intensive which makes the technology expensive.[27] In addition, reaction with dissolved organic matter, poor selectivity toward some contaminants, and being expensive when used to reach complete oxidation of OCs are among challenges of the oxidation methods.[28, 29] Thus, efficient removal of OCs requires development of new treatment technologies. Polymeric resins are a promising alternative for removal of OCs because of their adjustable structures for target contaminants.[30, 31] However, regeneration or disposal of used resins requires additional efforts and cost.

Palladium (Pd)-based catalysis has been introduced as a promising water treatment method for reductive transformation of various priority drinking water contaminants such as oxyanions (e.g., bromate and chlorate),[32, 33] halogenated alkanes,[34] and halogenated aromatics (e.g., chlorinated benzenes, and polychlorinated biphenyls (PCBs)).[1] Catalysts activity, stability, and selectivity for desired products significantly influence on the cost and applicability of catalytic treatment methods. Existing Pd-based catalysts have shown different catalytic activity for different contaminants. For example, higher reactivity was observed for dehalogenation of chlorinated aromatics and alkenes than oxyanions.[35] Inhibition and fouling of Pd-based catalysts are among major problems associated with catalyst stability. Inhibition of Pd on alumina catalysts by halide ions and sulfide has been reported by many studies.[36, 37] However, there are some catalysts such Pd-Re on activated carbon that exhibited better resistance to Cl^-.[32] Therefore, it is important to develop more active, stable Pd-based catalysts for target contaminants.

1.2 Problem Statement

Compared to many technologies available for treating water and wastewater containing neutral organic compounds, including photocatalytic oxidation,[38] electrolysis,[39] adsorption,[40] oxidation,[41] biodegradation,[42, 43] and membrane,[44] there is much less effort for removal of ionic organic contaminants (IOCs) such as aromatic amines from contaminated water. For example, adsorption of aniline (pK_a= 4.67) by activated carbon dramatically decreased with decreasing pH.[45] Ion exchange resins can be a promising approach to removing IOCs[46-48] by exchanging with ionic solutes in solution. However, due to the vast number of different contaminants and available sorbents, it is difficult to select a proper sorbent for a specific treatment scenario. To address this problem, it is important to understand the overall sorption process and to estimate the sorbed concentration of a target contaminant by a given sorbent. This process requires accurate predictive modeling and mechanistic understanding of major interactions taking place within the system. Currently, such information is largely not available.

Moreover, although regeneration of the exhausted resin is attainable at ambient temperature with low attrition rates, as opposed to activated carbon whose thermal regeneration process is costly, energy intensive, and with high attrition rates, it requires additional efforts.[49, 50] To overcome challenges in regenerating exhausted resins, palladium-based catalysis by hydrogen gas is a promising technology.[51] Loading palladium metals onto support enhances dispersion and facilitates separation of the catalysts after reaction.[52] The advantages of using palladium-based catalysts include greater catalyst activity and selectivity toward desirable reaction products.[2, 28] Indeed, palladium-based catalysis has been known as a key component in sustainable development of water treatment technologies.[53-55] Nevertheless, development of catalytic methods requires improvement of catalyst synthesis, including catalytic activity, lifetime, stability, selectivity, and susceptibility to poisoning.[28, 53]

Typical supports that have been used for palladium nanoparticles are activated carbon, alumina, silica, and zeolites.[28, 56] Low stability and activity loss of the developed catalysts is a major barrier in a widespread application of Pd-based catalysis. Catalyst deactivation is mainly a result of binding of anions such as halide ions and other constituents in natural water to Pd sites and leaching of the reactive sites.[53, 57, 58] Polymeric resins have rarely been explored as support for Pd. Many polymeric resins are commercially available with a diverse range of structures and functional groups. With mechanically strong, chemically inert, and porous structures, resins might be a proper support for Pd catalyst. Moreover, physical and chemical properties of resins, such as pore size distribution, functional groups, surface area, and the amount of crosslinking, are designable during synthesis which will enable us to improve their structures for better metal immobilization and catalytic activity.[59] It has been reported that immobilization of nanoparticles on ion exchange resins can be enhanced by the presence of ionic functional groups and porosity, which promotes electrostatic and steric stabilization.[56, 60] It has been shown that resin functional groups and nanoparticles have synergistic effects on reaction performance.[59, 61] Thus, these unique characteristics of polymeric resins make them potentially useful candidates for studying and developing new Pd-based catalysts.

An important feature of using polymeric resins as the support for Pd-based catalysts is that simultaneous detoxification of OCs, recovery of the reduction products, and in situ regeneration of the resin support can be achieved. To achieve these goals, the resin should have a high adsorption affinity for the target compound and a low adsorption affinity for the reduction product(s). This is mainly because high adsorption affinity enhances catalytic reduction of the target contaminant, which then produces products with low adsorption affinity for the catalyst support so that they can be easily released to the aqueous phase. The adsorbed reactants to the resin surface can be reactive because of possible spillover effects of the adsorbed hydrogen (H_{ads}) onto active metal sites.[62] Hydrogen spillover is defined as migration of the chemisorbed H_2 from an active metal site onto the surface of the support.[63]

1.3 Research Objectives

This research includes two main goals: first, to gain a mechanistic insight into and develop predictive models for the sorption of various cationic OCs on two commercially available cation exchange resins, and second, to develop novel Pd-based catalysts supported on polymeric ionic and neutral resins. The specific aims for this research are as follows:

i) To quantitatively examine the contribution of various molecular interactions to the overall selectivity of a number of environmentally relevant cations toward the selected resins using Poly-Parameter linear free-energy relationships (PP-LFERS).

ii) To develop a predictive model to calculate sorbed concentrations and selectivity of a diverse range of organic compounds on the selected cationic resins under changing pH.

iii) To synthesize a number of Pb-based resin composites by varying the types of resin support (neutral or ionic polymeric resins) and Pd loading.

iv) To understand the reduction mechanisms and identify the rate-limiting steps of reduction of 4-chlorophenol (4-CP) and 4-nitrophenol (4-NP) by the synthetized Pd-based catalysts.

iv) To optimize the developed catalysts based on the observed reaction mechanisms, removal efficiency, and catalyst longevity.

Predictive models for different resins can be used for selecting an efficient sorbent in the treatment of a given contaminant without conducting trial experiments. Ultimately, results of this work can be used by environmental and chemical engineers for a better understanding of individual interaction mechanisms, designing more efficient water treatment processes, and advancing new technologies to effectively treat contaminated water. Also, the mechanistic findings about sorption are applicable to other industries such as separation and purification processes. The developed catalysts can be used in other industrial chemical reactions as well.

CHAPTER 2

LITERATURE REVIEW

2.1 Organic Contaminates (OCs)

2.1.1 Aromatic Amines

Many organic compounds are ionic in the aquatic environment. Aromatic amines such as substituted anilines, extensively used as pesticides, dyestuffs, and pharmaceuticals, can exist in aqueous solution as either cationic species under solution pH less than their pKa values or neutral species at pH greater than their pKa.[18, 64-66] Estimated annual production of aniline in the U.S. alone has been reported 4.57×10^5 tons.[67] More than 30,000 tons of anilines are discharged into the environment annually.[68] A concentration of 600 ng/L for 3-chloroaniline and 2000 ng/L for 4-chloroaniline have been detected in the aquatic environment near an industrial area.[69] Aromatic amines have also been frequently found in drinking water and surface water due to excessive usage.[18, 68] They have been classified as very toxic compounds for the environment and humans. It is reported that a concentration of 10 ppm can kill 50% of the exposed aquatic organisms in 96 h.[70] Aniline is carcinogenic and also can easily convert hemoglobin in blood into methahemoglobin, which prevents oxygen uptake. Therefore, there is a potential risk for adverse effects on human health over a long period of time, even at low concentrations > 1 ng/L that are much less than the highest concentration observed in the environment.

2.1.2 Quaternary Ammonium Compounds (QACs)

Quaternary ammonium compounds (QACs), commonly found in effluents from disinfectant, surfactant, fabric softener, antistatic agent, and wood preservation industries, exist in the permanently charged cationic form in wastewater effluents.[71, 72] The U.S. consumption of QACs was reported to be more than 32,000 tons with an average concentration higher than 1 mg/L in wastewater effluents.[63, 73] World-wide annual consumption of QACs was 500,000 tons, and most uses of these compounds (75%) can be released to wastewater effluents to have toxic effects on aquatic organisms.[74, 75] The range of total QACs concentration was 25–300 mg/L, 0.3– 3.6 mg/L, 22–103 mg/kg (weight/dry-weight), and 0.2–3.0 mg/L for domestic wastewater, effluent wastewater, sewage sludge, and surface water in Austria, respectively.[76] QACs are very stable chemicals in the environment and can be adsorbed to a large extent to organic or inorganic surfaces such as suspended solids, sediments, and organisms.[77] Hence, they could attach to non-target organisms in activated sludge during wastewater treatment and in natural surface water.

2.1.3 Chlorophenols

Many halogenated compounds are among priority contaminants in water and wastewater effluents due to their highly toxic effects on human health and persistence in the environment.[3, 4] Chlorophenols (CPs) are commonly found in effluents of pesticide, dyestuff, and wood preservative industries.[1-4] World-wide production of CPs is estimated at ca. 100,000 tons per year.[63] The concentrations of CPs in surface water ranged from 2 to 2000 ng/L.[22] Moreover, CPs are biodegradation byproducts of complex molecules such as herbicides and pesticides in the environment.[22] .[3] Chlorophenols have a strong taste and odor. Very small amounts of chlorophenols can also change the taste of fish. Chlorophenols can form while disinfecting drinking water if certain compounds are present.[78] Therefore, most people can be exposed to very low levels of chlorophenols (< ppb) in drinking water.[78]

2.1.4 Nitrophenols

Nitrophenols (NPs) are highly toxic, carcinogenic, and persistent contaminants in waste waters of explosives, pesticides, and dye-stuffs.[5, 79] They can also be produced in the environment through microbial hydrolysis or photodegradation of some pesticides.[80 81] NPs can also be produced in the atmosphere as a result of photochemical reaction between aromatic compounds and nitrogen monoxide.[80] NPs are resistant to microbial degradation in soil and groundwater.[81] NPs have been listed among the top 114 priority pollutants by the U.S. Environmental Protection Agency (U.S. EPA) due to their chemical stability, water solubility, persistence, and toxicity to human health and the environment.[82, 83] It has been reported that 54,500 pounds of 2-NP and 12,750 pounds of 4-NP were released into the air and disposed in landfills from manufacturing industries in 1989.[84] Many studies have shown the presence of NPs in surface waters including lakes and rivers. For example, the maximum concentration of 2,4- dichloro-6-nitrophenol was 2.46 μg/L in aquatic environment near an agricultural area in southern France,[85] and the highest median concentrations in the Danube river were measured for 4-nitrophenol (29 ng/L) and 2,4-dinitrophenol (19 ng/L).

2.2 Water Treatment Technologies to Remove Organic Compounds (OCs)

Current water treatment technologies for removal of organic contaminants from aqueous solution include physical,[86] chemical,[87] and biological processes.[88] These methods include coagulation, sedimentation, lime/soda ash softening, adsorption, ion exchange, membrane filtration, chlorination, ozonation, and ultraviolet photolysis.[12, 89] In physical processes such adsorption and ion exchange, contaminants are concentrated and transferred from one phase to another, therefore, additional processes are required for regeneration and further contaminant treatment.[35] Coagulation, sedimentation, and lime/soda ash softening are common and cheap treatment methods for removal of water hardness and colloidal suspensions, they exhibited low efficiency for removal of OCs such as pharmaceuticals.[12, 90] Adsorption is commonly used for treatment of a wide range of OCs from water and wastewater effluents.[91] Granular activated carbon (GAC)[25] and powdered activated carbon (PAC)[92] are the most common adsorbents in water treatment plants. Although activated carbon is an efficient method for removal of hydrophobic OCs (removal efficiency > 97%), they have lower adsorption affinity toward polar and ionic compounds.[93] This is a major problem for many OCs that exist in ionic forms under typical water treatment pHs. In addition, thermal regeneration with high attrition rates of activated carbon makes this method economically unfavorable.[49] Ion exchange by anion/cation exchange resins is an efficient method that can selectively remove ionic organic compounds. Moreover, comparing to activated carbon, regeneration of saturated resins with pollutants is amenable under mild conditions.[94]

Application of nanofiltration and reverse osmosis in water treatment has been attracted attention of many researchers in the past few years because of high efficiency in removing different classes of OCs.[95] However, application of these methods are not common in water treatment plants due to high cost.[12]

The ability of oxidation processes such as chlorination, ozonation, and ultraviolet photolysis[89] to remove OCs has been the focus of many studies. Chlorination is the most common disinfection process that is mandatory for all water treatment plants in the U.S., where removal efficiency for different OCs ranged from 40% to 90%.[96] Ozonation has been found as a highly effective method for removing OCs (removal efficiency >95%).[96] Ultraviolet photolysis has been used for treatment of OCs such as chlorinated and nitrated aromatic compounds, phenols, and pharmaceuticals.[97] This procedure generally has low efficiency compared to other oxidation methods and requires high UV light fluences.[97] Advanced oxidation processes (AOPs) have been defined as oxidation processes that primarily use the hydroxyl radical in the mechanism(s) for destruction of a target pollutant. AOPs include ozone in combination with ultraviolet light (O_3/UV), ozone and hydrogen peroxide (O_3/H_2O_2), hydrogen peroxide and ultraviolet light (UV/H_2O_2), Fenton (H_2O_2/Fe^{2+}), and photocatalysis $TiO_2/h\nu/O_2$.[98] AOPs are relatively efficient methods for removal of many pharmaceuticals and organic compounds (>90% removal).[83] The main disadvantage of AOPs is the high costs. One major concern for oxidation methods is generation of toxic by-products that are more harmful to human health and the environment.[96]

2.3 Polymeric Resins

Macroporous nonionic resins were introduced as an alternative to activated carbon in the 1960s partly to overcome the expensive thermal regeneration of activated carbon. The structure of polymeric resins is composed of an insoluble polymer matrix, commonly made up of either styrene or acrylate monomers while occasionally including other monomers such as vinylpyrindine.[99] Cross-linked and hypercross-linked resins have been later synthesized by adding crosslinking agents, typically divinylbenzene, which enables manufactures to increase surface area and adjust pore size distribution of the resins.[100]

Ionic resins containing charged functional groups are used to perform ion exchange processes. [47] Anion exchange resins (AXRs) typically contain amino functional groups on the monomer while cation exchangers commonly contain sulfonate or carboxylate functional groups.[47, 101] Strong base anion exchangers have a quaternary amino functional group on the monomer structure. Weak base anion exchangers use tertiary, secondary, primary, or mixed amino groups. For cation exchange resins (CXRs), the functional groups are mostly sulfonate for strong CXRs and carboxylate groups for weak CXRs.[101, 102]

Resins have been primarily used for chromatographic separation, treatment of industrial wastewater, and recovery of usable organic chemicals. Ion exchange resins have been widely used for decades for removal of ionic species. Nonionic resins were introduced to water and wastewater treatment after development of porous resins with high surface areas in the 1960s.[30] It has been reported that a wide range of OCs such as ketons, benzenes, phenols, anilines can be effectively removed by macroporous resins.[30] Many studies have shown that sorption of OCs is promoted by hypercrosslinked resins, this is because crosslinkage modifies the surface properties of the polymeric structure.[103] Resins can be tailor-made to target specific compounds and remove a diverse range of OCs by varying resin structure, internal surface area, pore size distribution, and surface polarity during synthesis.[100]

2.4 Sorption Mechanisms

Generally, sodium or hydrogen cations are attached to the functional groups in CXRs and exchange with cations in solution. A typical cation exchange reaction between sodium and a target compound A^+ is as follow:

$$\overline{R^- Na^+} + A^+ \rightleftharpoons \overline{R^- A^+} + Na^+ \tag{2.1}$$

where the overbar denotes the resin phase, R^- is the negatively charged functional group attached to the resin, and A^+ represents the solute of interest.

Electrostatic interaction is the main sorption mechanism during ion exchange, while the selectivity of a compound to the resin is controlled by nonelectrostatic interactions between the nonpolar moieties (NPM) of the compound and those of the resin.[104, 105] The nonelectrostatic interactions include hydrophobic or nonspecific interactions due to London dispersive forces, Debye forces, and Van der Waals interactions, π-π electron donor/acceptor interaction, and hydrogen bonding interactions. Thus, the presence of nonpolar moieties such as aromatic ring or long aliphatic chain can result in higher selectivity.[104 106, 107 108] For example, selectivity of alkanesulfonic anions toward polystyrene anion exchange resins increased with increasing chain length of the anions:[104] higher selectivity was observed for larger aliphatic quaternary ammonium cations toward polystyrenesulfonic CXRs;[106, 107] and selectivity increased with increasing number of aromatic rings in the solutes due to the possibility of π-π interactions between the aromatic compounds and the resin.[108]

In addition, sorption reflects differences in interactions forces between solute-sorbent and solute-solvent, thus solvent-associated interactions (e.g. water-solute, water-sorbent, water-water interactions) have a profound effect on selectivity of sorption. For instance, sorption of ions with higher hydration energies or by resins with higher moisture contents is more difficult because expelling water molecules from the organic ions or from the resin matrix is more energy demanding.[105, 109, 110]

2.5 Pd-based Catalysts

Palladium (Pd) catalysis has been widely used in fine chemical reactions because it provides high reaction rate, high turnover number, and high selectivity.[52] Pd also has high affinity to adsorb hydrogen which can be used as electron donor in catalytic reactions.[111]

The main goal of deposition of nanoparticles onto solid supports is their separation and recovery.[35, 52, 112] Homogenous palladium catalysis has been reported in many chemical reactions; problems in recovering metal nanoparticles and loss of the expensive metals are among the major disadvantages of using such catalysts.[52, 56]A proper catalyst support provides a matrix for the dispersion of the metal element (palladium), increases surface area of the metals, and enhances catalysts' activity, hydrophobicity, and thermal, hydrolytic and chemical stability.[28] The support should be mechanically stable and highly porous to maximize mass transfer rate, important for heterogeneous catalytic reaction in the liquid phase.[113]

The deposition method of palladium nanoparticles on a solid support depends on the support type. Wet or dry impregnation, deposition-precipitation, deposition-reduction, and ion exchange methods can be used for oxides and carbon supports by using a suitable aqueous solution of Pd(II) precursors, such as $PdCl_2$, $Pd(NH_3)Cl_2$, $Pd(NO_3)_2$, and

H_2PdCl_4.[52, 112] Hydroxylated metal oxide surfaces enhance the interaction with palladium nanoparticles. Thus, introducing oxygen containing groups to a support surface like carbon can improve palladium interaction with the support. Support properties such as particle size, surface area, pore structure, and acid-base properties influence the catalyst activity and selectivity [59] by affecting surface area, dispersion, size and location of the metal nanoparticles.[52] For example, it has been shown that microporous and mesoporous materials such as zeolites can improve the reactivity and selectivity of the catalysts. [61]

Pd-based catalysts in bimetallic or monometallic forms on different inorganic and organic supports have been investigated for removal of halogenated compounds, N-nitrosoamines, and oxyanions.[32, 114-116] Reduction of nitrate with different Pd-based bimetallic catalysts such as Pd-In, Pd-Cu, and Pd-Sn in various supports such as γ-Al_2O_3, silica, activated carbon, TiO_2, and organic resins has been studied.[57, 117, 118] Pinter et al. investigated a combination of ion exchange with reduction processes by a bimetallic catalyst (Pd-Cu/Al_2O_3) for the removal of nitrate (NO_3^-).[119, 120] In their study, a strong anion exchange resin column was used to remove nitrate from other ions, then, the nitrate ion from regeneration of the ion exchange column was introduced to the catalyst reactor for denitrification. The main advantage of this method is the elimination of secondary waste streams of nitrate, but it still requires operation of ion exchange column and regeneration. A similar approach was studied by Liu et al. for reduction of perchlorate in waste ion-exchange regenerant brine by a Re-Pd bimetallic catalyst.[121] In a study by Kim and Choi, a Pd-supported ion-exchange resin was developed for complete decomposition of perchlorate through adsorption onto a strong anion exchange resin followed by catalytic decomposition of the adsorbed ClO_4^-.[122] Other work also looked into the activity and selectivity of catalysts supported on anion and cation exchange resins. For example, Gasparovicova et al. studied nitrate reduction by bimetallic Pd-Cu catalysts on two microporous cation and anion exchange resins and γ-Al_2O_3.[123, 124] The results showed that the activity of the catalysts on the anion exchange resin was four times more than that on the cation exchange resin. This is due to the sorption of nitrate anions through electrostatic interactions in the cationic resin. In comparison with the cationic resin, γ-Al_2O_3 showed higher activity of nitrate removal which was related to the diffusive effects of the active sites which are inside the polymeric resin but are on the outer surface of the inorganic support. However, selectivity of the resin-based catalyst to production of N_2 as oppose to NH_3 was better than γ-Al_2O_3. Reduction of nitrate by Pd catalysts leads to the production of hydroxide ions which increased solution pH up to 10-11. It has been shown that higher pH favors the formation of ammonium which is not acceptable for drinking water.[125, 126] There are some studies that used H^+ form of cation exchange resins as the support for bimetallic catalysts to help buffer the pH value and to prevent NH_4^+ from forming in nitrate reduction.[124, 127, 128]

2.6 Reduction of Chlorophenols by Pd-based Catalysts

Pd-based catalytic reduction of chlorophenols has been widely investigated by other researches. Most studies have used Al_2O_3 or activated carbon (AC) as the support. In hydrodehalogenation (HDC) reaction, one or more halogen atoms are replaced with atomic hydrogen. For reduction of a target compound with Pd catalysts, the presence of electron donor is essential. Using hydrogen gas (H_2) as an electron donor is very common because H_2 has a very high affinity to Pd surfaces. Metallic palladium dissociates the adsorbed hydrogen and converts it to the adsorbed hydrogen (Pd-H_{ads}) which is reactive in reducing the co-adsorbed compounds.

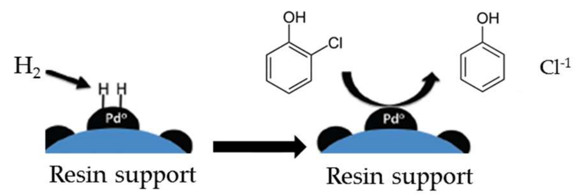

Figure 2-1: Schematic reduction of 4-CP on Pd-based catalyst in the presence of hydrogen gas.

It has been proven in some studies that adsorption of the target compound on the catalyst surface is the rate-determining step.[35, 62, 129] Hydrogenation of aromatic rings has been observed after dehalogenation in the presence of hydrogen gas as the electron donor. Both cyclohexanone and cyclohexanol have been produced as a result of ring hydrogenation.[129-131] Destruction rates of CPs over palladium/carbon catalysts were more than 98%.[1] It has been shown that HDC of CPs over Pd/C and Pd/Al_2O_3 is dependent on solution pH. Higher pH is more favorable for HDC because it limits the inhibition effect of Cl^-. However, Pd/Al_2O_3 is less sensitive to deactivation due to strong interactions between Pd and the support. Pd/C showed significant reactivity loss because of decrease in surface areas due to pore blockage and loss in Pd contents due to Cl^- poisoning.

2.7 Reduction of 4-Nitrophenol by Pd-based Catalysts

4-Nitrophenol has been widely used as a model compound for testing activity of different supported metal nanoparticles such as gold, silver, nickel, and platinum using hydrogen gas or sodium borohydride as the electron donor.[132-137] The catalytic hydrogenation of p-nitrophenol mainly resulted in formation of p-aminophenol (4-AP,

Figure 2-2). P-aminophenol is an important intermediate for manufacturing of pharmaceuticals, polymers, and dyes.[138, 139] Formation of 4-AP as the only product of hydrogenation of 4-NP is one of the advantages of Pd-based catalysts[134, 137] comparing to other commercial methods that lead to the formation of other side products such as aniline and phenylhydroxylamine.[140] Hydrogenation of 4-NP can also be followed by oxidation of p-aminophenol to other products such as hydroxyaniline, depending on experimental conditions. Catalytic reduction by homogenous polymer palladium complex catalysts can result in formation of other byproducts such as hydroxyaniline.[141, 142]

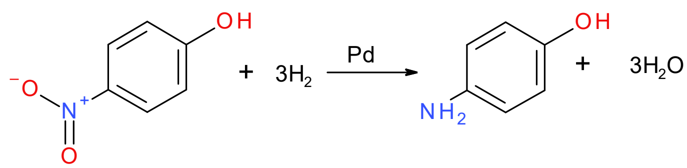

Figure 2-2: Schematic reduction of 4-NP on Pd-based catalyst in presence of hydrogen gas.

In many studies, the kinetic mechanism of catalytic reduction of 4-NP is believed to be a surface reaction, and thus, the Langmuir–Hinshelwood model has been successfully applied for studying kinetic mechanisms of 4-NP reduction while assuming surface reaction as the rate determining step.[143, 144] In addition, adsorption equilibrium of both reactants (4-NP and hydrogen donor) onto catalyst surface is required prior to reaction. Esumi et al. proposed that 4-NP reduction by Ag, Pd, and Pt/dendrimer catalysts is controlled by diffusion of 4-NP.[145] They also showed that Pd/dendrimer catalyst exhibited higher reactivity than Pt and Ag/dendrimer catalysts, due to its smaller metal nanoparticle size.

Pd-based catalysts supported on various supports, such as activated carbon and natural and synthesized polymers, have been used for hydrogenation of 4-NP. [83, 134-137, 146-148] Different factors have been found to influence catalytic reduction of 4-NP such as pH, metal loading, and catalyst support. It has been shown adsorption affinity of the reactants onto the catalyst surface has significant effects on the catalytic activity, and it is highly dependent on solution pH because pH influences on catalyst surface charge and dissociation of the reactants.[83, 98] Choudhary et al. showed that intra and extra mass transfer has significant effects on 2-NP reduction by Pd/C catalyst.[134] They showed large tortuosity factor and activation energy for intra diffusion of 2-NP in the catalyst, that is, adsorption or surface diffusion influences on the intraparticle mass transfer of 2-NP. By studying 4-NP adsorption binding energy, Pozun et al. showed that 4-NP reduction by bimetallic dendrimer catalysts such as Pd/Au and Pd/Cu is directly related to adsorption of 4-NP onto the catalyst surface.[149]

CHAPTER 3

SORPTION MECHANISMS AND PREDICTIVE MODELS FOR THE REMOVAL OF CATIONIC ORGANIC CONTAMINANTS BY CATION EXCHANGE RESINS

Results presented in this chapter have been published in Jadbabaei and Zhang (2014).[150]

Abstract

Understanding the sorption mechanism of organic contaminants on cation exchange resins (CXRs) will enable application of these resins for the removal of cationic organic compounds from contaminated water. In this study, sorption of a diverse set of 12 organic cations and 8 neutral aromatic solutes on two polystyrene CXRs, MN500 and Amberlite 200, was examined. MN500 showed higher sorbed concentrations due to its microporous structure. The sorbed concentrations followed the same trend of aromatic cations > aliphatic cations > neutral solutes for both resins. Generally, solute-solvent interactions, nonpolar moiety of the solutes, and resin matrix can affect selectivity of the cations. Sorbed concentrations of the neutral compounds were significantly less than those of the cations, indicating a combined effect of electrostatic and non-electrostatic interactions. By conducting multiple linear regression between Gibbs free energy of sorption and Abraham descriptors for all 20 compounds, polarity/polarizability (S), H-bond acidity (A), induced dipole (E), and electrostatic (J^+) interactions were found to be involved in the sorption of the cations by the resins. After converting the aqueous sorption isotherms to sorption from the ideal gas-phase by water-wet resins, a more

significant effect of J^+ was observed. Predictive models were then developed based on the linear regressions and validated by accurately estimating the sorption of different test-set compounds with a root mean square error range of 0.91 to 1.1 and 0.76 to 0.85 for MN500 and Amberlite 200, respectively. The models also accurately predicted sorption behavior of aniline and imidazole between pH 3 and 10.

3.1 Introduction

Many organic compounds such aromatic amines and quaternary ammonium cations exist in ionic form in the aquatic environment. The toxic effects of cationic organic contaminants (COCs) on human health and the environment require their efficient removal from contaminated water.[71, 72] Ion exchange resins that consist of polymeric matrices and different functional groups can effectively remove ionic organic compounds (IOCs)[46-48] by exchanging with ionic solutes in solution. For cation exchange resins (CXRs), the functional groups are mostly sulfonate or carboxylate groups.[101, 102] Although activated carbon has been structurally modified for removing ionic compounds, it has shown lower selectivity and sorption capacity (about 100 times lower) than ion exchange resins in the removal of IOCs.[151]

Poly-parameter linear free energy relationships (pp-LFERs) have been widely used for predicting partition behavior of neutral compounds from water to organic solvents[152, 153] or sorption of neutral compounds by various sorbents (eq 3.1).[154, 155] In the pp-LFERs method all possible interactions between a solute and a sorbent are considered in a general equation developed by Abraham:[156-159]

$$SP = eE + sS + aA + bB + vV + c \tag{3.1}$$

where SP represents a solvation property that is related to solute and solvent properties in a linear free energy relationship, and independent variables or descriptors E, S, A, B, and V account for the properties of the solute. E is the excess molar refraction accounting for nonspecific interactions due to London dispersive forces and Debye forces; S is a combined dipolarity/polarizability descriptor; A and B are the overall solute hydrogen bond acidity and basicity; V is McGowan's characteristic molecular volume that accounts for cavitation energy and some additional nonspecific interactions; and c is a constant used to capture all other additional forces and might be entropy related.[30] The regression coefficients *e*, *s*, *a*, *b*, *v*, and *c* are determined by multiple linear regression analysis and reflect differences in the interaction forces between the solvent and the sorbent.[160]

Interactions that are responsible for sorption of organic ions by ion exchange resins should include the same nonspecific and specific (e.g. H-bonding, π-π) interactions for neutral solutes.[105, 161] In addition, electrostatic interactions are an important part of the specific interactions.[103, 162] To take into account any additional interactions in partition of an ion between two solvents, Abraham's group introduced new descriptors J^+ and J^- for cationic and anionic solutes respectively, where J^- is zero for cations and J^+ is zero for anions. Also, both descriptors are zero for neutral solutes:[163-165]

$$SP = eE + sS + aA + bB + vV + j^+J^+ + j^-J^- + c \tag{3.2}$$

Like other regression coefficients in eq 3.1, j^+ and j^- represent differences in the additional interaction forces between the two solvents.

Our recent work has successfully used the pp-LFERs approach to examine sorption of neutral organic solutes onto three non-ionic resins[166] or organic anions and neutral solutes onto three anion exchange resins.[94] Dorge and Goss[167] developed a model for the sorption of organic cations to soil as a sum of sorption to organic matter and sorption to clay minerals based on McGowan's characteristic molecular volume and charged surface area. Despite these, only a very limited number of studies have reported the uptake of organic cations by CXRs[106, 161] with little variation in the structures of the cations, understanding of the molecular interactions remains phenomenological, and there is no *quantitative* model available to determine either sorption capacity or the level of electrostatic and non-electrostatic interactions between cations and CXRs. Toward this end, we investigated sorption mechanisms of 12 cationic and 8 neutral organic compounds over a wide range of aqueous concentrations on two CXRs (MN500 and Amberlite 200). Using the isotherm data and the pp-LFERs approach (eq 3.2), we interpreted the sorption mechanisms and developed predictive models to calculate sorbed concentration and selectivity of a diverse range of organic compounds on the studied resins under changing pH. Solvent-associated interactions of the solutes were then removed using ideal gas phase conversion to separate the effect of solvent-associated interactions from that of solute-sorbent interactions.[166] In this method, aqueous sorption was converted to sorption by a water-wet sorbent from the ideal gas phase where there are no intermolecular interactions.[166, 168, 169] The aqueous sorption isotherms were then reconstructed to analyze differences in the solute-sorbent interactions which were obscured in the original aqueous sorption.

3.2 Theoretical Approach

3.2.1 Model Development

The Gibbs free energy change of the transfer of solute *i* from the aqueous phase to the sorbent phase ($\Delta G_{S\text{-}W,i}$) can be related to the equilibrium sorbent-water distribution coefficient ($K_{S\text{-}W,i}$):

$$\Delta G_{S-W,i} = -RT \ln K_{S-W,i} \tag{3.3}$$

where R is the universal gas constant [0.008314 KJ/(mol·K)] and T (K) is the absolute temperature of the system. $K_{S\text{-}W,i}$ for ions is believed to be equal to the selectivity (or separation factor $\alpha_{A/Na}$) and can be estimated from the mole fraction of *i* in the exchanger phase (y_i) and in the aqueous phase (x_i):[105]

$$K_{S-W,i} = \frac{y_i x_{Na}}{y_{Na} x_i} = \frac{Q_e}{Q_c - Q_e} \cdot \frac{[Na^+]_0 + Q_e \dfrac{m}{V}}{C_e} \tag{3.4}$$

where Q_e (μmol/g) is the equilibrium sorbed concentration, Q_c is the resin ion exchange capacity (μeq/g), $[Na^+]_0$ is the initial Na^+ concentration in the aqueous phase (μM), C_e (μM) is the solute equilibrium concentration, the term $Q_e \frac{m}{V}$ represents the effective concentration of Na^+ exchanged by the sorbed organic ions where m is the mass of the resin (g), and V is the solution volume (L). The ratio of m to V was determined as a function of Q_e based on the experimental data for all cationic compounds (**Table 3-1**). Using the same approach as reported in our recent work for neutral and anionic compounds,[94, 166] a predictive model can then be developed for sorption of a training set of cationic compounds on a CXR (**Flowchart A-1**).

$\Delta G_{S\text{-}W,i}$ and selectivity ($\alpha_{A/Na}$) can be related to solute descriptors by pp-LFERs equation (eq 3.2 in the main text):

$$\Delta G_{S-W,i}(\text{or}\,\alpha_{A/Na}) = eE + sS + aA + bB + vV + j^{+}J^{+} + c \tag{3.5}$$

Similar to our recent work,[94] a predictive model can be developed for the sorption of a training set of compounds on a cation exchange resin based on the following steps:

1. For any arbitrary value of Q_e, the corresponding value for C_e can be calculated based on the Polanyi Dubinin-Astakhov model for fitting the sorption isotherms:[162]

$$\log Q_e = \log Q^0 - \left(\frac{\varepsilon}{E_0}\right)^b \tag{3.6}$$

where ε (KJ/mol) is the adsorption potential which can be calculated by:

$$\varepsilon = -RT\ln\left(\frac{C_w}{C_w^{sat}}\right) \tag{3.7}$$

where C_w is the aqueous equilibrium concentration and C_w^{sat} is the solute solubility in the aqueous phase. Q^0, E_0 and b are the fitting parameters, where E_0 (KJ/mol) is the sorption energy which accounts for all the interaction forces involved in sorption, Q^0 (µmol/g) is the maximum adsorption capacity, [162, 170, 171] and b is related to heterogeneity of the interaction energy.[172]

The corresponding $\Delta G_{S\text{-}W,i}$ can then be calculated based on the eqs 3.3 and 3.4.

2. For each Q_e, by performing multiple linear regression between a set of $\Delta G_{S\text{-}W,i}$ values and the solute descriptors for all training-set compounds based on eq 3.5, a

set of regression coefficients *e*, *s*, *a*, *b*, *v*, j^+, and *c* can be determined. The best regression model is determined by the lowest Mallow's C_p value while keeping the p-value of each parameter less than 0.1 to ensure each involved term statistically significant.

3. Multiple correlations are performed to develop relationship for each regression coefficient as a function of Q_e. These functions will be denoted as $f^e(Q_e)$, $f^s(Q_e)$, $f^a(Q_e)$, etc. for each coefficient.

4. After substituting the regression coefficient functions and eqs 3.3 and 3.4 into eq 3.5, we can obtain:

$$-RT\ln\left(\frac{Q_e}{Q_c-Q_e}\cdot\frac{[Na^+]_0+Q_e\dfrac{m}{V}}{C_e}\right)=f^e(Q_e)E+f^s(Q_e)S+f^a(Q_e)A+f^b(Q_e)B+f^v(Q_e)V+ f^{j^+}(Q_e)J^+ + f^c(Q_e) \tag{3.8}$$

After rearranging to solve for C_e the predictive model becomes:

$$C_e=\frac{Q_e}{Q_c-Q_e}\cdot\left([Na^+]_0+Q_e\frac{m}{V}\right)\cdot e^{\frac{f^{TOT}(Q_e)}{RT}} \tag{3.9}$$

where $f^{TOT}(Q_e)$ is equal to the right hand side of eq 3.8. Therefore, for sorption of a cation with known Abraham descriptors by a CXR with a known Q_c, C_e can be predicted at any given Q_e and m/V value, its selectivity can then be calculated based on eq 3.9.

It should be mentioned that for neutral compounds, their abundance in both aqueous and sorbent phases is not in the form of mole fraction, therefore, a constant (C_{ads}) accounting for the conversion to mole fraction is needed:[169]

$$\Delta G_{S-W,i} = -RT \ln K_{S-W,i} + C_{ads} \tag{3.10}$$

Zhu and Pignatello[173] approximated C_{ads} based on the Flory-Huggins theory for the chemical activity of a compound in a macromolecular phase:[174]

$$C_{ads} / RT = \ln \gamma_{w,i} + \ln \frac{V_w}{V_i} - [(1 - \frac{V_i}{V_s}) + X_{S-i}] + \ln \frac{1}{\rho_{resin}} \tag{3.11}$$

where $\gamma_{W,i}$ is the solute activity coefficient in water; V_i, V_W, and V_S are the molar volumes of solute, water, and sorbent, respectively; X_{S-i} is the Flory-Huggins solute-sorbent interaction parameter; and ρ_{resin} (g/mL) is density of resin. $\gamma_{W,i}$ can be calculated based on the solute solubility and melting point when the solute behaves non-ideally in water.[169]. Because there is entropy loss upon sorption of solutes by resins,[175] we assume X_{S-i}=-1. Since V_i <<V_S, C_{ads}/RT is thus calculated based on the eq below:

$$C_{ads} / RT = \ln \gamma_{w,i} + \ln \frac{\bar{V}_w}{\bar{V}_i \rho_{resin}} \tag{3.12}$$

Table 3-1: Linear correlations between the experimentally used m/V (g/L) and Q_e (μmol/L).

	MN500		Amberlite 200	
Solute	m/V=f(Q_e)	R^2	m/V=f(Q_e)	R^2
$Aniline^+$	0.0006Q_e	0.95	0.0111Q_e	0.93
DMA^+	0.0009Q_e	0.74	0.0137Q_e	0.94
Imidazole	0.0013Q_e	0.86	0.0118Q_e	0.97
NMe_4^+	0.0128Q_e + 0.7047	0.96	0.0334Q_e+2.366	0.99
NEt_4^+	0.0134Q_e + 0.014	0.98	0.048Q_e+1.136	0.99
NPr_4^+	0.0249Q_e -0.3047	0.96	0.1305Q_e-1.2205	0.97
NBu_4^+	0.0351Q_e + 1.3567	0.98	0.0993Q_e+2.5671	0.99
$CETM^+$	0.0082Q_e + 0.4735	0.93	0.0253Q_e+2.2239	0.98
$BETM^+$	0.0076Q_e+ 0.74	0.95	0.0989Q_e+0.9035	0.98
PTM^+	0.004Q_e + 0.5841	0.99	0.0136Q_e+0.4073	0.94
BTM^+	0.0018Q_e	0.90	0.0325Q_e	0.97
$VBTM^+$	0.0012Q_e	0.93	0.0118Q_e+0.0567	0.99

3.2.2 Gas Phase Transfer

The phase transfer method was applied to eliminate the effect of solvent-associated interactions from $\Delta G_{S\text{-}W,i}$ in order to yield insights into solute-sorbent interactions. It is assumed that solutes are sorbed by a water-wet sorbent from the ideal gas phase where the solute does not undergo any interaction.[166, 168] Figure 1 illustrates the thermodynamic cycle after the phase conversion from the aqueous phase to the ideal gas phase.

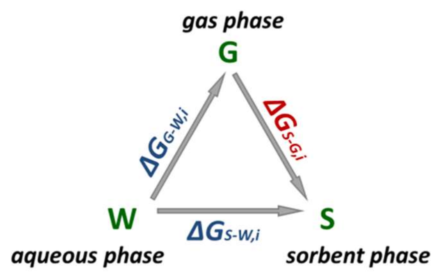

Figure 3-1: Gibbs free energy change between different phases (adopted from ref[166])

The net Gibbs free energy change for sorption of solute i from the aqueous phase to the sorbent phase can be defined as:

$$\Delta G_{S-W,i} = \Delta G_{G-W,i} + \Delta G_{S-G,i} \tag{3.13}$$

where $\Delta G_{G\text{-}W,i}$ is the free energy change for the partition of solute i from the aqueous phase to the gas phase, and $\Delta G_{S\text{-}G,i}$ is that for the sorption of solute i from the gas phase to the sorbent phase. $\Delta G_{S\text{-}G,i}$ and $\Delta G_{G\text{-}W,i}$ can be calculated based on the respective equilibrium distribution coefficients. [166, 169]

The free energy change for the partition of solute i from the aqueous phase to the gas phase ($\Delta G_{G\text{-}W,i}$) is:

$$\Delta G_{G-W,i} = -RT \ln K_{G-W,i} + RT \ln \frac{\bar{V}_W}{\bar{V}_G} \tag{3.14}$$

After substituting eqs 3.10 and 3.14 into eq 3.13 in the main text, ΔGS-G,i for neutral solutes is:

$$\Delta G_{S-G,i} = -RT(\ln \mathrm{K}_{S-W,i} - \ln \mathrm{K}_{G-W,i}) + RT\left(\frac{C_{ads}}{RT} - \ln \frac{\bar{V}_W}{\bar{V}_G}\right) \tag{3.15}$$

and for ionic solutes is:

$$\Delta G_{S-G,i} = -RT\left(\ln\left(\frac{Q_e}{Q_c - Q_e}\cdot\frac{[Na^+]_0 + Q_e\frac{m}{V}}{C_e}\right) - \ln K_{G-W,i}\right) - RT\ln\frac{\bar{V}_W}{\bar{V}_G} \tag{3.16}$$

where $K_{G\text{-}W,i}$ is the equilibrium distribution coefficient between the aqueous phase and the gas phase (i.e. Henry's law constant), $K_{S\text{-}W,i}$ (L/kg) is the equilibrium distribution coefficient for adsorption of solute i from the aqueous phase to the solid phase, $\bar{V}_G$ is the molar volume of ideal gas (24.73 L/mol) and $\bar{V}_W$ is the molar volume of the solute. C_{ads} is calculated from eq 3.12 for neutral compounds and is equal to zero for ionic compounds. $\Delta G_{S\text{-}G,i}$ can be related to solute descriptors by the pp-LFERs equation (eq 3.2):

$$\Delta G_{S-G,i} = eE + sS + aA + bB + vV + j^+J^+ + c \tag{3.17}$$

Following the model development steps, the predictive model after the gas phase conversion for neutral solutes is:

$$C_e = \exp(\ln(Q_e) + \frac{-f^{tot}(Q_e)}{RT} - \frac{C_{ads}}{RT} + \ln\frac{\bar{V}_W}{\bar{V}_G} - \ln K_{G-W,i}) \tag{3.18}$$

and for ionic solutes is:

$$C_e = \exp(\ln\left(\frac{Q_e([Na^+]_0 + Q_e\frac{m}{v})}{Q_c - Q_e}\right) + \frac{-f^{tot}(Q_e)}{RT} + \ln\frac{\bar{V}_W}{\bar{V}_G} - \ln K_{G-W,i}) \tag{3.19}$$

3.3 Materials and Methods

3.3.1 Materials

Two strong CXRs, MN500 and Amberlite 200, and one weak CXR, Amberlite IRC-76, were provided by Purolite® and Dow® (U.S.) respectively (properties in **Table**

3-2). Both strong CXRs are polystyrenic, MN500 is microporous while Amberlite 200 is porous; Amberlite IRC-76 is polyacrylic. Prior to use, the resins were sequentially washed by HCl, NaOH, NaCl and methanol (details in **section 3.3.2**). Six aliphatic and three aromatic quaternary ammoniums, four substituted phenols, four substituted anilines, imidazole, and nitrobenzene (NB) were purchased from Fisher Scientific. Analytical grade chemicals were used as purchased to prepare solutions with nanopure deionized water. The properties of solutes and their abbreviations are listed in **Table 3-3**.

Table 3-2: Properties of the selected ionic and non-ionic resins.

Name	Structure [a]	Functional Group [b]	Exchange Capacity [c]	BET Surface Area	Pore volume	BJH pore volume distribution %			Moisture content [c]	Contact angle [c]	Density [a]
			meq/g-dry	**m^2/g**	**mL/g**	**<2μm**	**2-50 μm**	**>50μm**	**%**	**degree**	**g/ml**
MN500	Polystyrene	SA	1.07	414[d]	0.65[e]	48.4[d]	32.5[d]	18.4[d]	52	0.0	1.19
Amberlite-200	Polystyrene	SA	2.43	42[f]	0.46[f]	0.4[f]	29.8[f]	69.8[f]	45	0.0	1.22
IRC-76	Polyacrylic	SA	3.36[a]	NA	NA	NA	NA	NA	63	0.0	1.16
IRA-910	Polystyrene	DMEA	5.33	NA	NA	NA	NA	NA	53	0.0	1.10
IRA-96	Polystyrene	TA	6.19	NA	NA	NA	NA	NA	59	13.1	1.05
MN200	Polystyrene	–	–	1021[g]	0.49[g]	69.5[g]	17.9[g]	12.6[g]	58	110.5	1.04
XAD-4	Polystyrene	–	–	829[g]	1.25[g]	12.4[g]	86.8[g]	0.8[g]	56	155.1	1.02
XAD-7	Polyacrylic	–	–	495[g]	1.12[g]	2.3[g]	90.7[g]	7.0[g]	67	110.2	1.07

[a] reported by the manufacturer; [b] Sulfonic acid (SA), Carboxylic acid (CA), Dimethylethanolammonium (DMEA), Tertiary amine (TA), ; [c] this work, Texts S6-S8; [d] ref [176]; [e] ref [177]; [f] ref [178]; [g] ref [166].

Table 3-3: Physical-Chemical Properties of the Selected Organic Compounds.

Compound	$\log K_{GW}$[a]	Hydration Energy[c] (KJ/mol)	Solute Descriptors[d] E	S	A	B	V^g	J^+
Aniline	-4.03	-5.09	0.96	0.96	0.26	0.41	0.82	0
4-Nitroaniline (4-NA)	-7.12	-22.72	1.24	1.83	0.51	0.34	0.99	0
2-Nitroaniline (2-NA)	-5.13	-11.36	1.18	1.37	0.30	0.36	0.99	0
4-Chloroaniline (4-CA)	-4.35	-6.91	0.91	1.36	0.36	0.25	0.96	0
Phenol	-4.59	-8.28	0.81	0.89	0.60	0.30	0.78	0
4-Nitrophenol (4-NP)	-7.66	-25.80	1.07	1.72	0.70	0.22	0.95	0
2-Nitrophenol (2-NP)	-3.1	0.22	1.02	1.05	0.05	0.37	0.95	0
4-Chlorophenol (4-CP)	-5.05	-10.91	0.92	1.24	0.55	0.22	0.90	0
2,6-Dichlorophenol (2,6-DCP)	-3.96	-4.96	0.90	0.90	0.38	0.24	1.02	0
4-Methylphenol (4-MP)	-4.15	-5.77	0.82	0.87	0.57	0.31	0.92	0
Nitrobenzene (NB)	-3.12	0.10	0.87	1.11	0.00	0.28	0.89	0
Protonated aniline (Aniline$^+$)	-14.5[b]	-64.82	0.81	1.62	1.93	0	0.84	0.62
Protonated N,N-dimethylaniline (DMA$^+$)	-14.2[b]	-63.11	0.81	1.85	1.84	0	1.12	0.81
Protonated Imidazole (Imidazole$^+$)	-16.5[b]	-76.23	0.56	2.5	1.61	0	0.56	1.05
Tetramethylammonium (NMe_4^+)	-9.76	-37.80	-0.20	1.48	0.82	0	0.81	1.24
Tetraethylammonium (NEt_4^+)	-9.27	-35.00	-0.52	1.81	0.57	0	1.41	1.52
Tetrapropylammonium (NPr_4^+)	-8.67[b]	-32.17	-0.07	1.72	0.49	0	1.92	1.64
Tetrabutylammonium (NBu_4^+)	-8.16[b]	-29.36	-0.10	1.90	0.40	0	2.48	1.65
(2-Chloroethyl)trimethylammonium (CETM$^+$)	-14.4[b]	-64.25	0.11[e]	1.83[f]	0.85[f]	0	1.06	1.80[f]
(2-Bromoethyl)trimethylammonium (BETM$^+$)	-15.4[b]	-69.95	0.29[e]	1.86[f]	0.82[f]	0	1.11	2.00[f]
Phenyltrimethylammonium (PTM$^+$)	-16.5[b]	-76.23	0.67[e]	2.07[f]	0.82[f]	0	1.26	2.00[f]
Benzyltriethylammonium (BTM$^+$)	-15.8[b]	-72.23	0.53[e]	2.40[f]	0.57[f]	0	1.82	2.20[f]
Vinylbenzyl trimethylammonium (VBTM$^+$)	-17.8[b]	-83.64	0.89[e]	2.17[f]	0.87[f]	0	1.64	2.15[f]

[a] K_{GW} is the dimensionless Henry's law constant[103] ; [b] estimated based on the modified bond contribution method[165]; [c] estimated based on $\Delta G_{G\text{-}W,i} = -RT\ln K_{GW} + RT\ln V_W/V_G$ where V_W and V_G are the molar volume of water and the gas phase, respectively[166]; [d] Abraham descriptors[153, 163]; [e] estimated from refractive index[163] ; [f] estimated based on the group contribution method (Table 3-4)[179]; [g] McGowan's characteristic molecular volume[179].

3.3.2 Resin Cleaning

The resins were subjected to wash by 10 bed volumes of 1M HCl, 1M NaOH and 1M NaCl, respectively in fixed-bed column runs in order to remove residual impurities. After washing resins with acid and base, distilled water was passed through the column to reach neutral pH in the effluent. The effluent flow rate was adjusted to 5 mL/min using a constant-flow pump to provide sufficient contact time between resin and solution. After column wash, the resins were transferred to a Soxhlet apparatus to be extracted with methanol for 8 hours for removing organic residues.

3.3.3 Measuring Resin Moisture Content

Three replicate resin samples of 1 gram were mixed with distilled water for 24 hours. The saturated resin samples were centrifuged for 20 minutes at 2000 rpm to remove free water from the resin beads. These samples were then immediately transferred to aluminum weighing dishes, weighed, and dried to constant weight at 105 ^oC. After drying, the samples were weighed again. The moisture content of each sample was calculated by:

$$moisture\% = \frac{m_2 - m_3}{m_2 - m_1} \times 100 \tag{3.20}$$

where m_1 is the weight of the empty weighing dish; m_2 is the weight of the resin and the weighing dish before drying; and m_3 is the weight of the resin and the weighing dish after drying. The average moisture content of the three replicates was reported as the moisture content.

3.3.4 Measuring Resin Cation Exchange Capacity

To measure ion exchange capacity of the strong cation exchange resins, 1 gram resin was transferred to a column and washed with 80 ml of 1 M of HCl solution at 5-7 ml/min to convert the resin beads to the H^+ form. Then the resin beads were washed with distilled water at 25-30 ml/min to reach neutral pH in the effluent followed by 70 ml of 1M of NaCl solution at 3-5 ml/min. After that 10-20 ml of distilled water was passed through the column. The effluents of the last two steps were collected and combined. The combined effluent was titrated with 0.1M of NaOH to obtain neutral pH. The resin beads were dried at 105 ^{o}C for 24 hours and after that the dry weight was measured (W). The exchange capacity (Q_c) was calculated using the eq below:

$$Q_c = \frac{(0.1 mol/l) \times V}{W} \tag{3.21}$$

where V is the volume of NaOH used for titration.

3.3.5 Measuring Resin Contact Angles

The contact angles were measured by professor Bingcai Pan at Nanjing University, China by a contact angle goniometer using the sessile drop method. The goniometer instrument consists of an optical system, a horizontal stage for holding samples, and a micrometer syringe to add a liquid drop on the surface of solid. The optical system captures the profile of water on the solid surface. The angle between the solid and the liquid interface is the contact angle. For measuring contact angles a solid sample was placed on the sample stage, and then the syringe was filled with distilled water. The instrument was turned on and the height of the syringe and the solid sample was adjusted so the tips of the syringe and the solid surface were visible on the screen. Then, a water droplet was added on the solid surface and contact angles were measured.

3.3.6 Adsorption Experiments

Batch experiments for adsorption isotherms were carried out in amber glass bottles with Teflon-lined screw caps at ambient temperature (22±1^{o}C). For each isotherm at least 17 experimental data points were collected. The concentration of NaCl was 20 mM in all samples to keep ionic strength constant, and the aqueous concentration of all ionic solutes was between 0.003 and 4 mM. For neutral solutes, the equilibrium concentration range was selected based on the compound solubility. Trial experiments were conducted to determine solid to solution ratios to achieve 25%-75% removal of the solutes. The pH was adjusted using 0.2 M NaOH and HCl to keep the solutes in the desired charged form. The amber bottles containing resin and the target compound solution were shaken under 175 rpm for 48 hours. Preliminary kinetic experiments showed that all sorption reached equilibrium within a few hours and there was no significant removal after about 10 hours. After reaching equilibrium, NB, anilines, and phenols were analyzed using high-performance liquid chromatography (HPLC-Agilent) and the quaternary ammonium cations and imidazole were analyzed using a total organic carbon analyzer (TOC-Shimadzu). Sorption of the target compounds was determined from the differences between the initial and final concentrations.

3.3.7 Analytical Methods

Agilent Technologies 1200 Infinity Series HPLC was used to analyze aromatic solutes except quaternary ammonium cations. To convert all solutes into predominately neutral species, diluted phosphoric acid at a pH of 3.00 was used as the mobile phase for the phenols with pKa values between 6.7 and 7.2, and ammonium acetate solution at pH=7.2 was used as the mobile phase for aniline and 4-CA (pKa value of 4.67 and 3.86). For the acidified mobile phase a Zorbax RX-C18 column was used. For the neutral compounds with a mobile phase of nanopure water and methanol a Zorbax XDB-C18 column was used. The DAD detector was set at 230–382 nm.

An Agilent Technologies 8453 UV/visible Spectrometer was used to measure the concentrations of aromatic quaternary ammonium cations. All samples were dissolved in DI water. The maximum detection wavelengths were adjusted to 203, 208 and 254 nm for

PTM^+, BTM^+, and $VBTM^+$ respectively. TOC analysis using a Shimadzu TOC-VCSH was necessary to determine concentrations of the aliphatic quaternary ammonium cations which cannot be analyzed by UV/Visible. Potassium hydrogen phthalate was used to calibrate the total carbon measurements with a range of 0.25 – 10 mg of carbon per liter. Injections of 100 μL were used and repeated three times for accuracy. Inorganic carbon tests were found to be negligible when measuring these samples. Concentrations from the TOC machine were converted from mg/L of carbon to molar concentrations based on the number of carbons within the compounds. The detection limit of TOC analysis (~700 μM) was higher than the other two methods and thus was used only on compounds that are incapable of detection via the other analytical methods.

3.3.8 Estimating Abraham Descriptors

Estimating descriptors for solutes that do not have reported descriptor values is important for using pp-LFERs. Descriptor V is the McGowan characteristic volume and was estimated based on the volumes of all atoms and the number of bonds in the molecular structure.[157, 179] Descriptor E can be estimated from refractive index.[163] Cations typically have negligible H-bond basicity, so we fixed their B values at 0. Two methods were examined for estimating descriptors A, S, and J^+ for the quaternary ammonium cations: the modified group contribution method,[179] and the method based on the reported pp-LFERs between compound's partition coefficients from water to any given organic solvent (lnP) and solute descriptors.[153] In the first method, the properties of each compound arise from the contributions of all functional groups in the structure. Thus, solute descriptors can be estimated as the sum of descriptor values of all functional groups. Tetramethylammonium (NMe_4^+) was used as the basic structure and its reported descriptor values (**Table 3-3**) were modified based on the contributions of all additional functional groups in each solute structure. Detailed calculations are in **Table 3-4**. The modified group contribution approach was validated by yielding comparable descriptors to the reported ones for NEt_4^+, NPr_4^+, and NBu_4^+ (data not shown). Descriptors estimated for $CETM^+$, $BETM^+$, PTM^+, BTM^+, and $VBTM^+$ using this approach can also reasonably reflect solute properties (**Table 3-3**).

Table 3-4: Calculation of descriptors S and A for the investigated quaternary ammoniums based on the reported descriptors for tetramethylammonium. J^+ values were initially assumed to be equal to the value of tetramethylammonium and then slightly adjusted to improve precision of the predictive model.

Compound	Functional group	S	A
PTM^+	Phenyl[a]	0.59	0
	Tetramethylammonium[b]	1.48	0.82
	total	**2.07**	**0.82**
BTM^+	Benzene[a]	0.59	0
	Tetraethylammonium[b]	1.81	0.57
	Ethyl[a]	0	0
	total	**2.4**	**0.57**
$VBTM^+$	Benzene	0.59	0
	Vinyl[a]	0.1	0.05
	Tetramethylammonium	1.48	0.82
	total	**2.17**	**0.87**
$CETM^+$	(2-Chloroethyl)[a]	0.35	0.03
	Tetramethylammonium	1.48	0.82
	total	**1.83**	**0.85**
	2-Bromoethyl[a]	0.38	0
$BETM^+$	Tetramethylammonium	1.48	0.82
	total	**1.86**	**0.82**

[a] ref [179]; [b] ref [163]

In the pp-LFERs approach, the descriptors of a solute can be estimated based on the reported regression coefficients (c, e, s, a, b, v, and j^+) for multiple solvent-water systems and the respective experimental lnP values of the solute in these systems. First, the experimental lnP values were estimated based on the ion transfer energy ($\Delta G^{o}_{tr} = -RT \ln P$) from SPARC (http://www.archemcalc.com/sparc.html), an online chemical properties calculator.[180, 181] Second, the lnP values of the solute in the solvent-water systems were calculated based on the known regression coefficients for each solvent using eq 3.2 and hypothetical descriptor values. Then, mathematical procedures such as Solver® in Microsoft Excel were used to calculate the unknown descriptors by minimizing differences (i.e. mean weighted square errors MWSE) between the experimental lnP values and the calculated ones.[157] Note that it is necessary to have solvents with different physical chemical properties, and the number of solvent-water systems should be greater than the number of unknown descriptors. The pp-LFERs approach was tested for all the solutes with unknown descriptors. However, we were not able to estimate the descriptors properly using this method, mainly due to the inaccuracy in the estimated lnP values (data not shown). For example, we expected positive S and A values for the quaternary ammoniums due to their high polarity and H-bond acidity, but the estimated S and A values were small positive or even negative values. The descriptors for DMA^+ and $imidazole^+$ were estimated based on the descriptors for the corresponding neutral solutes. Abraham and Acree[153] have developed a set of equations to predict descriptors for protonated amines based on the descriptors for neutral amines.

3.3.9 Estimating Henry's Law Constants ($LogK_{GW}$) for Cationic Solutes

Henry's law constants are required for the gas phase conversion analysis. Two approaches were examined for accuracy in estimating $LOGK_{GW}$ values. The first approach is based on $\Delta G_{G\text{-}W} = -RT\ln K_{GW}$, where $\Delta G_{G\text{-}W}$ were calculated in SPARC or Gaussian in WebMO (http://www.webmo.net/demo/index.html), a web-based interface for computational chemistry programs. In comparison with the reported Henry's law constants, neither programs estimated $\Delta G_{G\text{-}W}$ accurately (data now shown). The second approach is the modified bond contribution method[182] where $\log K_{GW}$ can be estimated from $\log K_{GW}$ of a structurally-related compound by adding or subtracting contributions of all additional bond values in the molecular structure (see one example in **Table 3-5**). Since, for Aniline$^+$, DMA$^+$, and aromatic quaternary ammoniums a less structurally similar compound was available as the base compound the obtained $\log K_{GW}$ values were then slightly adjusted ($<\pm 0.55$ log units which is similar to the reported error for experimentally determined lnP[153]) to improve precision of the predictive model (root mean square error values or RMSE) after the gas-phase conversion.

Table 3-5: Calculation of $\log K_{GW}$ for tetrapropylammonium based on the $\log K_{GW}$ of tetramethyl-ammonium NMe_4^+ (-9.76).

Additional Bonds	No	Value
Single-bonded aliphatic carbon (C-C)	8	0.1163
C-H	16	-0.1197
$-\log K_{GW}$ of NPr_4^+ = $-\log K_{GW}$ of NMe_4^+ + $\sum$(No × Value) = 8.77		

3.4 Results and Discussion

3.4.1 pH Effect on Sorbed Concentration on Resins

The pH effect on sorption of neutral aromatic and quaternary ammonium compounds by MN500 and Amberlite 200 was studied to examine the relative contribution of electrostatic versus non-electrostatic interactions to sorbed concentration. PTM$^+$ and NB were chosen as the representative cation and neutral solute. **Figure 3-2** shows that the sorbed concentration of PTM$^+$ on both resins is pH-independent between pH 4 and 10. The lower Qe at pH < 4 is mainly due to competition of H^+ for the exchange sites. The quaternary ammonium is permanently charged and removed mainly by the ion exchange mechanism,[105] therefore, electrostatic interactions are pH independent. Sorption of NB on the ion exchange resins is also pH independent but is significantly less than that of PTM^+. This is because neutral NB does not have any electrostatic interactions with the ion exchange resins. The pH effect was then investigated for aniline ($pK_a = 4.67$) and imidazole ($pK_a = 6.9$) as compounds that undergo proton transfer reaction under changing pH conditions. Aniline and imidazole are protonated at $pH<pK_a$, and neutral at $pH>pK_a$. **Figure 3-2** shows that sorption of aniline and imidazole decreased significantly when the fraction of the protonated compounds (i. e. aniline$^+$ and imidazole$^+$) decreased, suggesting that aniline$^+$ and imidazole$^+$ have higher sorbed concentrations than the neutral ones. This is because aniline$^+$ and imidazole$^+$ undergo ion exchange (electrostatic) in addition to hydrophobic (nonelectrostatic) interactions. Also, sorption of both compounds slightly decreased when pH was lower than 3 due to competition with H^+ for the sorption sites.

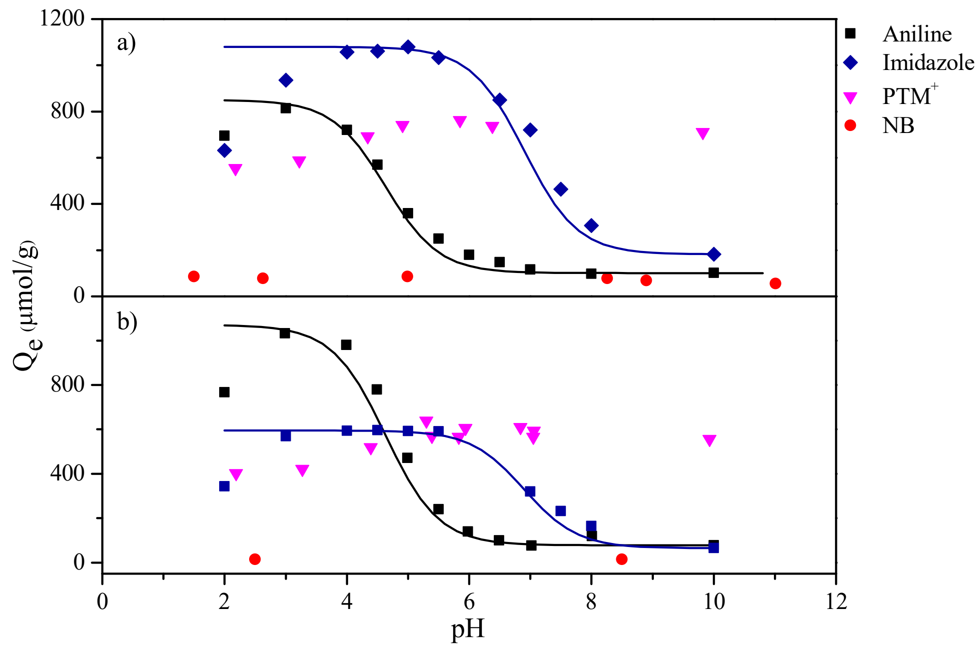

Figure 3-2: Effect of pH on the sorption of aniline, imidazole, phenyltrimethylammonium (PTM^+), and nitrobenzene (NB), on a) MN500 and b) Amberlite200. The solid lines show the estimated sorbed concentrations of aniline and imidazole over the tested pH range based on eq 3-23 (details in the **section 3.4.6**).

3.4.2 Original Aqueous Sorption Isotherms

The sorption isotherms of 20 organic compounds on MN500 and Amberlite200 are shown in **Figure 3-3**. The sorption isotherms were fitted well by the Polanyi Dubinin-Astakhov (D-A) model except for low concentrations where the sorbed concentrations of the cationic compounds were slightly overestimated. The D-A model fitting parameters and their MWSE are listed in **Table 3-6**. In general, MN500 exhibits higher sorbed concentrations than Amberlite 200, because MN500 has a high proportion of micropores (more than 48% of pore volume) which enhanced sorption energy due to superposition of force fields of the opposite walls.[183] More discussion on the effects of different resin structures is in SI (Text S9). We eliminated Amberlite IRC-76 for further study due to its poor removal of neutral solutes and low sorbed concentration of cations (**Figure 3-4**).

Sorbed concentration (**Figure 3-3**) and selectivity (**Figure 3-5**) of all solutes on MN500 and Amberlite200 follow the order of aromatic cations > halogenated aliphatic cations > non-halogenated aliphatic cations > neutral aromatic solutes. No significant difference was observed for the sorption of tetraalkylammonium cations on MN500 and on Amberlite200. The higher affinity of the cationic compounds than the neutral compounds indicates that the primary sorption process is ion exchange. As discussed more extensively in the "pp-LFERs" section, interactions between the nonpolar moieties of the ions and the resins are important in affecting resin selectivity. The highest selectivity of the aromatic cations can be attributed to the strong non-electrostatic interactions (i.e. π-π interactions) between the aromatic rings of the resin matrix and the aromatic cations. $BETM^+$ and $CETM^+$ exhibited higher sorption affinity than the non-halogenated aliphatic cations because the partial negative charges of -Br and -Cl can increase dipole-dipole and dipole-induced dipole interactions between the resin and the compounds. While neutral aromatic compounds have the ability to form π-π interactions, the lack of electrostatic interactions resulted in their much lower removal by the CXRs.

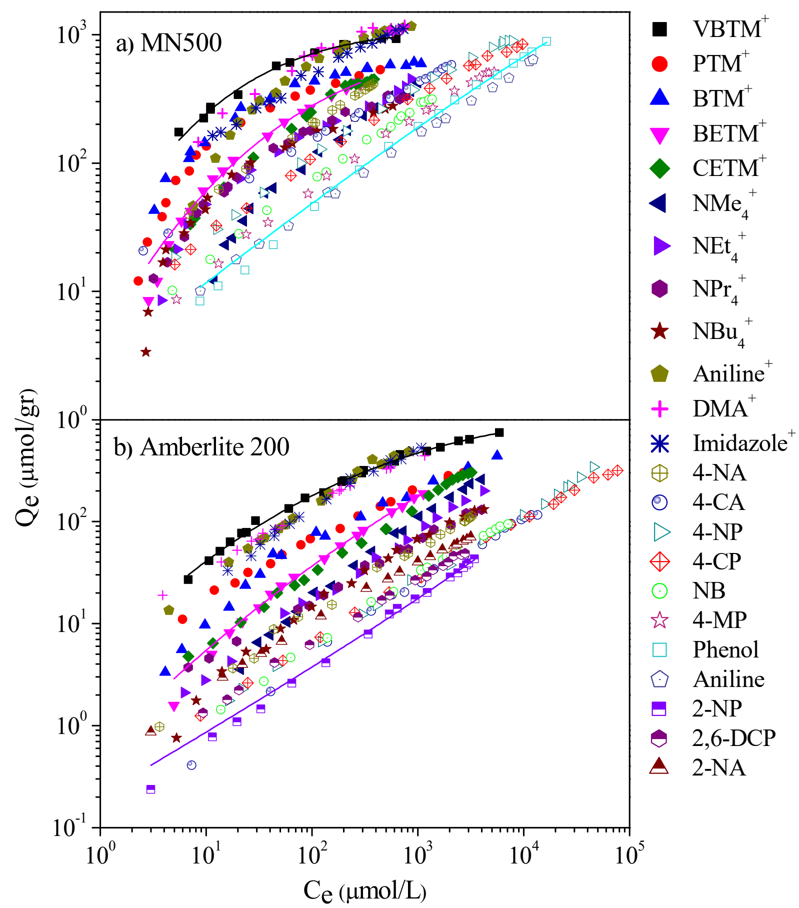

Figure 3-3: Original aqueous sorption isotherms of 12 cations and 8 neutral aromatic solutes on a) MN500 and b) Amberlite 200. Solid lines are examples of the model fittings by the Dubinin-Astakhov model.

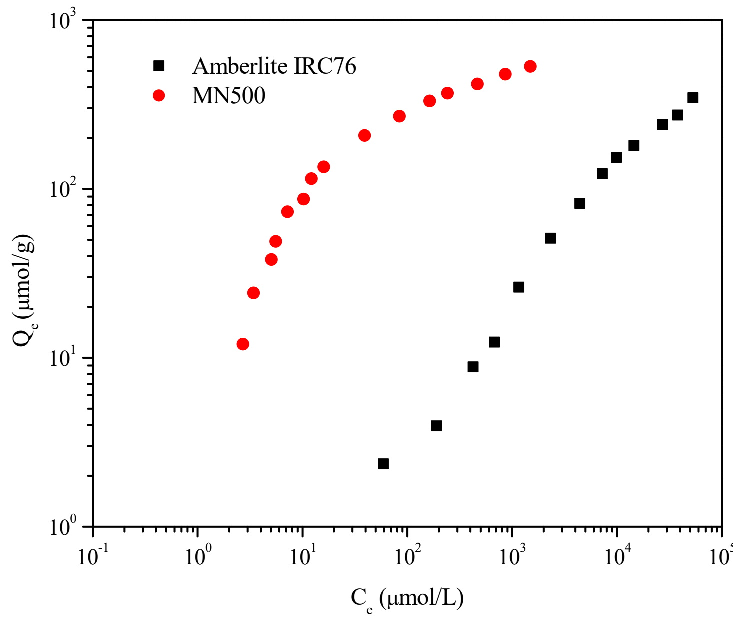

Figure 3-4: Original aqueous sorption isotherms of PTM^+ on MN500 and Amberlite IRC76.

Despite the importance of non-electrostatic interactions in ion selectivity, there is no direct correlation between selectivity and non-electrostatic interactions because solvent-solute interactions complicate the comparison. When using hydration energy (**Table 3-3**) to quantify solvent-solute interactions for all the cations, we found a positive correlation between selectivity and hydration energy ($R^2 = 0.575$ for all cations and 0.698 for aromatic and halogenated-aliphatic cations for MN500, and $R^2 = 0.452$ for all cations and 0.613 for aromatic and halogenated-aliphatic cations for Amberlite 200, **Figure 3-6**). Previous work has also reported the importance of hydration energy in determining selectivity for inorganic ions[184, 185] and organic anions.[94]

The sorbed concentration of the neutral compounds follows the order of 4-NA > 4-CA > 4-NP ≈ 4-CP > NB ≈ 4-MP > phenol ≈ aniline on MN500 and follows the order of 4-NA>2-NA>4-NP≈2,6-DCP≈4-CA≈4-CP>2-NP on Amberlite 200. This trend can be partly explained by the electronic effects of the solute functional groups. For example, the aromatic solutes with nitro groups were removed more than the ones with –Cl groups because $-NO_2$ is more strongly π e^--withdrawing.[103] Again, a more quantitative comparison among the neutral solutes is not possible due to the involvement of solute-solvent interactions.

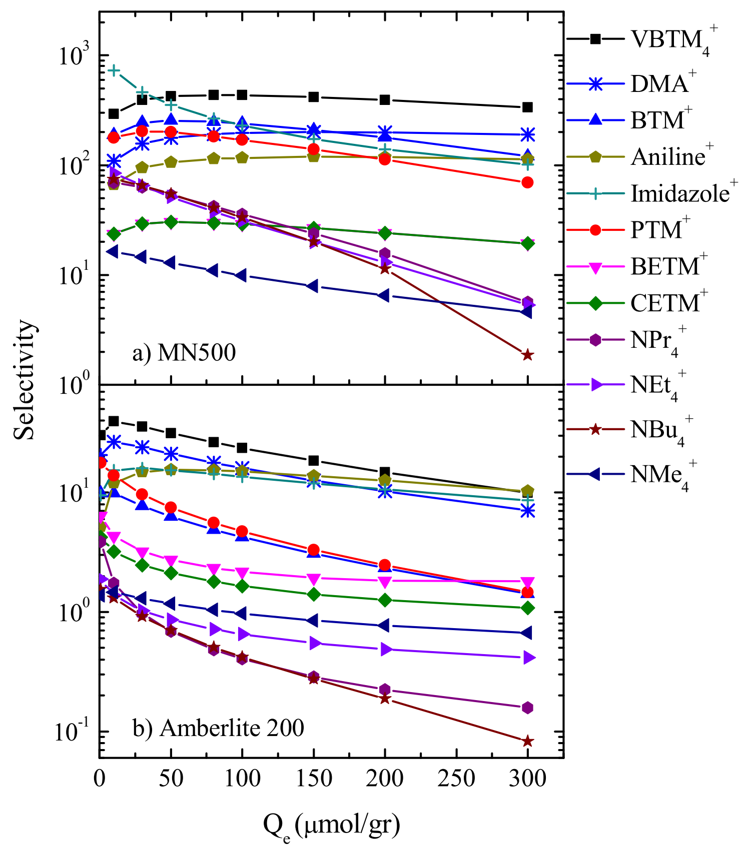

Figure 3-5: Selectivity at different sorbed concentrations for sorption of all ions onto the two resins.

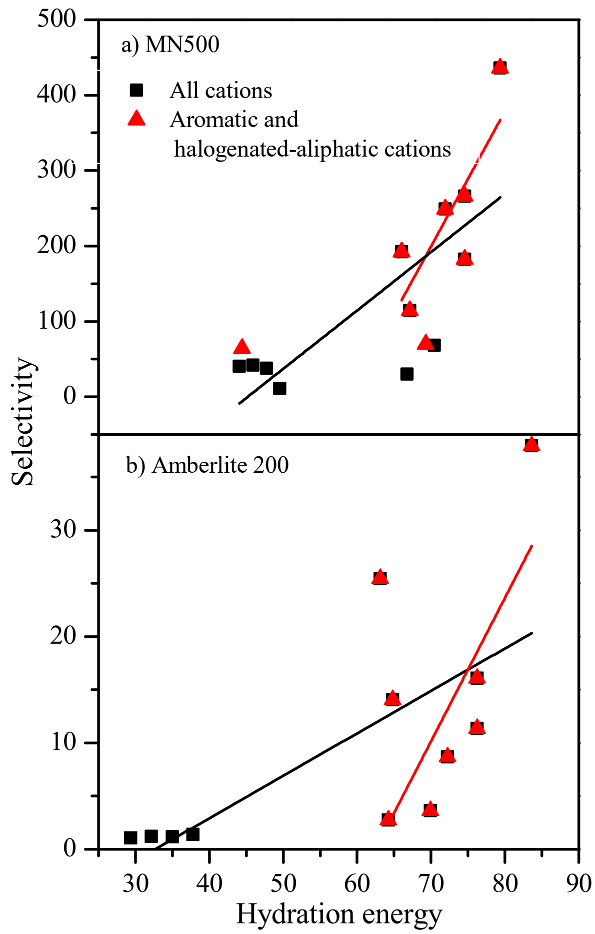

Figure 3-6: Correlation between selectivity and hydration energy for sorption of the investigated cations on a) MN500, $R^2 = 0.575$ for all cations and 0.698 for aromatic and halogenated-aliphatic cations, and b) Amberlite 200, $R^2 = 0.452$ for all cations and 0.613 for aromatic and halogenated-aliphatic cations.

Table 3-6: Original D-A model fitting parameters for the sorption isotherms measured for a) Amberlite 200 and b) MN500.

	Compound	C^{sat}_w	pK_a	Q_0 (μmol/g)	E (KJ/mol)	b	R^2	N	MWSE
	2-NA	7964	-0.26	97±2	11.2±0.1	1.21±0.04	0.999	17	0.004
	4-NA	8180	1	198±14	9.3±0.3	1.00±0.06	0.999	17	0.02
	4-CA	38009	3.86	220±65	9.1±1.0	1.04±0.27	0.991	17	0.02
	2-NP	14377	7.22	137±25	7.5±0.7	0.90±0.09	0.999	17	0.02
	4-NP	115025	7.15	961±81	6.6±0.3	0.76±0.04	0.999	17	0.05
	4-CP	204574	9.3	471±32	11.0±0.3	1.19±0.09	0.997	17	0.01
	2,6-DCP	10080	6.79	97±12	9.8±0.4	1.10±0.11	0.997	16	0.002
	NB	16982	NA	130±4	10.0±0.1	1.30±0.06	0.999	17	0.004
	$Aniline^+$	1000000[a]	4.67	1088±362	23.9±1.0	3.43±0.80	0.985	17	0.01
a)	DMA^+	1000000[a]	5.15	1050±89	24.2±0.3	2.67±0.15	0.999	17	0.002
	$Imidazole^+$	1000000[a]	6.9	1535±318	22.5±0.8	2.68±0.33	0.998	17	0.002
	$CETM^+$	1000000[a]	–	2570±1398	15.0±2.2	1.63±0.32	0.997	21	0.04
	$BETM^+$	1000000[a]	–	1930±587	16.6±1.2	1.75±0.18	0.999	17	0.04
	PTM^+	1000000[a]	–	938±180	21.2±1.0	1.93±0.21	0.998	16	0.004
	BTM^+	1000000[a]	–	1438±298	19.0±1.1	1.68±0.18	0.995	16	0.28
	$VBTM^+$	1000000[a]	–	1065±58	25.1±0.2	2.70±0.16	0.993	23	0.004
	NMe_4^+	1000000[a]	–	1584±410	15.7±1.0	1.81±0.19	0.999	17	0.004
	NEt_4^+	1000000[a]	–	1578±702	14.6±1.8	1.57±0.26	0.998	16	0.03
	NPr_4^+	1000000[a]	–	686±308	16.9±2.1	1.60±0.32	0.995	17	0.02
	NBu_4^+	1000000[a]	–	406±67	19.2±0.7	2.13±0.20	0.998	19	0.02
	Aniline	318909	4.67	1279±70	12.1±0.3	0.94±0.04	0.999	16	0.01
	$Aniline^+$	1000000[a]	4.67	1415±41	26.2±0.1	4.05±0.19	0.997	18	0.01
	4-NA	8180	1	835±42	13.1±0.2	1.14±0.05	0.999	15	0.0003
	4-CA	38009	3.86	962±44	15.2±0.2	1.03±0.05	0.999	17	0.01
	DMA^+	1000000[a]	5.15	1313±76	27.7±0.6	4.37±0.60	0.979	17	0.000
	$Imidazole^+$	1000000[a]	6.9	2592±390	24.2±0.74	2.01±0.22	0.997	21	0.000
	Phenol	852088	9.89	1848±124	13.4±0.3	1.13±0.05	0.999	17	0.02
	4-NP	115025	7.15	1092±22	15.4±0.2	1.32±0.04	0.999	17	0.0007
	4-CP	204574	9.3	1021±27	16.7±0.2	1.42±0.06	0.998	17	0.002
b)	4-MP	175714	10.17	869±48	14.6±0.3	1.29±0.07	0.999	18	0.001
	NB	16982	NA	493±32	12.3±0.3	1.11±0.08	0.997	17	0.001
	$CETM^+$	1000000[a]	–	822±52	24.3±0.2	3.59±0.22	0.999	17	0.01
	$BETM^+$	1000000[a]	–	840±83	26.2±0.4	3.03±0.23	0.998	17	0.14
	PTM^+	1000000[a]	–	617±28	29.6±0.2	4.18±0.29	0.991	19	0.20
	BTM^+	1000000[a]	–	627±9	30.3±0.2	4.80±0.2	0.991	19	0.006
	$VBTM^+$	1000000[a]	–	1058±32	30.2±0.2	4.52±0.29	0.996	14	0.003
	NMe_4^+	1000000[a]	–	830±153	21.7±0.7	2.50±0.33	0.994	16	0.02
	NEt_4^+	1000000[a]	–	491±36	27.0±0.3	2.95±0.21	0.991	16	0.007
	NPr_4^+	1000000[a]	–	491±22	27.2±0.2	3.06±0.26	0.995	19	0.02
	NBu_4^+	1000000[a]	–	343±19	28.4±0.2	3.67±0.28	0.995	19	0.006

[a] A hypothetical large value was assumed for the solubility of all cations due to their high solubility in order to fit the sorption isotherms for modeling purposes only.

3.4.3 Sorption Isotherms after Gas-Phase Conversion

The aqueous sorption isotherms were reconstructed after the gas-phase conversion in order to analyze the sorption behavior of solutes after eliminating the effect of solvent-associated interactions. The corresponding solute concentrations in the gas phase (C_{gas}) were calculated by:[166]

$$C_{gas} = C_w \exp\left(\frac{-\Delta G_{G-W,i}}{RT} + \frac{C_{ads}}{RT}\right) \tag{3.22}$$

where C_{ads} is a constant (eq 3.11). The general trend for the sorbed concentrations after the conversion is comparable to that before the conversion: i.e. aromatic cations > halogenated aliphatic cations > aliphatic cations > neutral solutes, but differences among the sorption isotherms after the conversion are more distinct (**Figure 3-7**). Particularly, the differences are much more pronounced between the aliphatic cations and the neutral solutes. Unlike the aqueous phase isotherms where the neutral compounds had comparable sorbed concentrations to those of the aliphatic cations, the aliphatic cations had much higher sorbed concentrations after the phase conversion. We believe this confirms the importance of electrostatic interactions in the sorption by CXRs. Quantitative examination of the dominant solute-sorbent interaction forces now becomes possible as details shown below.

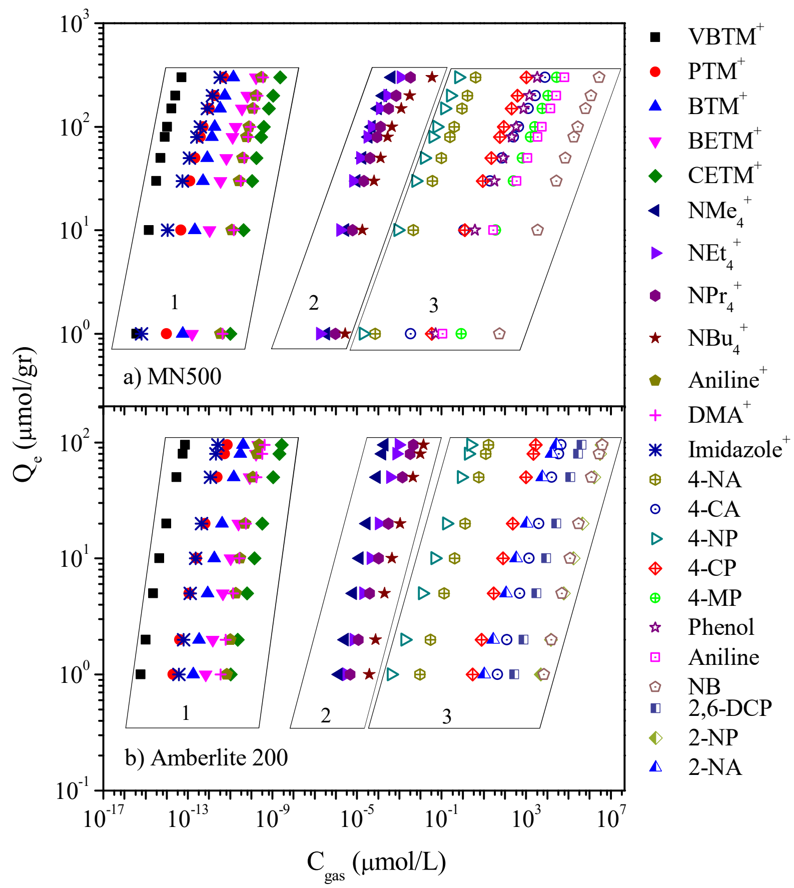

Figure 3-7: The reconstructed sorption isotherms after converting aqueous sorption to sorption from the ideal gas phase on a) MN500 and b) Amberlite 200: 1 – aromatic and halogenated aliphatic cations, 2 – aliphatic cations, and 3 – neutral solutes.

3.4.4 PP-LFERS

Multiple linear correlation between the natural logarithm of selectivity of all cations in sorption by both resins and solute descriptors was conducted at different sorbed concentrations to quantitatively examine the contribution of various interactions to the overall selectivity of the cations. The regression coefficients and the corresponding p-values in **Tables 3-7** and Appendix A A1-2 for MN500 suggest that selectivity was mainly promoted by dipolar/polarizability effects (S), induced dipole (E), H-bond accepting (A), and electrostatic (J^+) interactions. This result indicates that compounds with large S, E, A, or J^+ values will be strongly sorbed by MN500. With increasing Q_e , *e*, *a*, and j^+ values increased and *s* values decreased, indicating that although at lower concentrations dipole related interactions are the dominant force for the sorption of the cations, at higher concentrations H-bond accepting, electrostatic and somewhat induced-dipole interactions are also among the attractive forces. As the results show in **Tables 3-7** and A3-4 for Amberlite 200, selectivity was promoted mostly by induced dipole related interactions, dipolar/polarizability (S), H-bond accepting (A) interactions and electrostatic (J^+) interactions although they are not statistically significant, and the V term had a negligible contribution.

Table 3-7: Regression coefficients *e*, *s*, *a*, *v*, j^+, and c of the multiple linear regressions between selectivity ln($\alpha_{A/Na}$), $\Delta G_{S\text{-}W,i}$ or $\Delta G_{S\text{-}G,i}$ and solute descriptors for MN500 at Q_e=10, 50, and 200 µmol/g and Amberlite 200 (A200) at Q_e=2, 20, and 80 µmol/g.

	resins	Q_e	*c*	*e*	*s*	*a*	*b*	*v*	j^+	R^2
$\ln\alpha_{A/Na}$	MN500	10	-0.9±4.7	0.4±1.4	2.9±0.8	0.1±2.3	_	0.2±0.7	-0.4±1.5	0.819
	MN500	50	-1.7±3.4	0.8±1.0	2.0±0.6	0.9±1.7	_	0.5±0.5	0.3±1.1	0.908
	MN500	200	-3.0±3.3	1.3±1.0	1.1±0.5	2.0±1.6	_	0.5±0.5	1.2±1.1	0.948
	Amberlite200	2	-2.3±3.5	1.3±1.1	0.4±0.6	1.1±1.8	_	0.1±0.5	1.0±1.1	0.904
	Amberlite200	20	-1.9±3.2	1.8±1.0	0.7±0.5	1.0±1.6	_	0.0±0.5	0.5±1.0	0.946
	Amberlite200	80	-2.7±3.9	1.7±1.2	0.7±0.6	1.4±1.9	_	-0.2±0.6	0.6±1.2	0.938
$\Delta G_{S\text{-}W,i}$	MN500	10	-1.8±6.4	1.3±2.5	5.2±2.3	2.0±3.2	9.4±18.0	1.5±2.1	-0.7±2.4	0.502
	MN500	50	-7.1±4.6	1.3±1.8	4.0±1.6	4.8±2.3	10.2±12.8	2.3±1.5	1.7±1.7	0.825
	MN500	200	-11.5±3.4	2.3±1.3	2.8±1.2	6.9±1.7	11.1±9.6	1.9±1.1	3.8±1.3	0.939
	Amberlite200	2	-12.3±5.6	2.1±2.4	3.9±2.5	4.7±3.7	7.7±21.6	1.3±1.8	1.6±2.7	0.774
	Amberlite200	20	-11.6±3.7	2.9±1.5	3.7±1.6	4.7±2.4	-4.9±14.1	0.7±1.2	1.4±1.8	0.933
	Amberlite200	80	-13.1±3.7	2.6±1.5	3.5±1.6	5.7±2.4	-4.1±14.1	0.1 ±1.2	2.0±1.8	0.945
$\Delta G_{S\text{-}G,i}$	MN500	10	-24.6±6.4	19.9±2.3	15.5±2.2	23. 7±3.2	26.8±18.1	-12.2±2.0	34.8±2.4	0.994
	MN500	50	-27.9±5.7	20.6±2.1	14.7±2.0	25.4±2.8	20.9±16.1	-11.5±1.8	36.1±2.1	0.996
	MN500	200	-31.7±5.7	21.8±2.1	13.7±2.0	27.2±2.8	18.6±16.1	-11.9±1.8	37.6±2.1	0.996
	Amberlite200	2	-32.1±6.6	18.1±2.8	15.3±2.9	26.5±4.3	15.4±25.5	-10.7±2.1	31.5±3.2	0.995
	Amberlite200	20	-31.4±5.7	19.0±2.4	15.1±2.4	26.5±3.7	2.8±21.8	-11.3±1.8	31.3±2.8	0.997
	Amberlite200	80	-32.9±5.8	18.6±2.5	14.8±2.5	27.5±3.9	3.5±23.0	-11.9±1.9	31.8±2.9	0.996

Multiple linear correlations were also established between $\Delta G_{S\text{-}W,i}$ or $\Delta G_{S\text{-}G,i}$ and the solute descriptors for all neutral and cationic compounds on the studied resins. Regression coefficients and the corresponding p-values are listed in Tables 3-7 and A5-12. Lower R^2 values were obtained for the correlations at lower concentrations due to the overestimation of the D-A model fitting. For the aqueous sorption (i.e. $\Delta G_{S\text{-}W,i}$) on MN500, we observed similar regression coefficients as shown above where S was statistically significant over the entire range of Q_e, and the dependency of $\Delta G_{S\text{-}W,i}$ on E, A, and J^+ increased with Q_e. Also, descriptor V had a negligibly positive effect on sorption, and descriptor B had some positive effects which apply to the neutral compounds only because H-bond basicity (B) is almost zero for all cations. For aqueous sorption on Amberlite 200, descriptors A, E, S and J^+ had positive contributions, V showed a negligible effect, and B had some negative contribution but to the sorption of neutral compounds only. After the phase conversion (i.e. $\Delta G_{S\text{-}G,i}$), the contribution of solvent-associated interactions to the Gibbs free energy change has been eliminated, consequently the contribution of solute-sorbent interactions to $\Delta G_{S\text{-}G,i}$ can be examined. Unlike the aqueous phase sorption, electrostatic interactions (large j^+) have the most dominant effect on the sorption of the cationic compounds from the gas phase by both resins. There are also significant positive effects of descriptors E, S, and A, confirming the contribution of non-electrostatic interactions to the sorption of the organic compounds on CXRs. Therefore, cations with high E, S, and A values are more likely to be sorbed by the CXRs from the gas phase. In addition, negative contributions of V emerged, although there is no cavity formation in the gas phase. A similar effect of V was observed by Pan and Zhang[166] in sorption of neutral organic compounds on neutral resins after the gas phase conversion. As already reported,[166, 186] it is difficult to separate various interactions and a portion of London dispersive forces might be captured by the V term. Indeed, statistical calculations indicate that there is some correlation among the descriptors (pearson coefficient < 0.66, data not shown). Previous works also reported significant correlations among the descriptors.[94, 166, 186] Finally, descriptor B showed a more positive effect on the removal of the neutral compounds by the resins after the phase conversion.

3.4.5 Development and validation of Predictive Models

Based on the above pp-LFERs at different Q_e values, the regression coefficients *c*, *e*, *s*, *a*, *b*, *v*, and j^+ can be expressed as a function of Q_e i.e. $f^e(Q_e)$, $f^s(Q_e)$, etc. (**Figures A1-2** and Appendix A, **Text A1**). The predictive model based on eq 3-9 was then used to estimate C_e at any given Q_e for a given solute. **Figures 3-8** and **A3-4** compare the estimated C_e with the experimental ones. The results indicate that the predictive models are able to estimate the sorbed concentration well for both resins. To validate the models, they were reconstructed by randomly excluding one neutral compound, one or two quaternary ammonium cations, and one aromatic cation from the training-set. The new predictive models were examined by using these compounds (4-NA, PTM^+, and imidazole$^+$ for MN500 and 2,6-DCP, BTM^+, $ECTM^+$ and Aniline$^+$ for Amberlite 200) as the test-set compounds. Note that the test-set should have descriptors in the range of the descriptors of the training-set compounds. Comparison of the measured C_e values versus the predicted ones (**Figure 3-8**) indicates the accuracy of the models. Additional cross validation was conducted by selecting different solutes as the test-set (**Figures A5-6**), the obtained similar precisions (i.e. RMSE values in the range of 0.91-1.1 for MN500 and 0.76-0.85 for Amberlite 200) demonstrate the robustness of the developed models.

Similar precisions were obtained for the predictive models developed based on the gas-phase converted isotherms (**Tables A13-16** and **Figure A-7**). Our previous work also developed a predictive model for adsorption of neutral solutes by non-ionic resins after the gas-phase conversion,[166] this work shows that it is more convenient to develop predictive models based on aqueous sorption isotherms without sacrificing accuracy.

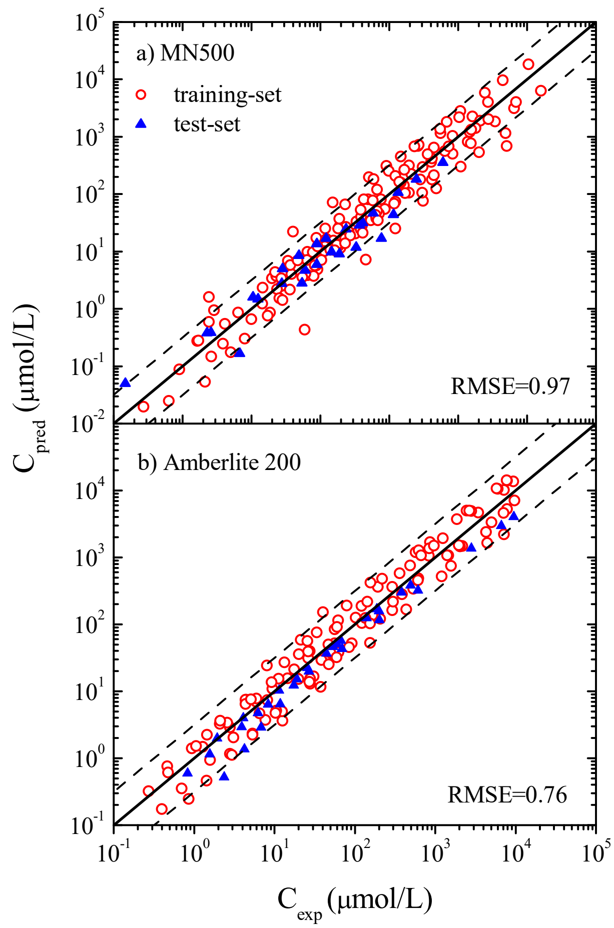

Figure 3-8: Aqueous equilibrium concentrations calculated based on the predictive model (eq 3-9) versus the experimental values for a) a training-set of 17 solutes with 153 data points and 3 test-set solutes (4-NA, PTM^+, and $imidazole^+$) with 27 data points for MN500; b) a training-set of 16 solutes with 128 data points and 4 test-set solutes (2,6-DCP, BTM^+, $CETM^+$ and $Aniline^+$) with 32 data points for Amberlite 200. The solid lines show a perfect prediction, where the predicted values for C_e exactly equal the experimental values; the dashed lines are 0.5 log units above or below the solid lines.

3.4.6 Predictive Model for pH Effects

The effect of pH on the sorbed concentration of compounds that can undergo proton transfer reaction under changes of pH can be estimated by using the developed predictive models. As ionic and nonionic forms of a solute have different sorption behavior, it was assumed that the overall sorbed concentration at any pH (q^T) is equal to the sum of the sorbed concentrations of all species:

$$q^T = \sum_{i=N} \alpha_i q^i \qquad (i = 1, \ldots N) \tag{3-23}$$

where q^i and α_i are the sorbed concentration and mole fraction of species i, respectively. q^i should be constant and can be estimated based on the constructed predictive model (eq 3-9) by using the respective solute descriptors for each species (e.g. neutral aniline and aniline$^+$). As shown in **Figure 3-2**, the sorbed concentrations of aniline and imidazole estimated using eq 3-23 over the tested pH range compare well with the experimental data, except at pH less than 3 when the sorbed concentration is lower than the predicted one due to competition with H^+. There is a slight difference between the measured and predicted sorbed concentrations at some pH points due to slight shifting of pH during the sorption experiments, although pH of the samples was adjusted to the desired one every 2-10 hours.

3.5 Conclusions and Implications

Overall, our results show that CXRs can be effective in the removal of COCs from contaminated water. Understanding the sorption mechanism is fundamental for selecting and synthesizing appropriate resin for a given contaminant. The sorption of organic solutes by CXRs is mainly affected by resin properties like moisture content, resin matrix, and surface area as well as solute structure. The selective removal of ionic organic contaminants by CXRs through ion exchange processes is promoted by non-electrostatic interactions between the non-polar moieties of the solutes and the resin matrix. pp-LFERs enable us to identify the predominant molecular interactions between solute and resin and to develop predictive models for estimating the sorbed concentration of a target contaminant on a given resin at any environmentally relevant pH. Therefore, predictive models for different resins can be used for selecting an efficient sorbent in the treatment for a given contaminant without conducting trial experiments. It should be mentioned that the applicability of a predictive model is limited to one resin and can not necessarily be extended to other resins. Inclusion of a large number of compounds with diverse structures in the training set will expand the ability of the predictive models to a large number of solutes. The gas-phase conversion is a useful approach for eliminating solute-solvent effects which obscure solute-sorbent interactions in the aqueous phase.

CHAPTER 4

DEVELOPMENT OF PALLADIUM-RESIN COMPOSITES FOR CATALYTIC HYDRODECHLORINATION (HDC) OF 4-CHLOROPHENOL

Abstract

Polymeric resins have been widely used for the removal of halogenated compounds, however, the sustainability of resin adsorption is compromised by frequent resin regeneration and further treatment/disposal of concentrated brine. Palladium (Pd)-based catalytic hydrogenation is promising to treat various classes of contaminants, including halogenated compounds, and the development of Pd-polymeric resin composites is advantageous because the composites can convert halogenated compounds to less toxic chemicals *in situ* and mitigate challenges associated with resin regeneration. In this work, three neutral resins (MN200, MN100, and XAD4) and two anion exchange resins (IRA910 and IRA96) were used as Pd supports to evaluate 4-chlorophenol (4-CP) hydrodechlorination reactivity. Similar 4-CP adsorption and reduction kinetics were observed, i.e., adsorption and reduction were both faster at acidic pHs for the neutral resins but faster at basic pHs for the anionic resins. With increasing initial 4-CP concentration from less than 1.5 mM to higher, 4-CP adsorption during reaction onto 1 wt% catalysts increased from non-detectable to detectable, indicating that the rate determining step changed from adsorption at low concentrations to surface reaction at high concentrations. The developed Langmuir−Hinshelwood kinetic models based on the two rate determining steps also suggested this mechanism. When adsorption was constant, the reactivity of the catalysts increased with increasing solution pH. This is because higher pH mitigates the adverse impacts of dehalogenation products (i.e., H^+ and

Cl^-) on catalytic reactions. The inhibition effect of Cl^- was more pronounced on IRA910 than on MN200. IRA910 with anion exchange functional groups facilitates Cl^- adsorption and promotes the production of $PdCl_3^-$ and $PdCl_4^{2-}$ species that are inactive for catalytic reduction. The accumulation of phenol, the major product in 4-CP reduction, resulted in catalytic activity loss over eight cycles when 4-CP was repeatedly spiked into the same reactor; catalytic activity was largely restored after resin regeneration.

4.1 Introduction

Chlorophenols (CPs) are among priority contaminants in water and wastewater effluents due to their high toxicity on human health (e.g., carcinogenic), adverse environmental impacts (e.g., inactivation of functional bacteria), and persistence in the environment.[3, 4] Conventional water treatment technologies such as ion exchange and adsorption by activated carbon or clays[19, 91, 187] are used for the removal of CPs, however, these processes produce large amounts of concentrated brine or secondary waste through regeneration and recycling of absorbents.[35, 98, 127, 188] Pd-based catalytic hydrogenation is beneficial for CP degradation because hydrogen is used as a clean reductant, CPs are converted to less toxic chemicals, secondary waste or byproduct generation is reduced, and catalysts can be reused over multiple cycles in principle.[189]

Reduction of CPs has been mostly demonstrated by Pd nanoparticles loaded on supports, such as alumina, and activated carbon.[53, 129, 130, 190] However, the use of polymeric resins as supports was largely underexplored. On the other hand, polymeric resins have been extensively used to remove organic and ionic pollutants such as halogenated phenols from industrial wastewater effluents.[30, 31] Resins with strong affinity to target contaminants may outperform conventional supports, because catalytic reduction is a surface mediated reaction and the overall reactivity could be limited by contaminant adsorption on catalyst.[31, 59] Pd enables the detoxification of CPs adsorbed on the resins and promotes the likelihood of *in situ* resin regeneration. Several pioneer studies demonstrated the advantages of using resin supported Pd for catalytic hydrogenation of anions, but none examined the removal of halogenated compounds. In these studies, however, the adsorbed amount of the target contaminant by the resins during the catalytic reactions was not tested. Therefore, it is difficult to attribute the decrease in soluble contaminant concentrations to either catalytic reduction or adsorption. In a few other studies, a combination of adsorption and catalytic reduction has been investigated to treat the secondary waste streams of used resins.

Therefore, it is important to explore the possibility of simultaneous removal of contaminants and regeneration of the Pd-loaded resin. One solution is to design Pd loaded resin catalysts with different adsorption affinity for the parent contaminant and the reduction products, i.e., to convert a target contaminant with high adsorption affinity to reduction product(s) with low adsorption affinity. The high adsorption affinity of the target contaminant enhances contaminant removal (i.e., adsorption and then catalytic reduction), and the reduction products with low adsorption affinity to the catalyst support can be easily released to the aqueous phase to minimize the need for resin regeneration.

The main goal of this work was to develop novel Pd-based catalysts supported on polymeric resins, and to evaluate their catalytic activity for CP reduction and the possibility of *in situ* regeneration of the resins. Resins with different structures and functional groups were selected to identify the key physical and chemical properties of the resins for impacting the catalytic activity. The catalysts were characterized by transmission electron microscopy (TEM) to determine Pd nanoparticle size distribution, energy dispersive X-ray spectroscopy (EDX) to analyze the surface composition of the catalysts, and X-ray powder diffraction (XRD) to evaluate the crystallinity of the nanoparticles. Ion exchange capacity and Brunauer-Emmett-Teller (BET) surface area of the resins were measured before and after Pd loading. 4-Chlorophenol (4-CP) was selected as the target contaminant for removal. Effects of pH and Cl^- and 4-CP concentrations on the reactivity of the catalysts were examined to investigate the poisoning effect of Cl^- and to identify the rate determining step(s) for kinetic modeling. Stability Longevity and the possibility of in situ regeneration of the catalysts over multiple cycles of 4-CP removal was also investigated, under extreme conditions where a high concentration of 4-CP (1 mmol L-1) was repeatedly spiked into the same reactor.

4.2 Materials and Methods

4.2.1 Materials and Chemicals

Three nonionic polymeric resins, cross-linked Amberlite XAD-4 and hyper-cross-linked MN200 and MN100, were provided by Rohm and Hass (U.S.) and Purolite® (U.S.), respectively. MN200 and XAD-4 have similar polystyrene structures but MN200 has a higher degree of cross-linkage which results in a larger surface area and additional micropores. The difference between MN200 and MN100 is that MN200 does not have any functional groups while MN100 has a small fraction of tertiary amine functional groups, with an ion exchange capacity of 0.1-0.3 meq/g (reported by the manufacture). Two polystyrene-based anion exchange resins (AXRs), Amberlite IRA910 and IRA96, were obtained from Dow® (U.S.). IRA910 is strongly basic with dimethyl-ethanolammonium functional groups. IRA96 is weakly basic with tertiary amine functional groups. Analytical grade 4-CP, NaPdCl4, and NaBH4 were purchased from Fisher Scientific and Sigma-Aldrich, and used without further purification. The 4-CP solution was prepared with ultrapure deionized water. Ultra high purity hydrogen gas (H_2-99.999%) was supplied by Air Gas.

4.2.2 Catalyst Preparation

Resin beads were soaked in a $NaPdCl_4$ solution, mixed gently overnight (300 rpm for at least 12 h), and collected after filtration. $NaPdCl_4$ was adsorbed onto the resin surface, and a nominal loading of 1% Pd (by weight) was achieved. The actual Pd loading was determined by inductively coupled plasma-optical emission spectroscopy (ICP-OES). Next, the $NaPdCl_4$ adsorbed resins were re-suspended in ultrapure water, and a $NaBH_4$ solution (pH 12) was added dropwise under violent stirring (600 rpm). The molar ratio of $NaBH_4$ to $NaPdCl_4$ was 20, and it is in excess to the stoichiometric ratio to convert all Pd precursor into Pd^0. The reaction lasted for 2 h, and resins were collected by filtration and rinsed thoroughly with ultrapure water to remove free Pd particles from the resins. In order to find the optimum cleaning procedure for the catalysts, the 1% Pd/resins were washed with ultrapure water for three times, and some resin beads were harvested for catalytic activity tests after each wash. The results of the reduction experiments at pH 3 and 11 indicated that the reactivity of Pd/MN200 and Pd/IRA910 catalysts decreased after two-time washing in comparison with one-time washing. This is due to the removal of some free or loosely attached Pd^0 particles after washing. Further washing did not affect reactivity, therefore, resins washed twice were used for all reduction experiments.

4.2.3 Experimental Setup

The semi-batch reduction experiments were carried out in 100 mL three-neck round bottom flasks at ambient temperature (22±1°C), with a continuous flow of hydrogen gas (50 mL min-1) and a mixing rate of 500 rpm (**Figure 4-2**). The hydrogen supply and mixing have been optimized to deliver sufficient reductant and minimize mass transfer limitations. One flask port was used to supply hydrogen, one for collecting samples, and one for venting the off-gas. Silicon rubber stoppers were used to seal the reactors to prevent hydrogen leakage into the atmosphere. First, 60 mL distilled water was added to the flask, then pH of the solution was adjusted to the desired value. 1 mol L-1 of HCl solution, 1 mol L-1 of acetic acid buffer, 0.1 mol L-1 of phosphate buffer, or 1 mol L-1 of NaOH solution was used to adjust solution pH to 3, 5, 7, and 11, respectively. Next, an appropriate amount of the catalysts was added to the solution (i.e., to achieve a Pd loading of 2.5 mg L-1), and the catalyst was pre-sparged with hydrogen gas for 30 min to restore the catalyst activity. Pd-based catalysts may be oxidized in air under ambient conditions, sparging hydrogen gas was shown to sufficiently restore the catalytic activity.[33] 4-CP solution was then amended to initiate reduction. Supernatants (0.5 ml) were collected at regular time intervals during the 150 minute reaction. Desorption experiments were also carried out to determine the amount of 4-CP sorbed by the catalysts during reaction. For the desorption experiments, the catalysts collected at different reaction times were filtered and transferred to amber glass bottles with Teflon-lined screw caps. Methanol (20 mL) was added for neutral resins, and a mixture containing methanol, water, and NaCl (20 mL, methanol/water=1/1 by volume, 8% NaCl by weight) was used for ionic resins. The amber bottles were shaken under 175 rpm for

48 hours, and 0.5 ml supernatants were taken for the analysis of contaminant and product concentrations. The catalysts were also reused to study their longevity. In these cyclic experiments, 1 mmol L-1 of 4-CP was repeatedly spiked to the reaction solution every three hours for eight reduction cycles (preliminary experiments showed that 4-CP was completed removed within three hours). Batch experiments for 4-CP adsorption onto the catalysts were carried out in a similar way except that hydrogen gas was not present.

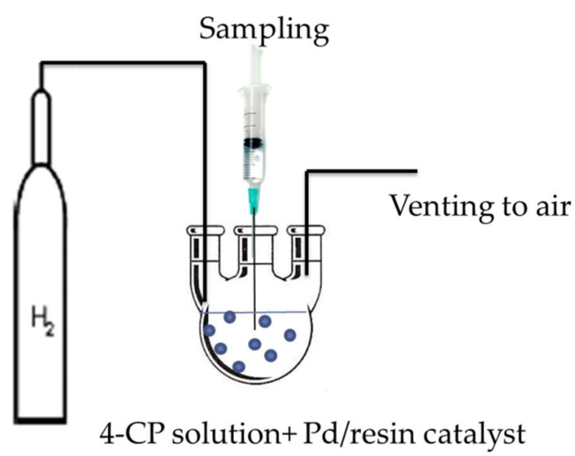

Figure 4-1: Semi batch reactor for hydrodechlorination of 4-CP.

4.2.4 Analytical Method

4-CP and phenol were analyzed using Agilent Technologies 1200 Infinity Series high-performance liquid chromatography (HPLC) with a Zorbax XDB-C18 column. A mobile phase composed of 70% methanol and 30% diluted phosphoric acid at a pH of 3.0 and flow rate of 1 mL min^{-1} was used. The DAD detector was set to 273 nm for phenol and 282 nm for 4-CP.

4.2.5 Characterization

TEM analysis was carried out with a JEOL JEM-1400 coupled with an energy dispersive X-ray spectrometer to determine Pd nanoparticle size distribution and to perform elemental analysis. To prepare samples, the resin beads were crushed finely and dispersed in methanol, and then deposited on a carbon/Cu grid. The samples were then dried under room temperature. XRD was used to characterize the crystallinity of the catalysts. A Bruker Kappa APEX II DUO single crystal X-ray diffractometer was used for collecting XRD data. The BET surface area of the resins was measured using a nitrogen gas adsorption apparatus. Pd loading of the catalysts was measured using ICP-OES after digestion in concentrated nitric acid and hydrochloric acid (3050B EPA method).

4.2.6 Mass Transfer limitations

Both extra- and intra-particle mass transfer rates were evaluated to determine whether the measured catalytic activity is limited by mass transfer. The extra-particle liquid-solid mass transfer rate was evaluated by calculating the overall liquid-solid mass transfer rate coefficient, k_c, based on the slip velocity approach of Hariott.[191] The transfer rate for single spheres is given by the semitheoritical equation:

$$N_{Sh} = \frac{k_c D_p}{D_v} = 2 + 0.6\left(\frac{D_p v \rho}{\mu}\right)^{0.5}\left(\frac{\mu}{\rho D_v}\right)^{0.33} \tag{4.1}$$

where N_{Sh} is the Sherwood number, D_p is the particle diameter, D_v is the diffusivity coefficient of the compound in water as estimated by the Hayduk and Laudie method, ν is the fluid mean velocity, ρ is the liquid density, and μ is the liquid dynamic viscosity.

The mass transfer rate constant was then calculated by multiplying the mass transfer coefficient (k_c) by the geometric surface area of the catalyst per volume of the solution, a:

$$a = \frac{total\ \ surface\ \ area}{total\ \ volume} = \frac{SA_p \times M}{\rho_p \times V_p} \times \frac{1}{V_R} \tag{4.2}$$

where SA_p and V_p are the geometric surface area and volume of one particle, M is the mass of the catalyst in the reactor, ρ_p is the catalyst particle density, and V_R is the reactor volume. In order to evaluate intraparticle liquid-solid mass transfer limitation, the Weisz and Prater criterion,[192] which is the ratio of the reaction rate to the diffusion rate, was used:

$$\frac{k_{obs} D_p^2}{D_e} \tag{4.3}$$

where k_{obs} is the observed reaction rate constant and D_e is the effective diffusivity which was approximately calculated as 0.02 $D_{v.}$[193] When the Weisz and Prater criterion is less than 1, the intraparticle mass transfer resistance is negligible.

4.3 Data Analysis

4.3.1 Reduction Kinetics

The removal of 4-CP by all the catalysts follows pseudo-first-order kinetics:

$$\frac{dC}{dt} = -k_{obs} C \tag{4.4}$$

where C is 4-CP concentration (μmol L^{-1}) in solution phase and k_{obs} (min^{-1}) is the observed pseudo-first order reaction rate constant. Rate constants were obtained from the linear regression of the natural log of solution phase concentrations versus time.

4.3.2 Turnover Frequency (TOF_0)

The initial turnover frequency values (TOF_0, min^{-1}), the number of molecules reduced per site per minute, were determined by dividing the product of the observed rate constant (k_{obs}, min^{-1}) and the initial 4-CP concentration (C_0, mol L^{-1}) by the concentration of surface Pd ($C_{surface\ Pd}$, mol L^{-1}), as following:[194]

$$TOF_0 = \frac{k_{obs}C_0}{C_{surface-Pd}} = \frac{k_{obs}C_0 M}{C_{Pd}D} \tag{4.5}$$

where $C_{surface-Pd}$ is the product of Pd loading (C_{Pd}, g L^{-1}) and dispersion divided by the Pd atomic weight (M, 106.4 g mol^{-1}). Preliminary TEM analyses suggested that Pd nanoparticles were near-spherical, and hence the nanoparticle shape was approximated by cuboctahedron.[67] The dispersion of cuboctahedrons is calculated by:[67]

$$D = \frac{30v^2 + 6}{10v^3 + 15v^2 + 11v + 3} \tag{4.6}$$

where *v* is the average order of cuboctahedral nanoparticles and calculated by:

$$v = \frac{d}{2d_{meatal-metal}} - \frac{1}{2} \tag{4.7}$$

where d is the nanoparticle diameter obtained from TEM analysis, and $d_{metal-metal}$ is the distance between metal atoms which is equal to 0.275 nm for Pd.

4.4 Results and Discussion

4.4.1 Characterization of the Catalysts

The actual Pd content, BET surface area, and ion exchange capacity of the resins before and after loading 1 wt % Pd are listed in **Table 4-1**. The BET surface area of the neutral resins and the ion exchange capacities of IRA96 and MN100 did not change significantly after loading Pd. The ion exchange capacity of IRA910 decreased by 17% after loading 1 wt % Pd. TEM images and particle size distributions are presented in **Figure 4-2** and **Figure 4-3**. To obtain particle size distribution, the diameter of at least 200 individual Pd particles at different locations was measured for each catalyst. The surface-area-weighted average size d_{Pd} was calculated according to:[122, 195]

$$d_{Pd} = \frac{\sum_i n_i d_i^3}{\sum_i n_i d_i^2} \tag{4.8}$$

where n_i is the number of particles of diameter d_i.

TEM and EDS results of the catalysts illustrated that Pd nanoparticles were highly dispersed in the porous structure of the resins. MN200, IRA910, and MN100 showed similar dispersion of Pd nanoparticles, mostly nanoclusters with some nanoparticles present. The nanoclusters are distributed non-uniformly within the resin structures. TEM images of XAD4 exhibited dispersion of mostly Pd nanoparticles with more uniform distribution and less nanoclusters, however, its particle size distribution was similar to the other two neutral resins. Note the much lower actual Pd loading on XAD4 compared with the other resins, even though with the same theoretical loadings of 1 wt% (**Table 4-1**). TEM images of IRA96 showed very poor dispersion of Pd nanoparticles. Low reactivity of this catalyst can also be related to the low Pd^0 loading of 0.31 wt% (the highest rate constant was measured to be 0.003 min^{-1} at pH 11 for IRA96). Pd particle dispersion in MN200 and IRA910 did not change after repeated usage (**Figure 4-2**). Pd particles supported on IRA910 exhibited a broader size range and larger particle sizes comparing to the neutral resins.

The X-ray diffraction (XRD) patterns of the catalysts were in agreement with the Pd^0 crystal reference pattern and Pd^0 was the only observed crystalline phase (**Figure 4-4**).

Table 4-1: Properties of the catalysts.

Resin Pd nominal weight	% Pd	Exchange capacity (meq/g)		BET surface area (m^2/g)	
		Before[a]	After[b]	Before[a]	After[b]
MN200 1%	0.67	–	–	937	920
MN200 0.2%	0.14	–	–	–	–
MN200 0.5%	0.44	–	–	–	–
MN100 1%	0.78	0.4	0.5	811	782
XAD4 1%	0.11	–	–	829	832
IRA910 1%	0.76	5.3	4.4	–	21
IRA96 1%	0.31	6.2	6.1	–	–

[a] Before loading 1 wt % Pd, [b] After loading 1 wt % Pd

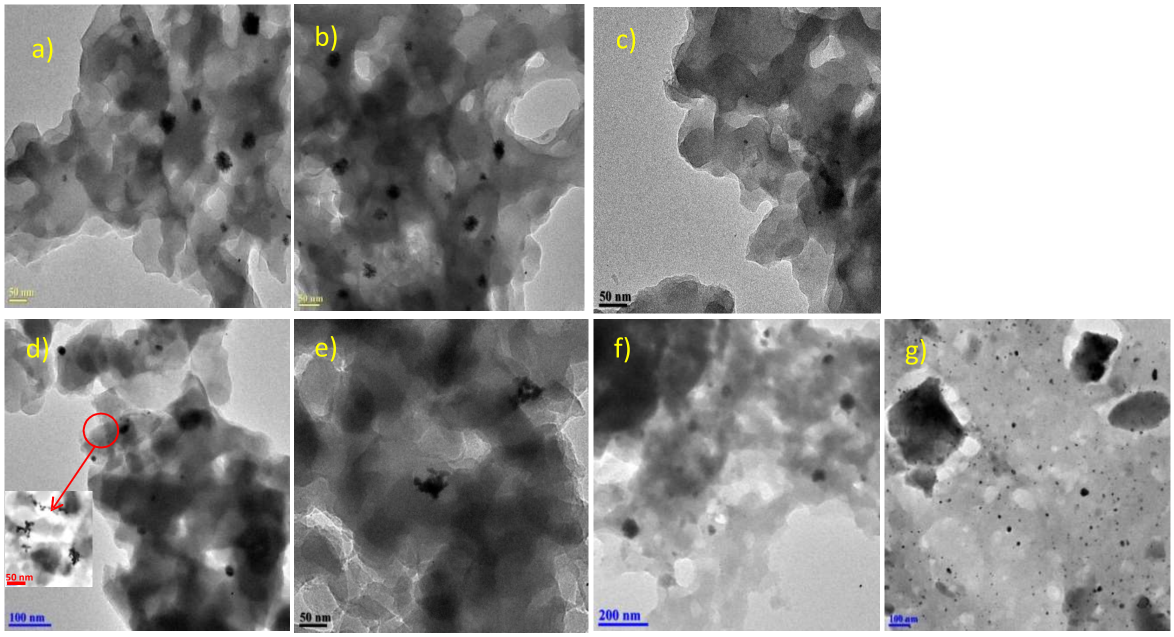

Figure 4-2: TEM images of a) fresh 1% Pd/IRA910, b) used 1% Pd/IRA910, c) Pd/IRA96, d) fresh 1% Pd/MN200, e) used 1% Pd/MN200, and f) 1% Pd/MN100, and g) 1% Pd/XAD4.

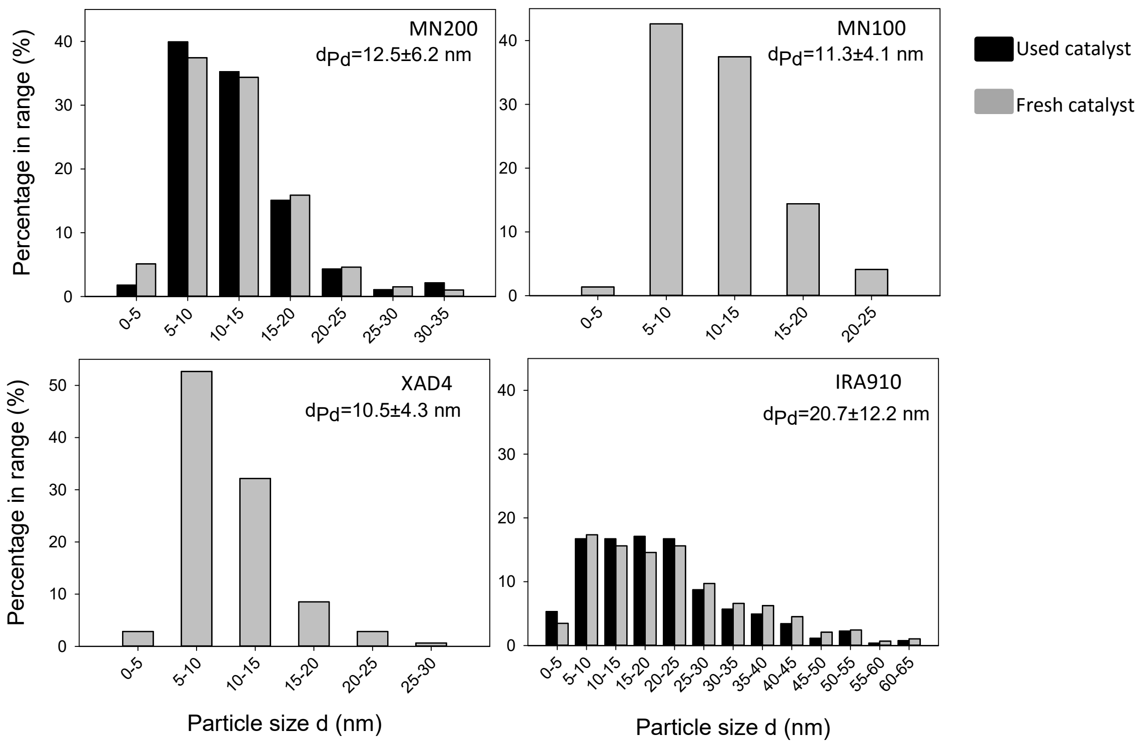

Figure 4-3: Particle size distribution of the fresh 1% Pd/catalysts and used 1% Pd/catalysts after eight times of usage.

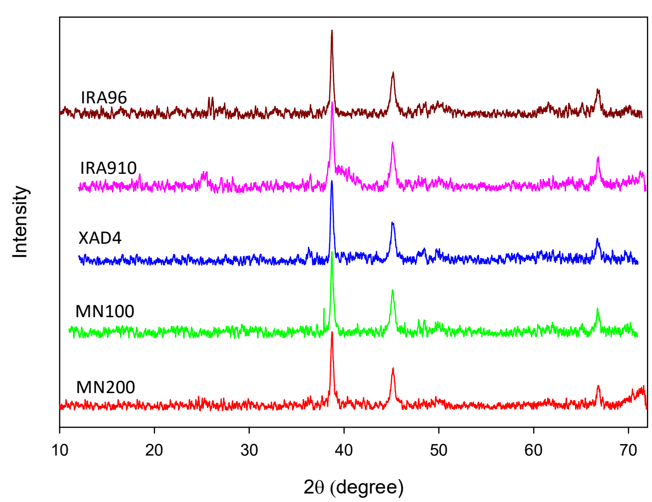

Figure 4-4: XRD patterns of palladium nanoparticles deposited on the resins.

4.4.2 Mass Transfer

Extra- and intra- particle mass transfer rates of a reactant can also influence its catalytic activity.[196] Particle size and mixing rate in reactions are two factors that can control mass transfer rates. Higher mixing rate and smaller particle size lower the likelihood of mass transfer limitation.[197] The calculated mass transfer rate constants were smaller than the measured k_{obs} for all the catalysts (**Table 4-2**). This indicates that liquid-solid mass transfer rate can limit the measured reactivity. An explanation for the observed extra-particle mass transfer limitation is that the resin beads are large particles (Dp > 500 μm). In addition, the calculation is conservative because it underestimates the contribution of mixing to the mass transfer rate from mixing in reaction (i.e., calculated based on the slip velocity of particles, only considering gravitational sedimentation) and of porous structure to a larger surface area for mass transfer (i.e., considering resins as solid spheres without pores). HighLarger reaction rate constants were observed when the catalyst beads were crushed (data not shown), confirming the existence of external mass transfer limitation. Though crushing resin beads improved the catalytic activity for contaminant removal, we did all other experiments with uncrushed resins to best simulate the application of resins in water treatment practices. For the commercially available resins with particle sizes larger than 500 μm, the external mass transfer limitation is inevitable and should be considered for catalyst development and evaluation. The estimated values of the Weisz and Prater criterion were less than 1 for all catalysts (**Table 4-2**). This suggests that the rate of 4-CP reduction on the Pd surface is much slower than its diffusion through the internal pores. Thus, there is no intra-particle mass transfer limitation.

Table 4-2: Extra-particle liquid-solid mass transfer rate constants ($a \times k_c$), experimentally measured reaction rate constants (k_{obs}), and Weisz and Prater criterion ($k_{obs}D_p^2/D_e$) for evaluating intra-particle liquid-solid mass transfer at pH 7 and 11 for neutral resins and AXRs, respectively. These pH values were selected because, as shown later, the resins had the highest reactivity under these pH conditions.

Resin	$a \times k_c$ (s^{-1})	$k_{obs,\,max}$ (s^{-1})	$\frac{k_{obs} D_p^2}{D_e}$
MN200	5.0×10^{-5}	2.4×10^{-4}	1.2×10^{-1}
XAD4	3.0×10^{-5}	1.5×10^{-4}	9.4×10^{-2}
MN100	7.0×10^{-5}	1.8×10^{-4}	1.3×10^{-1}
IRA910	7.0×10^{-5}	1.1×10^{-3}	1.8×10^{-1}
IRA96	5.0×10^{-5}	8×10^{-5}	6.1×10^{-2}

4.4.3 Adsorption Properties

The adsorption results of 4-CP on the resins indicated that adsorption capacity of the resins did not change much after loading 1 wt % Pd (**Figure 4-5**). Similar to the original resins, 4-CP was significantly adsorbed by the catalysts supported on the neutral resins (MN200, MN100, and XAD4) at pH<pK_a (pK_a=9.1), where the non-dissociated form (i.e., protonated form) of 4-CP has a higher adsorption affinity than the dissociated form (i.e., anionic form). The opposite is true for the adsorption of 4-chlorophenolate to the anion exchange resins (i.e., IRA910 and IRA96) at pH > pK_a. These results verify the fact that neutral resins exhibit much higher adsorption capacities toward neutral compounds, while anion exchange resins have higher adsorption capacities toward anionic compounds. Generally, MN200 and MN100 showed greater adsorption capacity to adsorb 4-CP at pH < pKa than XAD4. The larger proportion of micropores in MN200 and MN100 enhance adsorption energies due to the superposition of the force fields of the opposite walls.[183] As will be shown later, the different adsorption capacities of the resin supports have large effects on the overall catalytic reduction of 4-CP.

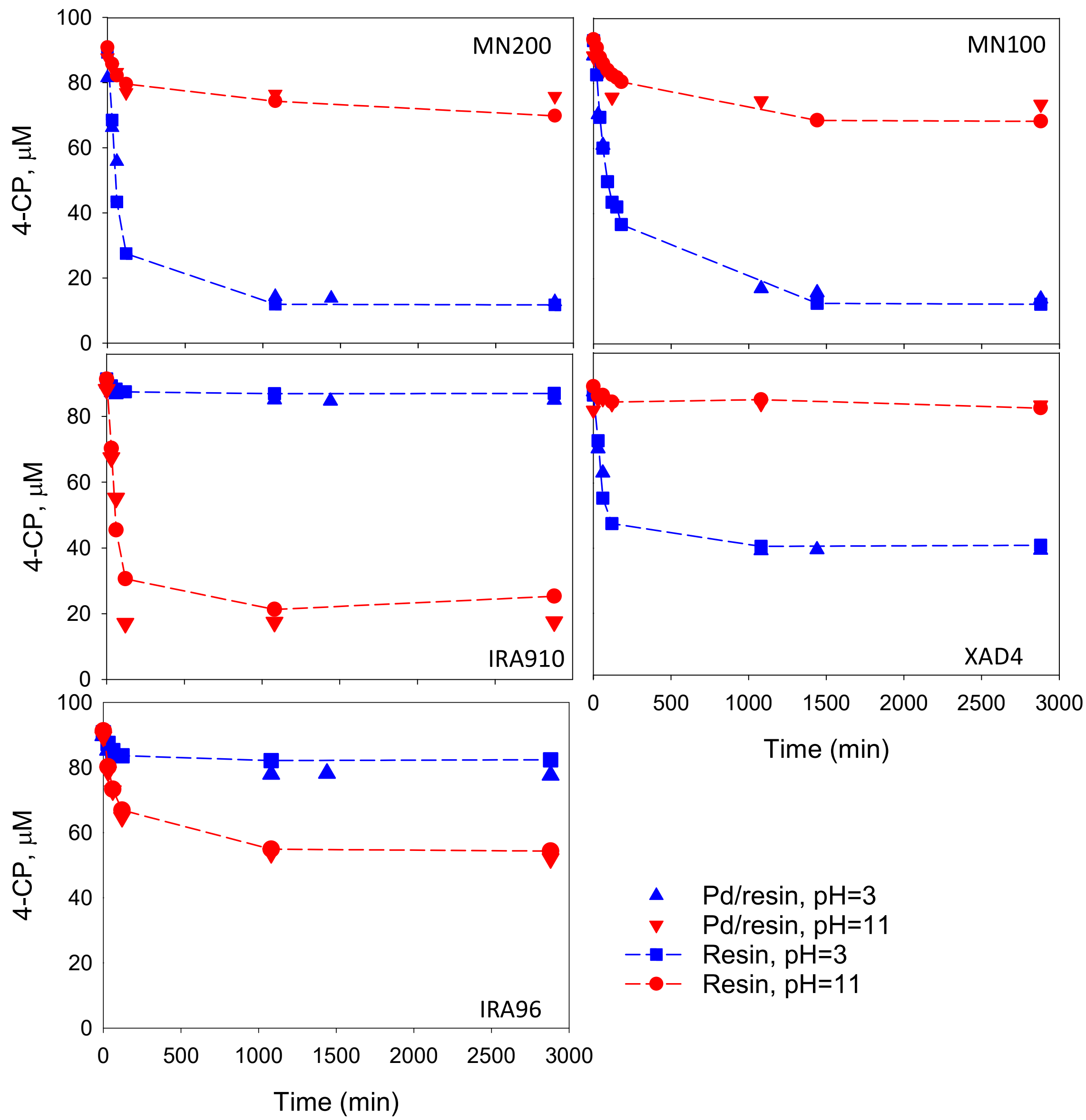

Figure 4-5: Comparing adsorption capacity of the resins before and after loading 1 wt % Pd. Reaction conditions: for initial 4-CP concentration of 100 µM, and 25 mg of resin andor 25 mg of 1 wt % Pd catalyst loading, no H_2 gas.

4.4.4 Reduction Kinetics

The activity of the developed catalysts in the reduction of 4-CP was measured at different pHs. The hydrodechlorination of 4-CP over the catalysts mainly resulted in the formation of phenol. After catalytic reactions, the sum of soluble and adsorbed 4-CP and phenol accounts for more than 90% of the initial amount of 4-CP. For example **Figure 4-6** shows the time course of 4-CP reduction of 4-CP, phenol formation, and the sum of 4-CP and phenol for XAD4 and IRA910. The amount of 4-CP and phenol adsorbed during reduction was measured by conducting reduction experiments in multiple reactors. Each reactor was sacrificed reactors for the desorption experiment at different reaction times. The desorption results in **Figure 4-7** confirmed that the 4-CP removal from solution by 1 wt% Pd-MN200, -MN100, and -IRA910 was resulted from the reduction of 4-CP rather than from adsorption onto the resins (less than 1%). Up to 9% of 4-CP was adsorbed by 1 wt% Pd-XAD4 during the reaction. Phenol, however, was adsorbed onto all the resins during the reaction (**Figure 4-7**). At pH 7, the amount of phenol adsorbed was the highest onto the MN200 and MN100 catalysts (30-40% of the total formed phenol), and for XAD4 was 11% of the total formed phenol. Phenol was moderately adsorbed onto IRA910 (about 34% of the total formed phenol) at pH=11 when phenolate is the dominant species (pK_a of phenol=10.0). Due to the negligible amount of 4-CP adsorbed during most of the reactions, pseudo-first-order rate constants for 4-CP reduction were obtained from the linear regression of the natural log of solution phase concentrations versus time (**Figure 4-8**).

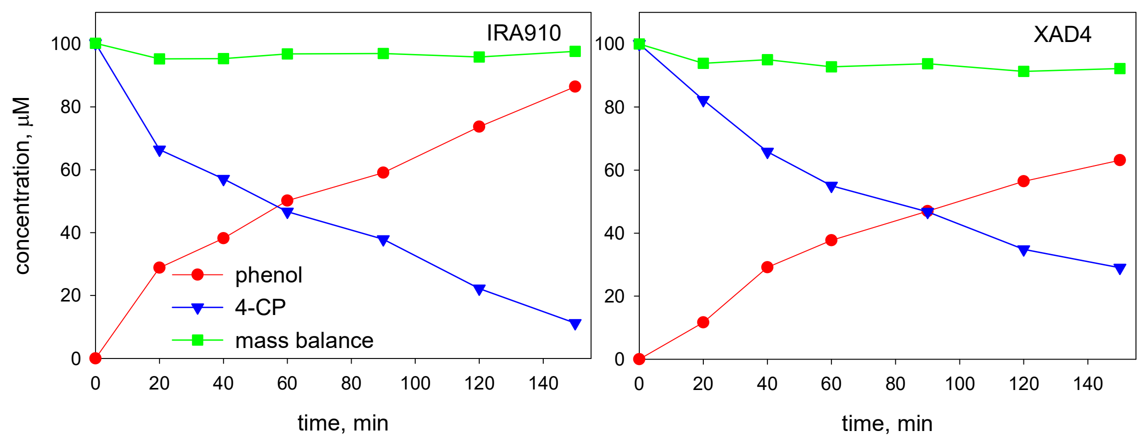

Figure 4-6: Reduction of 4-CP by XAD4 at pH 7 and IRA910 at pH 9. Consumption of 4-CP, production of phenol and mass balance i.e. the total concentration of 4-CP and phenol are shown in the figures.

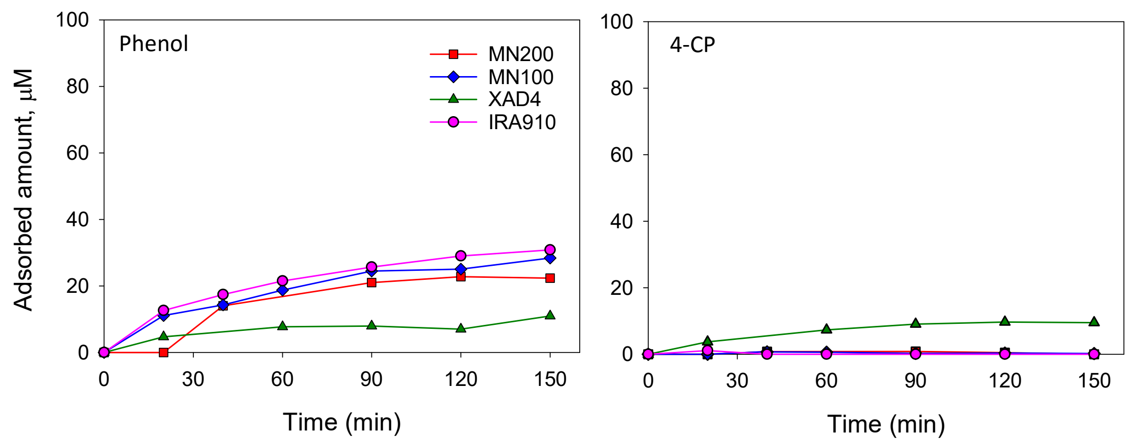

Figure 4-7: Adsorbed amounts of phenol and 4-CP onto MN200, MN100, and XAD4 at pH 7 and onto IRA910 at pH 11 during the reaction. Reaction conditions: initial 4-CP concentration of 100 µM, and 25 mg of 1 wt % Pd catalyst loading.

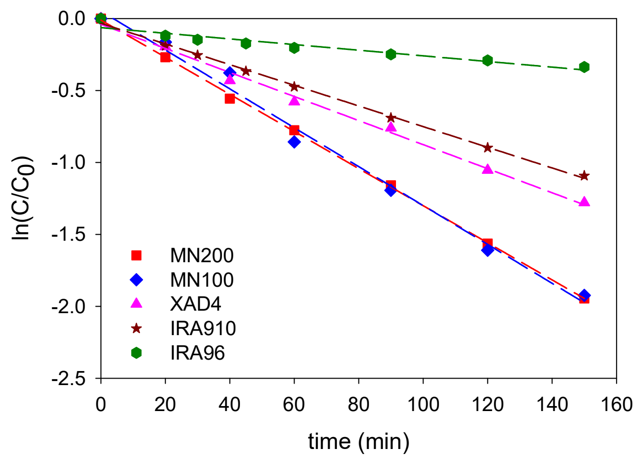

Figure 4-8: Linear correlation between the natural log of 4-CP concentration in solution phase versus time for the experiment of 25 mg of 1 wt% Pd/resin at pH 7. The initial concentration of 4-CP was 0.1 mM.

4.4.5 Effect of pH on Catalytic Activity

4-CP reduction rate constants for all catalysts at different pHs are shown in **Figure 4-9a**, where k_{obs} typically increased with pH increasing from 3 to 7. Different behavior was observed for 4-CP reduction at pH 11, that is, k_{obs} for the catalysts supported on the neutral resins decreased when pH reached 11 while a significant increase was observed for the catalyst supported on IRA910. The initial turnover frequencies (TOF_0) also followed the same trend (**Figure 4-9b**). Solution pH affects both Pd activity and adsorption properties of the resins. Comparing the reduction and adsorption results suggested that faster reactivity is consistent with higher adsorption capacity for all the catalysts, as detailed below.

As illustrated in **Figure 4-10**, the faster reduction of 4-CP on MN200 at pH 3, 5, and 7 than at pH 11 is compatible with its higher adsorption capacity at the lower pH values. The similar enhancing effect of adsorption on reduction was also observed for the reduction of 4-CP by IRA910 at pH 11 comparing to pH 3, 5, and 7. Thus, the ability of the catalysts to adsorb 4-CP molecules, which further react with activated hydrogen, facilitated the subsequent reduction of 4-CP.

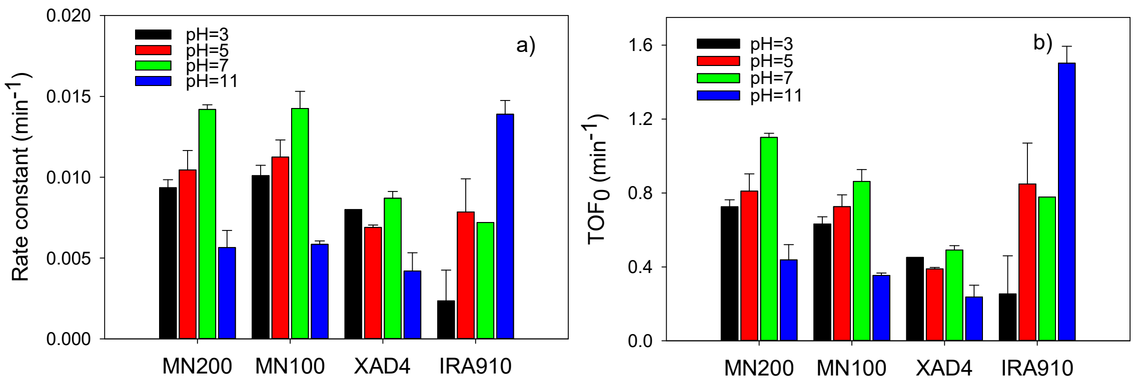

Figure 4-9: Catalytic 4-CP reduction rate constants (a) and initial turnover frequency (TOF_0) (b) over the catalysts at different pHs.

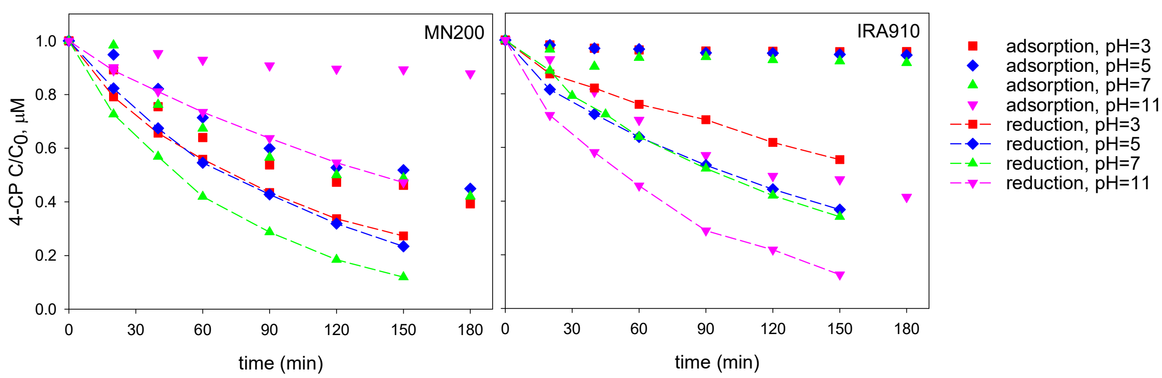

Figure 4-10: Comparing the reduction and adsorption kinetics at different pHs (pH 3 and, 5, 7, and 11) for 25 mg of 1 wt % Pd -MN200 and IRA910, and initial 4-CP concentration of 100 μM. The adsorption tests were carried out in the absence of hydrogen gas, and the reduction results are based on the loss of 4-CP due to HDC.

In addition to affecting adsorption, solution pH also influences catalyst activity.[83] The activity of the catalysts increased with an increase in solution pH from 3 to 7 when the adsorption capacity of the resins was constant for both 4-CP and phenol. This is because 4-CP and phenol are both non-dissociated at these pHs due to their respective pKa of 9.1 and 10.0. As reported by other studies, increasing pH enhances the conversion rate of 4-CP due to the mitigation of H^+ and Cl^- inhibition,[35, 129] which are the byproducts of 4-CP reduction. High concentrations of Cl^- at low pH are favorable for $PdCl_3^-$ and $PdCl_4^{2-}$ formation. These anionic Pd species are inactive for 4-CP reduction, in contrast to Pd^{n+} species that were found to be important for dehalogenation.[35, 53, 129] The formation of $PdCl_3^-$ and $PdCl_4^{2-}$ also results in the leaching of Pd into aqueous solutions, which further decreases the catalytic activity and compromises the longevity of the catalysts over multiple cycles.

4.4.6 Kinetic Modeling and Effect of initial 4-CP Concentrations

In the reported mechanisms, hydrodechlorination of chlorinated organic compounds can be described by the following steps: 1) adsorption of the target compound and hydrogen gas (H_2) onto the catalyst surface (Pd^0), typically following the Langmuir adsorption isotherm, 2) dissociation of the adsorbed hydrogen by metallic Pd and conversion to the adsorbed atomic hydrogen ($Pd\text{-}H_{ads}$), and 3) reaction between the adsorbed atomic hydrogen and the co-adsorbed compound. Step 3 is typically treated as the rate determining step (RDS).[198, 199] Kinetic models can be developed based on these sequential steps, considering either the adsorption or reaction as the rate determining step. Two models were developed for the reaction kinetics based on the Langmuir-Hinshelwood (L-H) model which has been extensively applied to investigating heterogeneous catalytic processes:[62, 200, 201] 1) surface reaction is the RDS, and 2)adsorption is the RDS. Note that although reaction may be limited by external mass transfer, the calculated mass transfer rates are not significantly smaller than the measured reactivity (**Table 4-2**). We assume the second model is applicable within the region where the reaction rate is controlled by the rate of both mass transfer and adsorption, whichever is smaller.

When surface reaction is the RDS, the L-H model can be expressed as the following elementary steps including adsorption of 4-CP and hydrogen gas and surface reaction. For the high concentration region, surface reaction is the RDS. Thus, L-H model can be derived as following:

Step 1: $4 - CP + * \overset{K_1}{\rightleftharpoons} 4 - CP^*$ (Adsorption of 4-CP)

Step 2: $H_2 + 2* \overset{K_2}{\rightleftharpoons} 2H^*$ (Adsorption of hydrogen gas)

Step 3: $4 - CP^* + 2H^* \xrightarrow{k_3} Phenol + H^+ + Cl^- + 3*$ (Surface reaction, RDS)

Where the active sites for chemisorption on the catalyst surface are described by *. $4\text{-}CP^*$ and H^* are the chemisorbed 4-CP and hydrogen on the active surface sites, and phenol, H^+, and Cl^- are the reaction products. The overall reaction rate is:

$$r = k_3\left[4-CP^*\right]\left[H^*\right]^2 \tag{4.9}$$

Assuming negligible adsorption of phenol, H^+, and Cl^- due to low concentrations of the products at the beginning of the reaction, the total adsorption sites $[*]_0$ can be expressed as the sum of the surface concentration of the vacant active sites [*] and the total adsorption sites that are occupied by 4-CP and H_2:

$$[*]_0 = [*] + \left[4-CP^*\right] + \left[H^*\right] \tag{4.10}$$

where $[4\text{-}CP^*]$ and $[H^*]$ are the total adsorption sites that are occupied by the reactant 4-CP and H_2, respectively.

The equilibrium adsorption constants for steps 1 and 2 are defined as:

$$K_1 = \frac{\left[4-CP^*\right]}{\left[4-CP\right]\left[*\right]} \Rightarrow \left[4-CP^*\right] = K_1\left[4-CP\right]\left[*\right] \tag{4.11}$$

$$K_2 = \frac{\left[H^*\right]^2}{\left[H_2\right]\left[*\right]^2} \Rightarrow \left[H^*\right] = \sqrt{K_2\left[H_2\right]}\cdot\left[*\right] \tag{4.12}$$

By substituting equations 4.11 and 4.12 in equation 4.10, we obtain:

$$\left[*\right]_0 = \left(K_1\left[4-CP\right] + \sqrt{K_2\left[H_2\right]} + 1\right)\cdot\left[*\right] \tag{4.13}$$

By substituting equations 4.11-4.13 in equation 4.9 and assuming $K_2 \approx 0$ because there is negligible adsorption of H_2 on the catalysts compared to the reactants:

$$r = k_3 K_1 K_2 \left[*\right]^3{}_0 \left[H_2\right] \frac{\left[4-CP\right]}{\left(K_1\left[4-CP\right]+1\right)^3} \tag{4.14}$$

Assuming $[*]_0$ is the amount of surface Pd sites of the catalysts, and $K_2[*]^3{}_0$ is constant, the initial reaction rate r_0 (mmol $g_{Pd}^{-1} \cdot h^{-1}$) as a function of initial 4-CP concentration ([4-CP]$_0$) can be rewritten as:

$$r_0 = k_r K_1 \left[H_2\right] \frac{\left[4-CP\right]_0}{\left(K_1\left[4-CP\right]_0+1\right)^3} \tag{4.15}$$

where $k_r = k_3 K_2 [*]^3{}_0$ (mmol $g_{Pd}^{-1} \cdot hr^{-1}$) is the intrinsic rate constant.

When adsorption of 4-CP is the RDS, the kinetics of the overall reaction can be describe by:

Step 1: $4-CP + * \xrightarrow{k_1} 4-CP^*$ (Adsorption of 4-CP, RDS)

Step 2: $H_2 + 2* \overset{K_2}{\rightleftharpoons} 2H^*$ (Adsorption of hydrogen gas)

Step 3: $4-CP^* + 2H^* \overset{K_3}{\rightleftharpoons} Phenol + H^+ + Cl^- + 3^*$ (Surface reaction)

The overall reaction rate is:

$$r = k_1[4-CP][*] \tag{4.16}$$

The equilibrium adsorption constants for steps 2 and 3 are defined as:

$$K_2 = \frac{[H^*]^2}{[H_2][*]^2} \Rightarrow [H^*] = \sqrt{K_2[H_2]} \cdot [*] \tag{4.17}$$

$$K_3 = \frac{[phenol][H^+][Cl^-][*]^3}{[4-CP^*][H^*]^2} \Rightarrow [4-CP^*] = \frac{[phenol][H^+][Cl^-]}{K_3 K_2 [H_2]} \cdot [*] \tag{4.18}$$

By substituting equations 4.17 and 4.18 in equation 4.10, we obtain:

$$[*]_0 = \left(\frac{[phenol][H^+][Cl^-]}{K_3 K_2 [H_2]} + \sqrt{K_2[H_2]} + 1 \right) \cdot [*] \tag{4.19}$$

By substituting equation 4.19 in equation 4.16 and assuming $K_2 \approx 0$:

$$r = k_1[4-CP] \frac{[*]_0}{\left(\frac{[phenol][H^+][Cl^-]}{K_3 K_2 [H_2]} + 1 \right)} \tag{4.20}$$

Assuming the concentrations of the products at the beginning of the reaction are low and do not change with time (i.e., $[phenol][H^+][Cl^-] \approx constant$), the reaction rate can be approximated as:

$$r = k_1 m [*]_0 [4-CP] \tag{4.21}$$

where m is a constant.

Assuming $[*]_0$ is the amount of surface Pd sites of the catalysts, the initial reaction rate r_0 (mmol $g_{Pd}^{-1} \cdot h^{-1}$) as a function of initial 4-CP concentration ($[4\text{-}CP]_0$) can be rewritten as following:

$$r_0 = k_r [4-CP]_0 \tag{4.22}$$

where $k_r = k_1 m [*]_0$ ($g_{Pd}^{-1} \cdot hr^{-1}$) is the intrinsic rate constant.

To test the two kinetic models and to investigate the relative contribution of 4-CP adsorption and surface reaction to the hydrodechlorination, the influence of 4-CP initial concentration was evaluated. The initial reaction rate was measured for various initial 4-CP concentrations from 0.1 to 7.5 mM. The initial rates were calculated based on the solution phase concentrations, where the loss of 4-CP includes the disappearance of 4-CP from the suspension due to both reaction and adsorption. The desorption results at the end of each reaction showed that with increasing initial 4-CP concentration, the amount of 4-CP adsorbed on the catalysts during reaction also increased (**Table 4-3**). Therefore, the rate determining step for hydrodechlorination by the catalysts changed from adsorption at low concentrations to surface reaction at high concentrations, as detailed below.

In general, r_0 increased with increasing initial 4-CP concentration for all the catalysts, and it followed the order of MN200 >= MN100 > IRA910 over the entire range of the tested concentrations (**Figure 4-11**). The first L-H model (eq 4.15) fits well initial reduction rate versus initial concentration for the high concentration range tested ($R^2 > 0.94$ **Table 4-4**). Comparable intrinsic rate constants k_r were obtained for MN200 and MN100 catalysts. The values of the equilibrium adsorption constant K_1 for MN200 and MN100 were almost equal, agreeing with their similar resin structure and adsorption capacity. The value of k_r and adsorption constant obtained for Pd/IRA910 were smaller. This is because IRA910 has lower adsorption affinity for the nondissociated form of 4-CP at pH=7.

The experimental data for the low concentration range were all well fitted to the second L-H kinetic model (eq 4.22), R^2=0.99. The intrinsic rate constant k_r follows the order of MN200 > MN100 > IRA910 (**Table 4-4**). The rate constant for MN200 was slightly higher than that for MN100 (276.2 vs 258.5 $g_{Pd}^{-1} \cdot hr^{-1}$), and IRA910 has a significantly smaller rate constant (140.1 $g_{Pd}^{-1} \cdot hr^{-1}$). This behavior can also be explained based on the adsorption properties of the resins, as discussed earlier.

Table 4-3: Adsorbed amounts of 4-CP (μM) at the end of the catalytic reduction for different initial 4-CP concentrations with 25 mg of 1 wt % Pd catalyst loading at pH=7. The adsorbed 4-CP was only detected when 4-CP initial concentration was above 1.5 mM.

Initial 4-CP concentration mmol L^{-1}	Catalyst		
	Pd/MN200	Pd/MN100	Pd/IRA910
0.1	0.0	0.0	0.0
0.5	0.0	0.0	0.0
1.0	0.0	0.6	0.0
1.5	9.4	14.0	2.6
2.5	38.4	37.1	60.1
5.0	287.0	255.0	87.6
7.5	546.8	510.8	123.9

Table 4-4: Fitting parameters of the L-H model for $[4\text{-CP}]_0$ > 1.5 mM and < 1.5 mM for 4-CP reduction at pH=7 for 25 mg of 1 wt % Pd catalyst loading.

Catalyst	High concentrations> 1.5 mM		Low concentrations < 1.5 mM
	k_r mmol $g_{Pd}^{-1} \cdot hr^{-1}$	K_1 L $mmol^{-1}$	k_r $g_{Pd}^{-1} \cdot hr^{-1}$
MN200	7127±156	0.047±0.002	276.2
MN100	6786±697	0.043±0.009	258.5
IRA910	4180±802	0.036±0.013	140.1

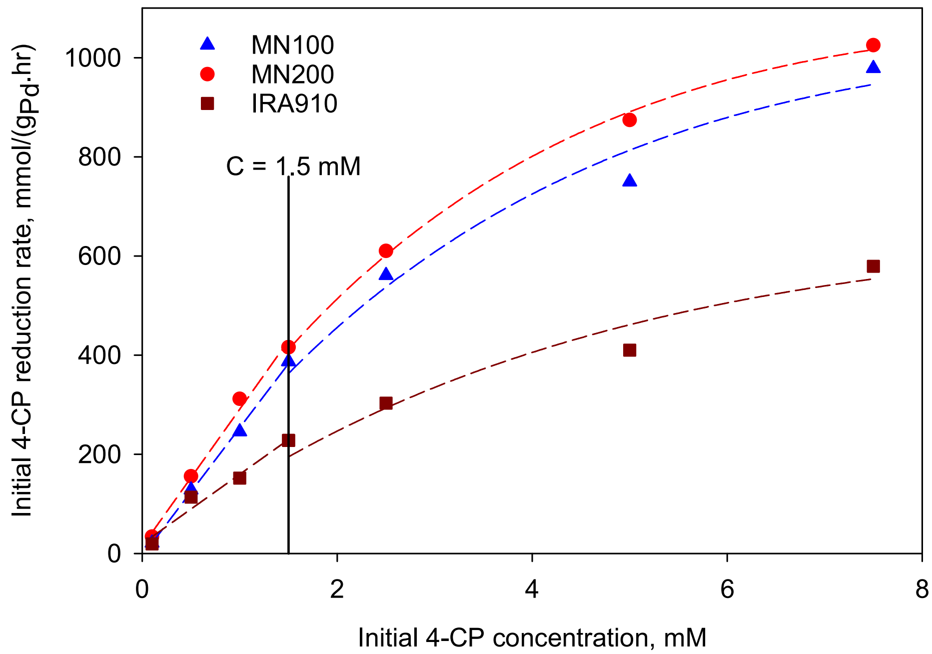

Figure 4-11: Influence of initial 4-CP concentration on the initial rate of 4-CP reduction by 25 mg of 1 wt % Pd catalyst at pH=7. Dashed lines are fitting curves to the two kinetic models. The vertical line shows when initial 4-CP concentration was 1.5 mM.

4.4.7 Effect of NaCl

The reactivity of the catalysts Pd/MN200 and Pd/IRA910 was further tested in aqueous solution with varying concentrations of NaCl from 0 to 2 mol L^{-1} at pH 7. The results indicated a more significant decrease in the rate constant of IRA910 than that of MN200 (70% vs 20% reduction in the rate constant) when NaCl concentration was increased from 0 to 0.1 M (**Figure 4-12**). Further increase of NaCl concentration from 0.1 to 2 M did not change the catalytic activity much. The adsorption experiments in the presence of NaCl at pH 7 showed that NaCl did not have any significant influence on the adsorption of 4-CP by MN200 and IRA910. The reduction of the catalytic activity could be related to the formation of palladium chloride species (i.e., $PdCl_3^-$ and $PdCl_4^{2-}$) and the subsequent leaching of the active sites as was reported by other studies.[130, 190] The difference in the effect of NaCl on the catalytic activity of the neutral and anion exchange resins could be attributed to the anion exchange ability of IRA910 which facilitates sorption of Cl^- and hence formation of more $PdCl_3^-$ and $PdCl_4^{2-}$ species.

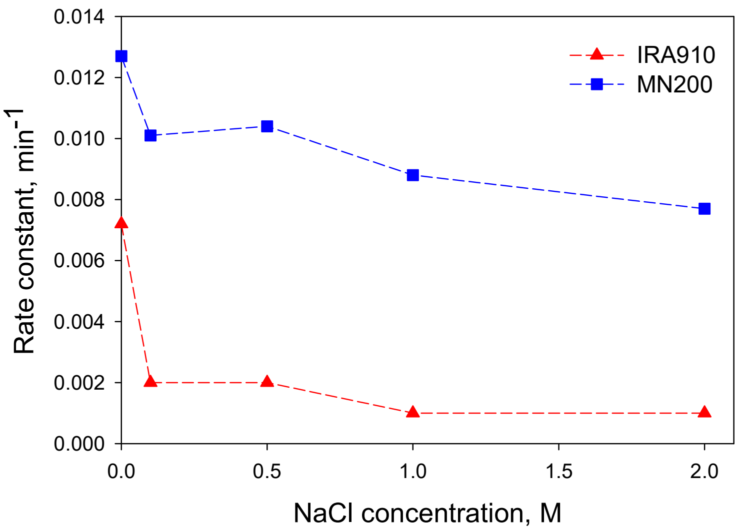

Figure 4-12: Effect of NaCl concentration on the reactivity of the 1 wt % Pd catalysts for initial 4-CP concentration of 100 μM, 25 mg of 1 wt % Pd catalyst loading, and pH=7.

4.4.8 Effect of Pd Content

MN200 resin was loaded with three different amounts of Pd in order to investigate the effect of Pd content on the catalytic activity. The Pd nominal loadings were 0.2, 0.5, and 1 wt%, and the actual Pd contents determined by ICP-OES are 0.14, 0.44, and 0.67 wt% (**Table 4-1**). The desorption results showed that, during the reduction, 4-CP was adsorbed on the catalysts with 0.14 and 0.44 wt% Pd (**Figure 4-13a**), but not onto 0.67 wt% Pd catalyst (**Figure 4-7**). The amount of 4-CP adsorbed during the reaction was the highest onto the 0.14 wt% Pd catalyst and increased when the reaction proceeded. The adsorbed amount of 4-CP onto 0.44 wt% Pd slightly increased at the beginning of the reaction and then decreased when reaction proceeded.

We believe the above results can be explained by the two kinetic models. For the low Pd content catalyst, the reaction follows the L-H mechanism when surface reaction is the RDS. The catalysts with lower Pd contents have less available Pd sites, thus surface reaction is slower. On the other hand, adsorption is the RDS for the reduction of 0.1 mmol L^{-1} 4-CP by 0.67 wt% Pd catalyst. In supporting this mechanism, no adsorbed 4-CP was observed during the reaction, suggesting surface reaction is faster than adsorption. Hydrodechlorination of 4-CP by 0.44 wt% Pd catalyst could be the turning point where the RDS changed from surface reaction to adsorption. This is, because the measured adsorbed amount of 4-CP during the reaction decreased from 15% to less than 5% of initial 4-CP concentration as reaction progressed. The 4-CP reduction rate constants for these three catalysts are shown in **Figure 4-13b**. The reduction rate constants were calculated based on the decay of 4-CP due to just HDC and amount of 4-CP adsorbed during the reaction was excluded from the total 4-CP loss. The apparent first order rate constant increased with increasing Pd content from 0.14 to 0.67 wt%. However, this increase is less significant when Pd content increased from 0.44 to 0.67%, suggesting that increasing Pd content would not necessarily result in much higher reactivity. The optimum Pd content is the point where RDS changes from surface reaction to adsorption, i. e. slightly above 0.44 wt%.

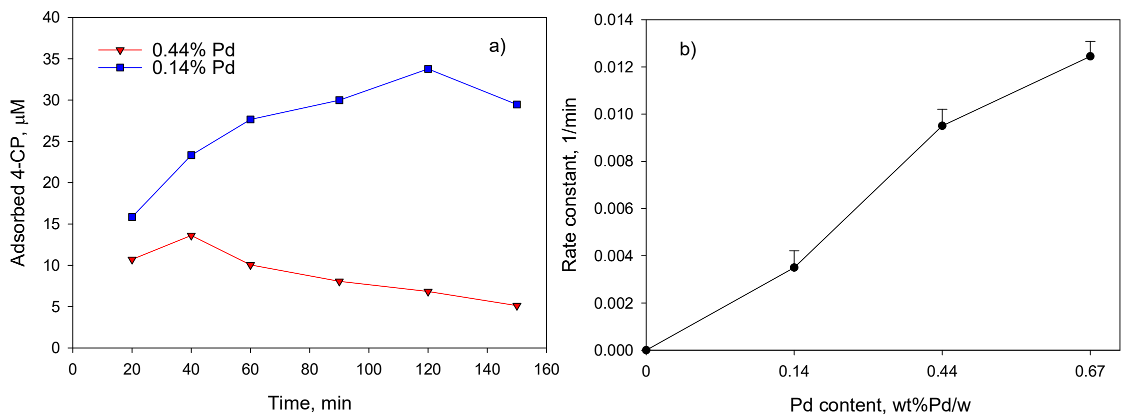

Figure 4-13: a) Amount of 4-CP adsorbed on 0.14 and 0.44 wt % Pd/MN200 during the HDC. b) 4-CP reduction rate constants for 0.14, 0.44 and 0.67 wt % Pd/MN200. Reaction conditions: pH 7, initial 4-CP concentration of 100 μM, and 25 mg of catalyst loading.

4.4.9 Catalyst Stability

The reactivity of the catalysts was tested in eight sequential reaction cycles to investigate the stability of the catalysts. 1 mmol L^{-1} 4-CP was repeatedly added to the reactor at the beginning of each cycle of three hours (**Figure 4-14**). Three-hour reaction was selected because less than 10% of the initial 4-CP remained in solution at the end of the first run for the most reactive catalysts (MN200 and IRA910). The repeatedly addition of high concentrations of 4-CP to the same reactor was selected to provide more severe condition for testing the catalytic stability (i.e., releasing more H^+ and Cl^- at the end of reactions and accumulation of reaction products). The catalytic activity decreased after the first run (**Table 4-5**), and leveled off in the next seven runs. The decrease in the removal efficiency may be partly related to the loss of the catalysts during sampling (mass loss of 21% for MN200 and IRA96 and 39% for IRA910 at the end of eight cycles). When desorption of the catalysts was conducted after the eight consecutive runs, it was found that significant amounts of 4-CP and phenol were adsorbed. Note that the majority of the formed phenol was in the solution phase (**Table 4-6**). In fact, the proportion of the dissolved phenol to the total phenol was more than 95% for the anion exchange resins and ca. 70% for MN200. Separate adsorption experiments also showed that 4-CP adsorbs more strongly on the resins than phenol (**Figure 4-15**), indicating that resins can be more easily regenerated after 4-CP has undergone catalytic reduction. During the first run, no 4-CP was adsorbed. The amount of phenol adsorbed after eight runs was more than 15 times higher than that after the first run for MN200. Therefore, the accumulation of phenol in the catalysts seems to be the major reason for the loss in the reductive activity.

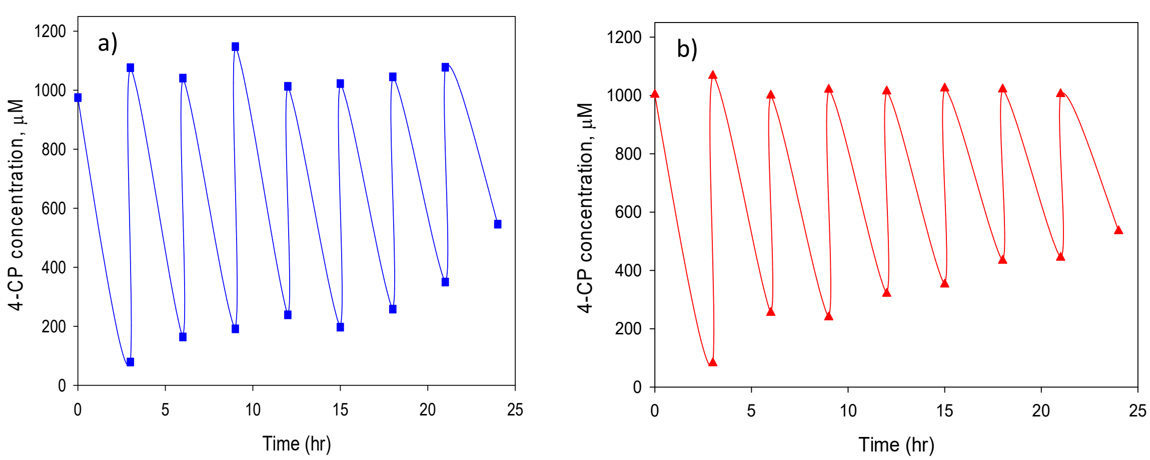

Figure 4-14: Changes of 4-CP concentration over eight cycles for a) IRA910 and b) MN200. Each cycle was 3 hours and then 1 mM of 4-CP was spiked again into the reactor.

Table 4-5: Removal efficiency during the cyclic reactions, i.e., % of 1 mM 4-CP reduced by 25 mg of 1 wt % Pd catalysts, after 3 hours at pH 7.

Cycle	MN200	IRA910	IRA96
1	91.8	91.9	43.4
2	76.1	84.8	34.9
3	76.1	81.6	29.1
4	68.6	79.2	24.9
5	65.3	80.5	25.9
6	57.7	74.8	22.6
7	56.5	66.5	22.2
8	46.8	49.3	19.4
after regeneration	82.9	114.8	34.1

Table 4-6: Amounts of phenol and 4-CP adsorbed (μM) by 25 mg of 1 wt % Pd catalysts after one and eight runs versus phenol concentrations (μM) in the solution phase, pH=7.

Catalyst	Adsorbed 4-CP		Adsorbed Phenol		Phenol in solution phase	
	1st run	8th run	1st run	8th run	1st run	8th run
MN200	0.0	365.5	156.6	2432.9	486.1	5539.8
IRA910	0.0	47.9	0.0	266.8	622.1	6103.3
IRA96	12.1	175.7	0.0	39.2	247.6	2623.0

To confirm the above hypothesis, the catalysts were regenerated and were tested again for 4-CP reduction. As shown in **Table 4-5**, MN200 regained ca. 90 percent of the original reactivity. Note, the original removal efficiencies and the removal efficiencies after regeneration have been normalized by the catalyst weight for comparison purposes. The reactivity of the regenerated IRA910 is surprisingly higher than the original one, this could be due to the breakage of the resin beads by the magnetic stir bars used for stirring and the mitigation of external mass transfer limitation. IRA96 regained about 80 percent of its original reactivity which could be attributed to its lower efficiency of removal of the adsorbed phenol and 4-CP from the catalysts, i.e. regeneration efficiency of 74% for IRA96 vs. 96% and 95% for IRA910 and MN200, respectively.

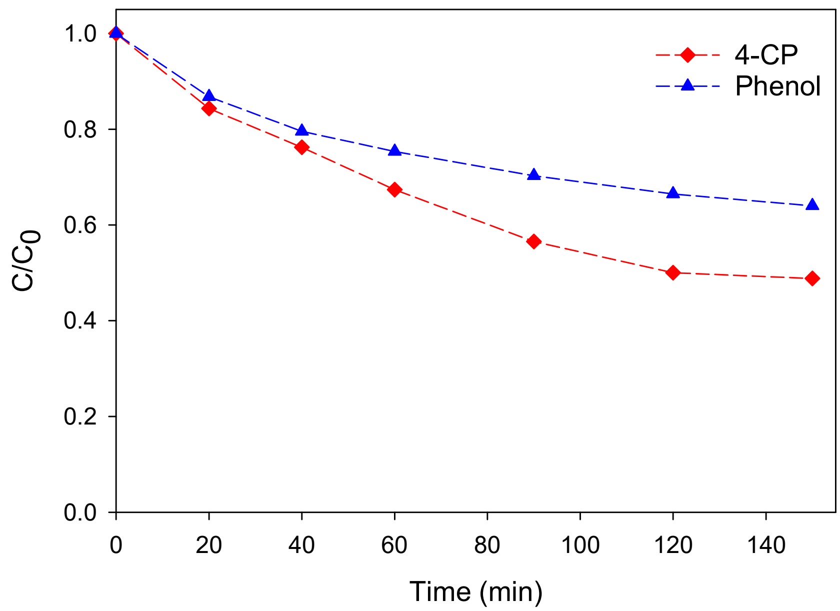

Figure 4-15: Comparing adsorption of phenol to that of 4-CP onto 1 wt% Pd-MN200 at pH 7. The adsorption tests were carried out in the absence of hydrogen gas.

It should be mentioned that the catalytic activity of all catalysts did not change after three cycles if the catalysts were simply rinsed with DI water and then mixed with fresh 1 mM 4-CP solution in the reactor after each 3-h cycle (**Figure 4-16**). This condition is similar to real applications when catalysts are in continuous contact with fresh influent such that the accumulation of the reaction product(s) is much less. This result further verified the ability of the catalysts to sustain their reactivity through multiple cycles.

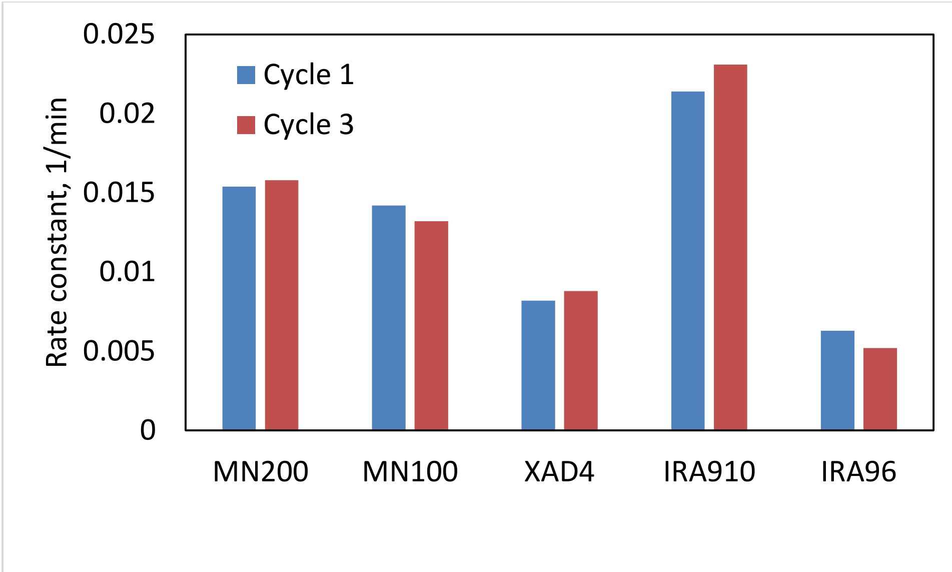

Figure 4-16: Comparing the reactivity of the catalysts over three cycles when the catalysts were rinsed with DI water after each cycle and then mixed with a new batch of reaction solution.

4.4.10 Effect of Resin structures

Overall, loading Pd on strong anion exchanger IRA910 and microporous neutral resins MN200 and MN100 was more successful than on macroporous neutral resin XAD4 and weak anion exchange resin IRA96. The Pd contents of MN200, MN100, and IRA910 were higher than IRA96 and XAD4 under the same preparation conditions (**Table 4-1**). This could be related to the higher adsorption of the Pd precursor by the microporous and strong anion exchange resins. Among the neutral resins, MN200 and MN100 showed similar reactivity. This behavior was expected as the two resins have very similar microporous structures and consequently similar adsorption behavior. The additional functional groups in MN100 did not seem to affect the catalytic reactivity. Comparing XAD4 to the other two neutral resins, XAD4 was less reactive due to a lower Pd loading. This could be associated with its lower proportion of micropores that results in lower adsorption capacity of the Pd precursor during synthesis. Among the resins, MN200 and MN100 showed the highest reactivity for hydrodechlorination of 4-CP at neutral pH where they have the highest adsorption capacity, and IRA910 had the highest reactivity at pH 11 due to its anion exchange ability (**Figure 4-9**). Neutral resins showed stronger mechanical rigidity than IRA910 as a higher proportion of IRA910 beads were broken apart by magnetic stirring. Our results also indicated that neutral resin MN200 was more resistant to the poisoning effect of Cl^- because of the lower sorption of Cl^-. On the other hand, IRA910 could be a better candidate for *in situ* regeneration purposes, because the adsorbed amounts of 4-CP and phenol onto IRA910 were much lower than those onto MN200 at neutral pH (**Table 4-6**).

4.5 Conclusions and Implications

Pd-based catalysis by hydrogen gas has been considered as a promising technology for reductive destruction of various classes of contaminants. Pd-based catalysts supported on polymeric resins can be used for detoxification of adsorbed organic contaminants and *in situ* regeneration of spent resin. In the present work, we developed Pd-based catalysts supported on two anionic and three neutral resins, and evaluated their catalytic activity in hydrodechlorination of 4-CP. The reactivity of the catalysts was dependent on solution pH and adsorption affinity of the resins. For neutral resins, neutral pH was more favorable for reduction of 4-CP due to the inhibition effect of Cl^- and H^+, however, lack of adsorption decreases catalytic reactivity at high pHs. For anionic resins, increasing pH resulted in higher reactivity due to higher sorption of 4-chlorophenolate through anion exchange. With increasing initial 4-CP concentration, the adsorbed amount of 4-CP onto the resins during catalytic reduction increased, indicating that the RDS for the hydrodechlorination changed from adsorption (including external-mass transfer) at low concentrations to surface reaction at high concentrations. Two kinetic models were developed based on the Langmuir-Hinshelwood model, one for low concentrations where adsorption/mass transfer is the RDS and the other for high concentrations when surface reaction is the RDS. Both kinetic models fit well and confirmed the enhancement effect of adsorption on the catalytic reactivity. Neutral resins are more resistant to the poising effect of Cl^- than ionic resins because the anion exchange nature of the latter facilitates adsorption of Cl^- and thus formation of more $PdCl_3^-$ and $PdCl_4^{2-}$ species. Adsorption of phenol over multiple reaction cycles resulted in the activity loss, and the regeneration of the used catalyst restored the catalytic activity. This study shows that the integration of adsorption and catalytic treatment is a promising strategy to significantly reduce the volume of the secondary waste from resin regeneration. Also, polymeric resins are a great candidate for developing new Pd-based catalysts due to their designable structures and unique physical and chemical properties that allow simultaneous removal of target contaminants and *in situ* regeneration of the spent resin. Future work should be carried out to examine if it is beneficial to run adsorption and catalytic reduction in sequence. In other words, Pd/resin catalysts will be used as an adsorbent first and then passing H_2 through the saturated Pd/resin to initiate catalytic reduction. This might decrease the need for H_2 consumption and increase treatment efficiency.

CHAPTER 5

CATALYTIC HYDROGENATION OF 4-NITROPHENOL BY PALLADIUM-RESIN COMPOSITES

ABSTRACT

Polymeric resins have been frequently used for the treatment of organic compounds, but regeneration of the spent resins has been a major problem in their application. Catalytic reduction of 4-nitrophenol (4-NP) by palladium-resin catalysts is promising for 4-NP detoxification, *in situ* regeneration of the catalysts, and recycling of the products. In this study, we examined the catalytic reduction of 4-NP by Pd-based catalysts supported on three neutral resins (MN200, MN100, and XAD4) and two anion exchange resins (IRA910 and IRA96), using hydrogen gas as the electron donor. The influence of pH, initial 4-NP concentration, and 4-NP adsorption was investigated in order to evaluate the catalytic reactivity and optimize catalyst synthesis. Reduction kinetics followed the same trend as the adsorption kinetic, i.e., faster adsorption and reduction were observed at acidic pHs for the neutral resins and at basic pHs for the anionic resins (4-NP $pK_a = 7.15$). This finding points to the significant role of adsorption in the overall catalytic reaction. Adsorption and surface reaction were believed to be the rate-determining step (RDS) for low and high concentrations of 4-NP, respectively. This is because 4-NP adsorption onto the catalysts was not detected during the hydrogenation reaction at low concentrations ($C_0 < 1.0$ mM), but was detected at high concentrations ($C_0 > 1.0$ mM). For each concentration range, the Langmuir-Hinshelwood model based on the respective RDS could fit the reaction kinetics well. The inhibiting effect of Cl^- on the reactivity of the catalysts indicated that the hydrophobic nature of the neutral resins enhanced their resistance to the impact of Cl^-. The accumulation of 4-NP and the sole

reduction product (4-aminophenol) on resin surfaces through eight cycles resulted in loss in the catalytic activity, which was largely restored after regeneration. Our findings support that Pd-resin composites are advantageous to water treatment because they allow less frequent catalyst regeneration and enable recycling of products.

5.1 Introduction

Nitrophenols (NPs) are persistent and toxic organic pollutants in the environment.[82, 83] Compared to current treatment methods such as biological treatment,[88] membrane,[95] and adsorption,[202] catalytic hydrogenation has been introduced as a more sustainable method that can convert NPs into more environmentally friendly products, as opposed to transferring contaminants from aqueous phase to solid phase that requires further efforts for regeneration and contaminant treatment.[132, 139, 203, 204]

Catalytic reduction of 4-NP has been widely investigated as a model reaction for examining the catalytic activity of supported metal nanoparticles such as gold, silver, nickel, and platinum, using hydrogen gas or sodium borohydride as the electron donor.[132-137] Among various supported metals, Pd-based catalysts received less attention in 4-NP reduction. Pd-based catalysts supported on supports such as activated carbon and natural and synthetic polymers have been used for hydrogenation of 4-NP.[83, 134-137, 146-148] Despite this, polymeric resins are rarely explored in developing Pd-based catalysts, although they have strong mechanical rigidity, high surface area, enhanced porosity, and tunable pore size distribution and surface functional groups. These properties allow selective removal of a specific contaminant by the resins and enhance deposition of metal nanoparticles in resin porous structures.[30, 31, 56, 59, 60, 100] Pd-based catalysts supported on anion and cation exchange resins were studied for reduction of anions such as nitrate and perchlorate.[122,

[123] Praharaj et al. investigated Au supported on anion exchange resins for 4-NP reduction with a focus on Au nanoparticle immobilization.[112] Neutral resins as support and reduction of organic contaminants such as NPs have not been explored. Additionally, integration of adsorption and reduction processes using Pd-resin composites can be designed for conversion of NPs to less toxic chemicals and in situ regeneration of the products. This can be done by development of Pd-resin catalysts to convert a target contaminant with high adsorption affinity to reduction product(s) with low adsorption affinity. High adsorption affinity is required for removing target contaminants by adsorption and then catalytic reduction, and low adsorption affinity is required to release the reduction products to the aqueous phase to minimize the need for resin regeneration. A similar concept has been used for the regeneration of ion exchange resins used for perchlorate and nitrate removal.[122, 127] However, adsorption and catalytic regeneration performed in subsequent steps. That is, the saturated resin or the regenerant brine was catalytically treated after the completion of adsorption.

In our recent work, Pd-based catalysts supported on neutral and ionic polymeric resins were developed and their catalytic reactivity was investigated for hydrogenation of 4-chlorophenol. The main goal of this work is to evaluate the catalytic activity of the developed catalysts for 4-NP reduction and the possibility of *in situ* regeneration of the resins. Toward this goal, effects of pH, Cl^-, and 4-NP concentration on the reactivity of the catalysts were examined. Reduction and adsorption kinetics were studied at different pHs to evaluate the role of adsorption in the catalytic reduction. Desorption experiments were carried out during 4-NP reduction to measure the amount of 4-NP adsorbed to the catalysts. The desorption results were used to show that 4-NP removal from solution was resulted either from catalytic reduction or from adsorption onto the resins. This would help determine the RDS of 4-NP reduction. Langmuir-Hinshelwood kinetic models developed based on the RDSs were used to study the kinetics of 4-NP reduction. Longevity of the catalysts over eight reaction cycles of 4-NP removal was also investigated. The optimum Pd content was obtained for 4-NP reduction by testing 4-NP catalytic reduction by the catalysts with different Pd contents (0.14, 0.44, and 0.67 wt% Pd MN200).

5.2 Materials and Method

5.2.1 Chemicals and Experimental Methods

Chemicals, materials, and methods including catalyst preparation and characterization, experimental set up, and analytical methods are provided in **Section 4.2**. Catalysts properties are reported in **Table 4-1**. Analytical grade 4-NP was purchased from Sigma-Aldrich and used without further purification. The 4-NP solution was prepared with ultrapure deionized water. The solution pH was adjusted to 3.0 using 1 mol L^{-1} of HCl solution, to 5.0 using 1 mol L^{-1} of acetic acid buffer, and to 7.0 and 9.0 using 1 mol L^{-1} of phosphate buffers. To avoid oxidation of 4-AP, reaction supernatants were immediately analyzed, and desorption experiments were carried out in an oxygen-free anaerobic chamber (N_2:H_2 of 95:5).

The extent of 4-NP disappearance and reaction product formation was monitored by an Agilent Technologies 1200 Infinity Series high-performance liquid chromatography (HPLC) with a Zorbax XDB-C18 column and a diode array detector. A mobile phase consisted of 70% methanol and 30% diluted phosphoric acid at a pH of 3.0 and flow rate of 1 mL min^{-1} was used. The DAD detector was set to 320 nm for 4-NP and

275 and 300 nm for 4-AP. 4-AP standard solutions were analyzed by HPLC to confirm the formation of 4-AP. No other peaks were observed during the reaction, indicating a stoichiometric conversion of 4-NP to 4-AP without formation of other side products.

5.2.2 Data Analysis

The decay of 4-NP by all the catalysts follows pseudo-first-order kinetics (eq 4.4). Rate constants were obtained from the linear regression of the natural log of solution phase concentration versus time plots. The initial turnover frequency values (TOF_0, min^{-1}), i.e., the number of molecules reduced per site per minute, were calculated by dividing the product of the observed rate constant (k_{obs}, min^{-1}) and the initial 4-NP concentration (C_0, mol L^{-1}) by the concentration of surface Pd ($C_{surface\ Pd}$, mol L^{-1}) (eq 4.5)

5.3 Results and Discussion

5.3.1 Mass Transfer

Generally, the possibility of mass transfer limitation can be lowered by increasing mixing rate and decreasing particle size.[196, 197] Because of the same particle size and mixing rate in the reactions, the mass transfer calculation results were similar to hydrodechlorination of 4-CP. The overall liquid-solid mass transfer rate coefficient, k_c, was calculated based on the slip velocity approach of Hariott[191] to investigate the possibility of extra-particle liquid-solid mass transfer. The calculation details are provided in **section 4.2.6**.The calculated values of mass transfer rate constants were smaller than the measured k_{obs} for all the catalysts (**Table 5-1**). Thus, liquid-solid mass transfer rate could limit the reduction kinetics. As mentioned in our previous work, large resin particles (Dp > 500 μm) and underestimation of the contribution of mixing in calculating the slip velocity of particles are the reasons for the observed extra-particle mass transfer. This conclusion was further supported by the greater 4-NP reduction rate constants when the catalyst beads were crushed (data not shown).

Weisz and Prater criterion was calculated in order to evaluate intra-particle mass transfer limitation (calculation details are in **section 4.2.6**). There was no intra-particle mass transfer limitation based on the estimated values of the Weisz and Prater criterion, being less than 1 for all the catalysts (**Table 5-1**). That is, 4-NP reduction on the Pd surface was much slower than its diffusion through the internal pores.

Table 5-1: Extra-particle liquid-solid mass transfer rate constants ($a \times k_c$), experimentally measured reaction rate constants (k_{obs}), and Weisz and Prater criterion ($k_{obs}D_p^2/D_e$) at pH 5 and 9 for 1 wt% Pd/ neutral and anion exchang resins, respectively. These pH values were selected because, as shown later, the resins had the highest reactivity under these pH conditions. Initial 4-NP concentration was 100 μM, the amount of Pd/resin catalysts was 250.0 mg/L.

Resin	$a \times k_c$ (s^{-1})	$k_{obs,\,max}$ (s^{-1})	$\frac{k_{obs} D_p^2}{D_e}$
MN200	5.6×10^{-5}	2.3×10^{-4}	1.2×10^{-1}
XAD4	3.2×10^{-5}	1.7×10^{-4}	3.3×10^{-2}
MN100	7.5×10^{-5}	2.6×10^{-4}	1.3×10^{-1}
IRA910	6.8×10^{-5}	2.3×10^{-4}	1.7×10^{-1}
IRA96	5.3×10^{-5}	6.8×10^{-5}	4.9×10^{-2}

5.3.2 Adsorption Properties

The adsorption results of 4-NP on the resins indicated that the adsorption kinetics by the resins did not significantly change after loading 1 wt % Pd (**Figure 5-1**). The adsorption behavior of 4-NP was similar to other phenolic compounds such as 4-CP. For the neutral resins (i. e., MN200, MN100, and XAD4), the adsorption of 4-NP (pK_a=7.15) decreased when solution pH increased from 3 to 9, indicating that the nondissociated 4-NP had higher adsorption than the dissociated one. In contrast, for the anion exchange resins (i.e., IRA910 and IRA96), with decreasing solution pH from 9 to 3, the adsorbed amount of 4-NP significantly decreased when 4-nitrophenolate concentration decreased. 4-NP was not adsorbed much at pH=3 compared to pH=5 when approximately 40% of 4-NP was adsorbed by IRA910 and IRA96. This could be related to the presence of some 4-nitrophenolate at pH 5, as indicated visually by the pale yellow color of the solution at pH=5. Among the neutral resins, MN200 and MN100 showed higher adsorption affinity toward 4-NP than XAD4 due to their microporous structures. Micropores can enhance adsorption energies due to the superposition of the force fields of the opposite walls.[183] Adsorption of 4-nitrophenolate by IRA910 was higher than by IRA96 because IRA910 is a strong anion exchange resin while IRA96 is a weak anion exchange resin with tertiary amine functional groups (pK_a~6.0). Tertiary amines are in the free base form at pH >pK_a, so the resin loses its ion exchange capacity.

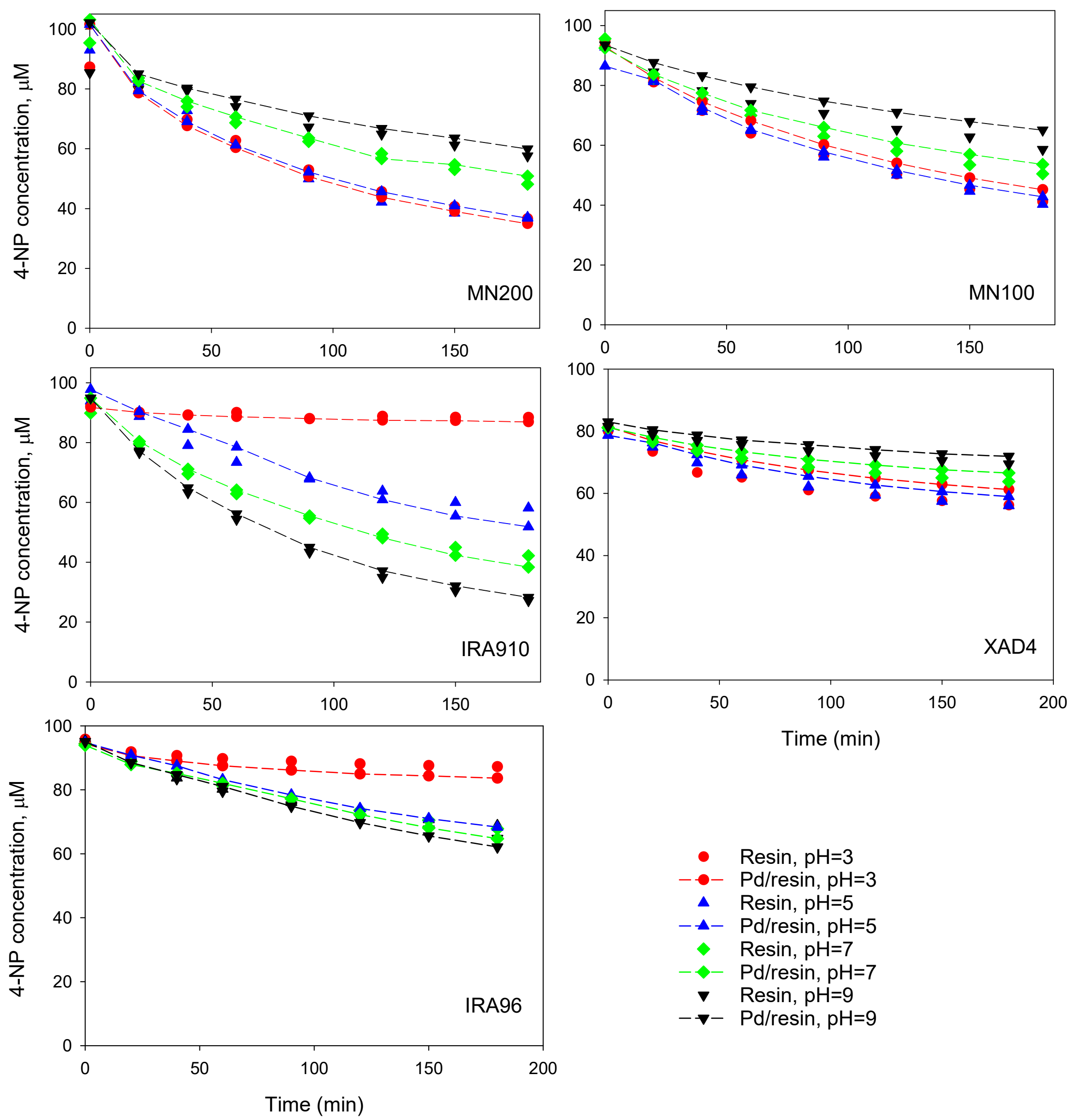

Figure 5-1: Time course of 4-NP adsorption by the resins before and after loading 1 wt % Pd. Experimental conditions: initial 4-NP concentration of 100 µM, 25 mg of resin or Pd/resin, volume of 100 mL.

5.3.3 Generic Reduction Kinetics

The reduction of 4-NP over the catalysts mainly resulted in the formation of 4-aminophenol (4-AP). No other reduction intermediates of 4-NP were observed. The sum of 4-NP and 4-AP was higher than 95% of the initial amount of 4-NP throughout the reaction. For example, **Figure 5-2** shows the time course of reduction of 4-NP, production of 4-AP, and the sum of 4-NP and 4-AP for Pd/XAD4 and Pd/IRA910. This finding suggests negligible adsorption of 4-NP and 4-AP during the reduction of 4-NP by all the catalysts under typical reaction conditions. Negligible adsorption of 4-NP during the reaction was observed over the tested pH range. To confirm this observation, the adsorbed amounts of 4-NP and 4-AP were measured during reaction by conducting reduction experiments in multiple reactors, and sacrificing different reactors for the desorption experiments at different reaction times. Desorption results confirmed that the 4-NP removal from solution by 1 wt% Pd-MN200, MN100, XAD4, and IRA910 was resulted from the reduction of 4-NP rather than from adsorption onto the resins (**Figure 5-3**). Due to the negligible amount of 4-NP adsorbed during the reaction, pseudo-first-order rate constants of 4-NP reduction were obtained from the linear regression of the natural log of 4-NP solution phase concentration versus time (**Figure 5-4**).

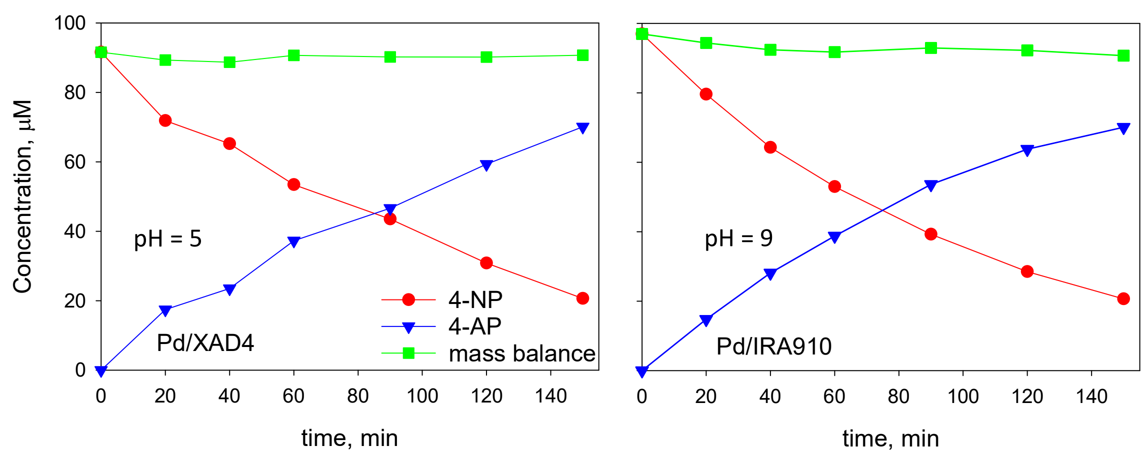

Figure 5-2: Reduction of 4-NP by Pd/XAD4 and Pd/IRA910. Consumption of 4-NP, production of 4-AP and mass balance i.e. the total concentration of 4-NP and 4-AP are shown in the figures. Experimental conditions: initial 4-NP concentration of 100 μM, 25 mg of Pd/resin, pH = 5 and 9, volume of 100 mL.

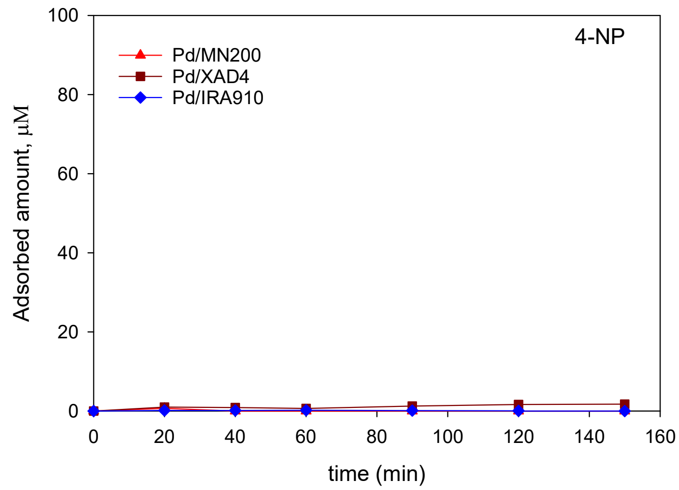

Figure 5-3: Adsorbed amounts of 4-NP onto 1 wt% Pd -MN200 and XAD4 at pH 5 and onto 1 wt% Pd-IRA910 at pH 9 during 4-NP catalytic reduction. The initial concentration of 4-NP was 100 μM, 25 mg of Pd/resin, volume of 100 mL.

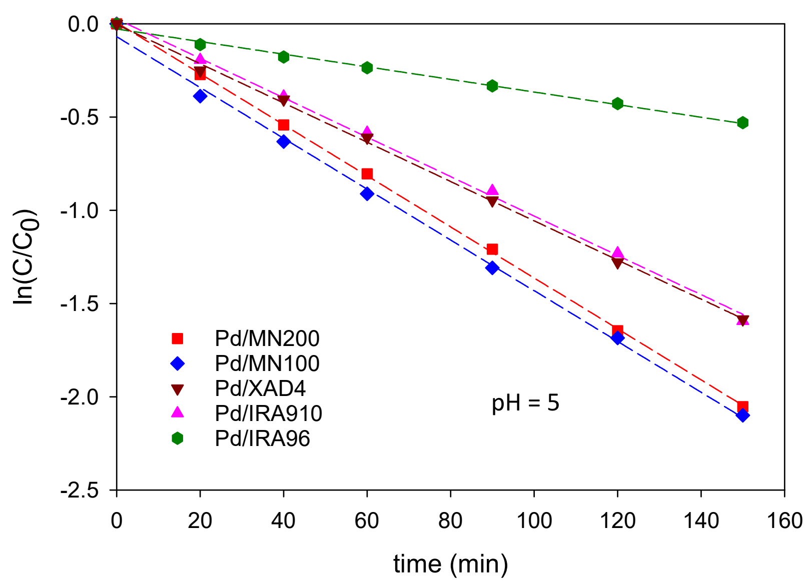

Figure 5-4: Linear correlation between the natural log of 4-NP concentration in solution phase versus time for the experiments of 25 mg of Pd/MN200, MN100, XAD4, IRA910,

and IRA96 at pH 5. The initial concentration of 4-NP was 100µM, solution volume 100 ml.

5.3.4 Effect of pH on Catalytic Activity

The effect of pH on catalytic reactivity was determined for each catalyst. Similar to the adsorption results, strong pH-dependency was observed for 4-NP reduction (**Figure 5-5a**). For all the catalysts supported on the neutral resins, the highest 4-NP reduction rate constant (k_{obs}) was observed at the pH of 3 and 5 when the adsorption capacity was the highest. Similar to the trend for adsorption capacity, k_{obs} for the catalysts decreased with pH increasing from 5 to 9. k_{obs} for the catalysts supported on the AXRs also showed comparable pH dependency as observed for adsorption, i. e., it increased when pH increased from 3 to 9. **Figure 5-6** shows the comparison between adsorption and reduction kinetics at different pHs for 1 wt% Pd-MN200 and IRA910. The initial turnover frequencies (TOF_0) also followed the same trend as observed above (**Figure 5-5b**). These are consistent with the results obtained for the catalytic reduction of 4-CP by the same catalysts, indicating the importance of adsorption in catalytic reduction is likely general for Pd-resin catalysts. Similarly, Vincent et al. showed that the pH dependent activity of catalytic 4-NP reduction by Pd/chitosan was attributed to the sorption behavior of the reactants.[83, 98] Also, it has been reported by many studies that the surface charge (pH_{pzc}) of supported catalysts such as Pd/Al_2O_3, ZrO_2, and Pd/SnO_2 significantly influences on oxyanion reduction kinetics.[205, 206] That is, negatively charged oxyanions can be repelled or attracted to the catalyst surface, depending on the surface charge, resulting in lower and higher reduction rate constants, respectively.

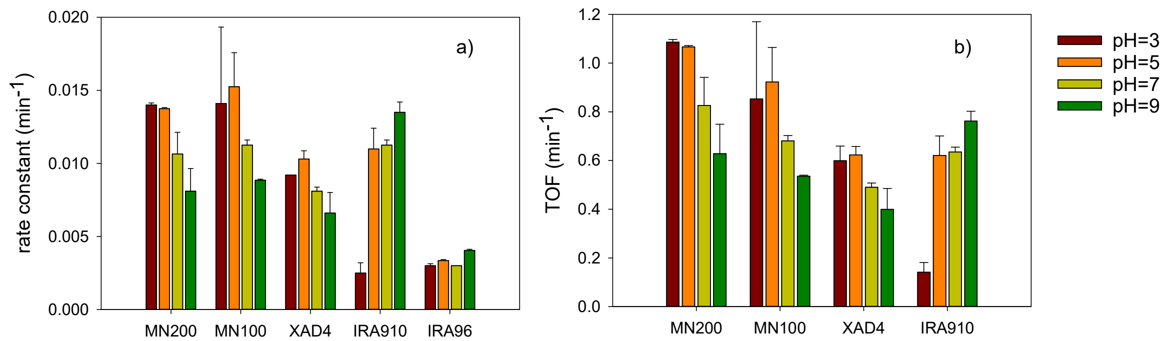

Figure 5-5: Catalytic 4-NP reduction rate constants (a) and initial turnover frequency (TOF_0) (b) over the catalysts at different pHs. Reaction conditions: 4-NP initial concentration of 100 µM, 25 mg of 1 wt% Pd/resin, solution volume of 100 mL.

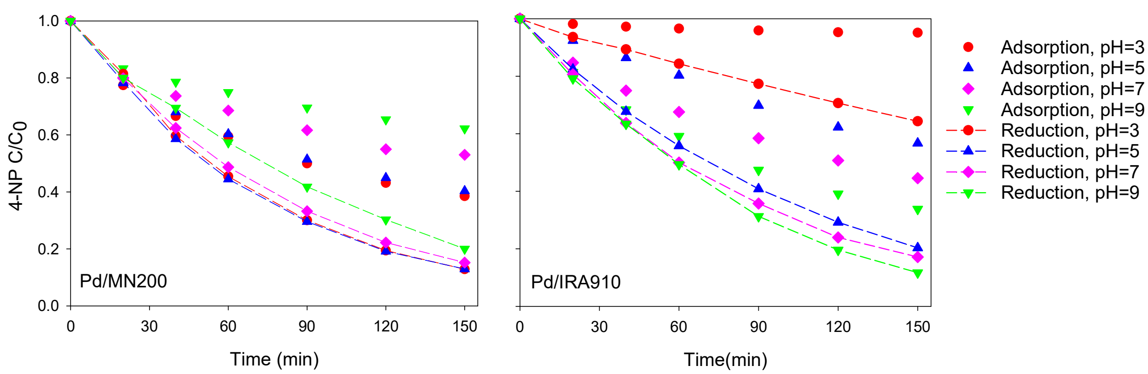

Figure 5-6: Comparing the reduction and adsorption kinetics at different pHs (pH 3, 5, 7, and 9) for the catalysts Pd/MN200 and Pd/IRA910. The adsorption tests were carried out in the absence of hydrogen gas, and the reduction results were based on the loss of 4-NP due to reduction. Reaction conditions: 4-NP initial concentration of 100 µM, 25 mg of 1 wt% Pd/resin, solution volume of 100 mL.

For 1 wt% Pd supported on the neutral resins the highest rate constant of 4-CP reduction at pH=7 is comparable to the highest 4-NP reduction rate constant at pH=5. Same thing is true for AXRs at pH 9 and 11. For neutral resins, 4-NP reduction rate constant is higher than 4-CP reduction rate constant at pH of 5 and 3 that could be related to inhibition effect of HDC products (Cl^- and H^+), however, 4-NP reduction rate constant at pH=9 is higher than 4-CP reduction rate constant at pH=11. For 1 wt% Pd supported on AXRs 4-NP reduction rate constants at pH of 7 and 5 is higher than 4-CP reduction rate constants that could be related to higher 4-nitrophenolate sorption. Generally, 4-CP exhibited higher adsorption affinity to the resins than 4-NP. On the other hand nitro group is strongly electron-withdrawing group and chloro group is weakly electron-withdrawing group. Therefore, it can be concluded that reduction rate shows the net effect of adsorption affinity and reduction potential of the reactants.

5.3.5 Kinetic Modeling and Effect of Initial 4-NP Concentration

Kinetics of 4-NP reduction can be modeled based on the Langmuir-Hinshelwood (LH) model. In this model, both reactants (4-NP and H_2) should be adsorbed onto the catalyst surface (Pd^0). After that, the adsorbed hydrogen dissociates by metallic Pd and converts to adsorbed atomic hydrogen (Pd-H_{ads}). The adsorbed species then react, and the products desorb from the surface. In our recent work, two kinetic models were developed based on the LH model for low and high concentrations where adsorption and surface reaction are the rate determining steps (RDS), respectively (details in **section 4.4.6**).
In order to study the reaction mechanism(s) of 4-NP reduction and to determine the relative contributions of 4-NP adsorption and surface reaction, the effect of initial 4-NP concentration on the catalytic activity was evaluated. The initial reaction rate was measured for varying initial 4-NP concentrations from 0.1 to 7.5 mM. The initial rates were calculated based on the concentration of 4-NP in the supernatant to account for the loss of 4-NP due to both adsorption and reduction. As shown in **Figure 5-7**, increasing initial 4-NP concentration resulted in higher initial rates, and it followed the order of

MN200 >= MN100 > IRA910 over the entire range of the tested concentrations (**Figure 5-7**). The desorption results at the end of each reaction showed that with increasing initial 4-NP concentration, the adsorbed amount of 4-NP on the catalysts also increased (**Table 5-2**). Therefore, similar to the hydrodechlorination of 4-CP, the rate determining step for 4-NP reduction by the catalysts could also have changed from adsorption at low concentrations to surface reaction at high concentrations. Indeed, the two L-H models were fit well to the initial rates of 4-NP reduction for both the high and low concentration ranges tested (eqs 4.15 and 4.22), $R^2 > 0.94$ (**Table 5-3**). For the high concentration range, the values of the equilibrium adsorption constant K_1 for MN200 and MN100 were comparable, agreeing with their similar resin structure and adsorption capacity. K_1 for IRA910 was however smaller, this is because IRA910 has lower adsorption affinity for the nondissociated form of 4-NP at pH=5. The highest value of the intrinsic rate constant k_r was obtained for MN200 and the lowest one for IRA910.

For the low concentration range, the intrinsic rate constant k_r for MN200 was slightly higher than that for MN100 (247.4 vs 234.4 $g_{Pd}^{-1} \cdot hr^{-1}$), and IRA910 has a significantly smaller rate constant (154.9 $g_{Pd}^{-1} \cdot hr^{-1}$). As was discussed earlier in the effect of pH section (**section 5-3-4)**, the adsorption properties of the resins can well explain the above behavior. That is, neutral resins have higher adsorption capacity at pH < pK_a, and consequently higher catalytic activity than AXRs.

Table 5-2: Adsorbed amounts of 4-NP (μM) at the end of the reaction with different initial 4-NP concentrations, 25 mg of 1 wt% Pd/resin at pH=5.

Initial 4-NP concentration mmol L^{-1}	Catalyst		
	Pd/MN200	Pd/MN100	Pd/IRA910
0.1	0.0	0.0	0.0
0.5	0.4	0.5	0.0
1.0	0.6	0.6	9.6
2.5	219.1	168.5	49.6
5.0	413.1	365.5	66.4
7.5	509.6	443.0	88.1

Table 5-3: Fitting parameters of the L-H model for $C_0 > 1.0$ mM and < 1.0 mM for 4-NP reduction by 25 mg of 1 wt% Pd/resin at pH=5.

Catalyst	High concentration		Low concentration
	k_r, mmol/g_{Pd}.hr	K_1 L $mmol^{-1}$	k_r 1/g_{Pd}.hr
Pd/MN200	3567	0.08	247.4
Pd/MN100	2940	0.09	234.4
Pd/IRA910	2505	0.05	154.9

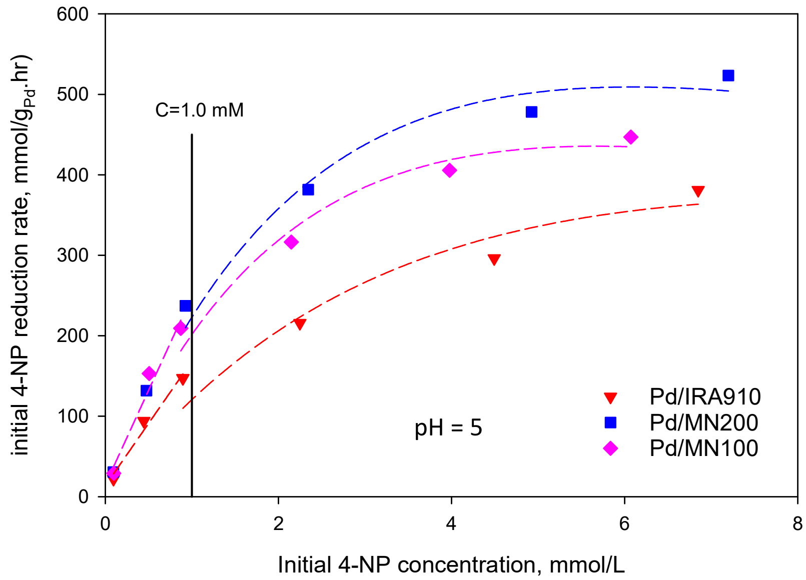

Figure 5-7: Influence of initial 4-NP concentration on the initial rate of 4-NP reduction. Dashed lines are fitting curves to the two kinetic models C_0 <1.0 mM: eq 4.22 and C_0 >1.0 mM: eq 4.15. Experimental conditions: pH=5, 25 mg of 1 wt% Pd-resin of catalyst loading.

5.3.6 Effect of Cl^-

To investigate the poisoning effect of Cl^- on the catalysts, the reactivity of 1 wt% Pd-MN200 and -IRA910 was examined in aqueous solution with varying concentrations of NaCl from 0 to 2 mol L^{-1} at pH 5 (**Figure 5-8**). Similar to 4-CP reduction by the same catalysts in the presence of Cl^-, 4-NP reduction rate constant decreased with increasing NaCl concentration from 0 to 0.1 mol L^{-1}. However, the decrease was more significant for IRA910 than for MN200 (52% vs 17% reduction in the rate constant). As showed in our recent work, the support structure has significant influence on the poisoning effect of Cl^-. MN200 with a neutral structure (hydrophobic) was more successful than anion exchange resin IRA910 (hydrophilic) to resist the inhibition effect of Cl^-. This is due to less sorption of Cl^- onto MN200. It has been reported that hydrophobic zeolites and encapsulated Pd/γ-Al_2O_3 with hydrophobic silicone polymers are more resistant to catalyst fouling by excluding Cl^- or sulfide. This will prevent both the formation of Pd species like $PdCl_3^-$ and $PdCl_4^{2-}$, which are much less reactive than Pd^{n+} species, and leaching of active Pd sites.[130, 190, 207, 208]

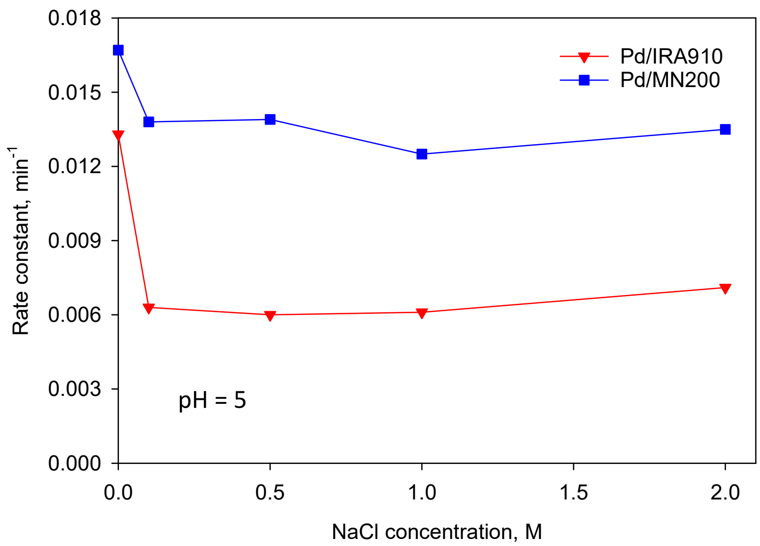

Figure 5-8: Effect of NaCl concentration on the reactivity of the catalysts in reduction of 4-NP. Initial concentration of 4-NP = 0.1 mmol L^{-1}, pH = 5, 25 mg of 1 wt% Pd-resin.

5.3.7 Effect of Pd Content

0.14, 0.44, and 0.67 wt% Pd/MN200 were prepared to investigate the effect of Pd content on the catalytic activity. In contrast to 4-CP reduction by 0.14 and 0.44 wt% Pd where 4-CP was significantly adsorbed onto the catalysts during the reaction, 4-NP was only slightly adsorbed onto the same catalysts (**Figure 5-9a**). Neither 4-CP nor 4-NP was adsorbed onto 0.67 wt% Pd catalyst during the reaction. The rate constants of 4-NP reduction at pH 5 by 0.14 and 0.44 wt% Pd catalysts were greater than those of 4-CP reduction at pH 7 (0.011 vs 0.004 min^{-1} by 0.14 wt%, and 0.014 vs 0.01 min^{-1} by 0.44

wt%). However, comparable rate constants were observed for reduction by 0.67 wt% Pd (0.014 vs 0.013 min^{-1}). It can be concluded that lower catalytic activity resulted in higher amounts of the reactant adsorbed during reaction. This higher reactivity could be related to higher reduction potential of 4-NP than 4-CP. The above findings can be well explained by the L-H mechanism: for 0.14 wt% Pd catalyst, surface reaction is the RDS due to less available Pd sites and hence slow reaction, and for 0.44 and 0.67 wt% Pd catalysts, adsorption is the RDS due to a non-detectable amount of 4-NP adsorbed during the reaction.

The 4-NP reduction rate constants for the three catalysts are shown in **Figure 5-9b**. The amount of 4-NP adsorbed during the reaction was excluded from the total 4-NP loss when calculating the reduction rate constants. The apparent first order rate constant slightly increased with increasing Pd content from 0.14 to 0.44 wt%. Further increase in Pd content from 0.44 wt% to 0.67 wt% did not change the rate constant value. Thus, high Pd content is not required to increase the catalytic activity. The optimum Pd content is therefore the point where the RDS changes from surface reaction to adsorption, i. e., about 0.44 wt% Pd at pH 5, while for 4-CP, it was slightly higher than 0.44 wt% Pd at pH 7. As showed earlier, catalytic reactivity decreased with increasing pH (pH > 5), this was consistent with decreasing adsorption affinity at high pHs. Thus, it is likely that the switch in the RDS from surface reaction to adsorption will take place at lower Pd content for higher pHs (pH of 7 and 9). That is, the optimum Pd content would probably be less than 0.44 wt% at pH > 5. Similar scenario can be true for 4-CP reduction at pH > 7 because the decrease in the catalytic reactivity was due to the decrease in 4-CP adsorption affinity to the catalysts. At pH < 7, a higher optimum Pd content is needed due to inhibition of active sites by the reduction products (H^+ and Cl^-) when the adsorption affinity of 4-CP is constant.

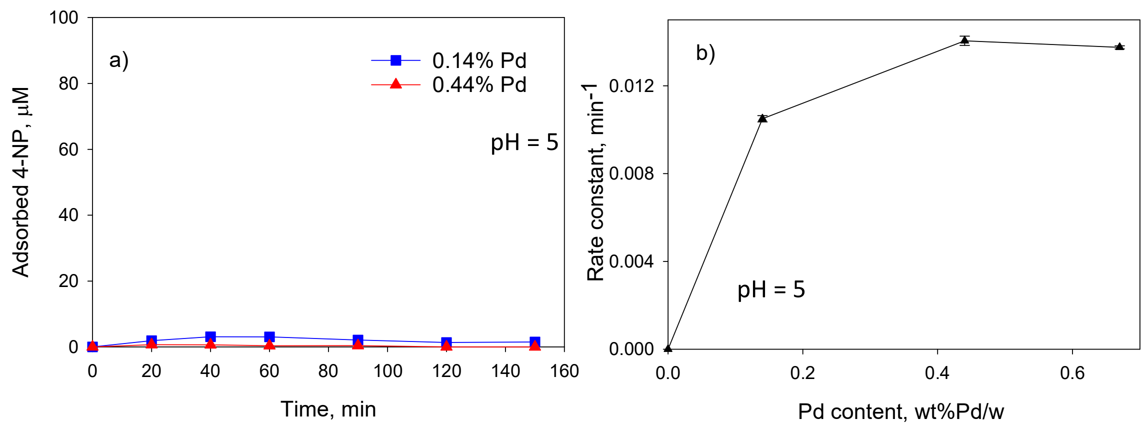

Figure 5-9: a) Amount of 4-NP adsorbed on 0.14 and 0.44 wt%Pd/MN200 during the reaction and b) 4-NP reduction rate constants for 0.14, 0.44 and 0.67 wt%Pd/MN200. Reaction conditions: pH 5, initial 4-NP concentration of 100 µM, and 25 mg of Pd/resin.

5.3.8 Catalyst Longevity

The longevity of the catalysts was examined by employing the catalysts in eight reaction cycles when 4-NP was repeatedly spiked to the same reactor every three hours for eight times. The initial concentration of 4-NP was adjusted to 1 mmol L^{-1} for each cycle. This severe testing condition was employed to test the longevity of the catalysts under the worst case scenario. Concentrations of 4-NP and 4-AP were measured after each three-hour reaction. The catalytic activity of the neutral resins started decreasing after the first run (**Table 5-4**); after four runs, it was less than half of the initial activity. IRA910 did not show any catalytic activity after five runs. Desorption of the catalysts after the eight consecutive runs showed some adsorption of 4-NP and 4-AP onto the catalysts, although the majority of the formed 4-AP was still in the solution phase (more than 98%) (**Table 5-5**). 4-AP is completely or partly protonated (ionic form) at pH of 3 and 5 (pK_a=5.48 and 10.46) so that it can be adsorbed by the AXRs, and it is in the neutral form at pH of 7 and 9 so that it can be adsorbed by the neutral resins. A significant amount of 4-NP was adsorbed by IRA910 at the reaction pH of 9 as compared to the other catalysts, this can explain the complete loss in IRA910's activity after five runs. Adsorption of 4-NP and 4-AP was not determined after the first run, however, both 4-AP and 4-NP were adsorbed onto the resins after eight runs. Therefore, the activity loss can be related to the accumulation of 4-NP and 4-AP in the catalysts. Indeed, as shown in **Table 5-4**, the neutral resins regained ca. 90 percent of the original reactivity after regeneration, while the reactivity of IRA910 actually increased. As reported in our recent work, IRA910 showed weak mechanical rigidity because IRA910 beads were easily broken by the magnetic stir bars used for stirring. Crushed IRA910 showed higher reactivity after regeneration than the original one due to the mitigation of the external mass transfer limitation. It should be mentioned that in real applications, catalysts are always in contact with fresh influent, therefore, the likelihood of product accumulation should be much smaller, and consequently longevity of catalysts should be much longer.

Table 5-4: Removal efficiency, i.e., % of reduction of 1 mM 4-NP by 25 mg of the catalysts at pH 5 for 1 wt% Pd-MN200, MN100, and XAD4, and at pH 9 for 1 wt% Pd-IRA910.

Cycle	MN200	MN100	XAD4	IRA910
1	87.4	80.1	78.3	66.9
2	72.3	71.5	74.3	47.8
3	70.3	71.9	75.2	62.6
4	58.2	50.4	54.9	29.2
5	53.3	52.4	69.7	20.2
6	44.3	56.1	65.0	0.0
7	41.5	43.5	59.6	0.0
8	32.1	28.0	54.4	0.0
after regeneration	74.0	73.8	74.2	92.9

Table 5-5: The adsorbed amounts of 4-AP and 4-NP (μM) after one and eight runs and 4-AP concentrations in solution phase. Reaction conditions: 25 mg catalysts, pH 5 for 1 wt% Pd-MN200, MN100, and XAD4, and pH 9 for 1 wt% Pd-IRA910.

Cycle	Adsorbed 4-NP		Adsorbed 4-AP		4-AP in solution phase	
	1st run	8th run	1st run	8th run	1st run	8th run
MN200	N.D.	50.6	N.D.	83.6	661.9	5772.9
MN100	N.D.	34.1	N.D.	66.8	648.2	6861.0
XAD4	N.D.	39.5	N.D.	N.D.	708.3	6099.6
IRA910	N.D.	364.7	7.0	53.7	447.3	3780.5

N.D.: not determined

5.3.9 Effect of Resin Support

Our results indicated that resin support has significant influence on loading Pd nanoparticles and on the catalytic activity. Higher Pd contents were obtained for resins MN200, MN100, and IRA910 than XAD4 and IRA96. This is because of stronger adsorption of the Pd precursors by microporous (MN200 and MN100) and strong anion exchange (IRA910) resins than by macroporous (XAD4) and weak anion exchange (IRA96) resins. As a result, higher reactivity was observed for MN200, MN100, and IRA910. Similar to 4-CP reduction, the catalytic reduction of 4-NP was dependent on the adsorption capacity of the resins. Anion exchange resin IRA910 showed better catalytic reactivity for the ionic form of 4-NP and neutral resins exhibited the highest reactivity for the neutral form of 4-NP. Neutral resins exhibited more resistant to the inhibition effect of Cl^-, and better longevity under cyclic usage. In many studies, catalyst deactivation by Cl^- has been observed for Pd-based catalysts such as Pd/C and Pd/Al_2O_3, two common Pd-based catalysts, although the extent of deactivation was different.[130, 209] For example, Pd/Al_2O_3 was found to be more resistant to Cl^- due to stronger metal/support interactions, however, activated carbon has a hydrophobic structure that helps excluding Cl^- form catalyst surface.[209] Therefore, polymeric resins are beneficial for developing resistant Pd-based catalysts since they can be tailor synthesized to provide stronger metal support binding and expel inhibiting agents.

5.4 Conclusions

In this study, we established that Pd-based catalysts supported on polymeric resins are efficient for hydrogenation of 4-NP. This is a promising method for stoichiometric conversion of 4-NP, a priority contaminant, to 4-AP, an important intermediate in industrial and pharmaceutical reactions, and for *in situ* regeneration processes. Several factors were studied to investigate 4-NP reduction and to determine the rate determining step, including intra and extra particle mass transfer limitations, effect of pH, and effects of initial 4-NP concentration, Cl^-, and Pd content. Extra particle mass transfer limitation was observed for all the catalysts, this is mainly due to the large particle size of the resin beads. Adsorption was a key factor controlling the catalytic activity of 4-NP reduction; the highest reactivity of the neutral resins was observed at pH lower than pK_a where the protonated form of 4-NP has higher adsorption affinity, and that of the anion exchange resins was observed at pH higher than pK_a where 4-nitrophenolate has higher adsorption affinity. RDS of the reaction changed from adsorption at low concentrations where no 4-NP adsorption was detected during reaction to surface reaction at high concentrations where 4-NP adsorbed onto the catalysts during reaction. The optimum Pd content was determined to be 0.44 wt% by studying the RDS of 4-NP reduction at pH 5 by 0.14, 0.44, and 0.67 wt% Pd-MN200. Neutral resins exhibited more resistance to the inhibition effect of Cl^- due to lower sorption of Cl^- onto neutral resins than onto anion exchange resin. Negligible adsorption of 4-AP onto the catalysts suggests the applicability of the developed catalysts for production and *in situ* regeneration of 4-AP. Despite the accumulation of 4-AP and 4-NP over multiple cycles to result in catalytic deactivation, frequent contact of fresh influent with the catalysts can prevent significant accumulation of reaction products.

The present study shows that combination of adsorption and catalytic treatment is a promising technology with smaller environmental impacts for simultaneous removal of target contaminants and in situ regeneration of the spent adsorbent. Regeneration of the spent adsorbent that produces large amounts of secondary waste can be largely avoided by catalytic reduction of the adsorbed compound. Polymeric resins are great support for developing Pd-based catalysts because they can be tailor-made to target specific compounds, improve catalyst resistance to inhibition effect of water constituents such as halide ions, and extend catalyst longevity.

CHAPTER 6

CONCLUSIONS AND FUTURE WORKS

This study has obtained mechanistic understanding of sorption of a broad spectrum of cationic organic contaminants by two cation exchange resins and provided predictive models for estimating sorption capacity of cations by the resins. It has also provided mechanistic insight into the hydrogenation of 4-CP and 4-NP and the possibility of *in situ* regeneration by the synthetized Pd-resin composites.

6.1 Sorption Mechanisms for the Removal of Cationic Organic Contaminants by Cation Exchange Resins

Cationic compounds were removed mainly by an ion exchange mechanism (electrostatic interactions), however, there are many factors contributing to the selectivity of the ions toward the resins. They include hydrophobicity and types of functional groups of the compound, size and nature of the resin functional groups, dielectric constant of the solvent, and moisture content and polymer matrix of the resin. It has been shown that nonelectrostatic interactions between the nonpolar moieties (NPM) of an organic ion and those of the resin matrix increased the sorption affinity. These nonelectrostatic interactions include $\pi-\pi$ interactions between the aromatic rings of the resin matrix and the aromatic cations, dipole−dipole and dipole−induced dipole interactions between halogenated compounds and the resin. A general preference of aromatic cations > halogenated aliphatic cations > aliphatic cations > neutral solutes was observed based on the amount sorbed by the resins. In general, microporous resins such as MN500 showed higher sorption capacities due to the enhanced sorption energy associated with micropores.

The presence of solvent-associated interactions complicated the comparison between the selectivity of different compounds, therefore, the gas phase conversion, which only considers solute-sorbent interactions, provided a better insight into solute−sorbent interactions.

6.2 Predictive Model for the Sorption of Cationic Organic Contaminants by the Cation Exchange Resins

Polyparameter linear free energy relationships (pp-LFERs) were used to predict sorbed concentrations of cations by both resins, and to quantitatively examine the contributions of various interactions to the overall selectivity of the cations. pp-LFERs analysis for both resins suggested that selectivity was mainly promoted by electrostatic interactions and nonelectrostatic interactions, including dipolar/polarizability effects, induced dipole, and H-bond accepting.

Two predictive models were constructed for the two cation exchange resins based on the pp-LFERs regression results at different equilibrium sorbed concentration values. The results indicated that the predictive models were able to estimate the sorbed concentrations well for both resins. The ability of the models to predict the sorbed amounts of similar compounds was validated for three test compounds, where the predicted sorbed concentrations of the test compounds were within the range of errors obtained for the training set compounds. The models were further expanded to predict the sorbed concentrations of compounds that can undergo protonation/deprotonation reactions under changes of pH. Overall, the predictive models for different resins allows selection of an appropriate resin for a given contaminant without conducting trial experiments, which are much more time-consuming and labor-intersive.

6.3 Catalytic Activity of the Synthesized Pd-Resin Catalysts

Our results indicated that resin properties such as BET surface area, ion exchange capacity, and adsorption capacity did not change significantly after loading Pd. TEM and EDS results of the catalysts illustrated that Pd nanoparticles were highly dispersed in the porous structures of the resins. The X-ray diffraction (XRD) patterns of the catalysts were in agreement with the Pd^0 crystal reference pattern and Pd^0 was the only observed crystalline phase.

External particle mass transfer limitation was observed for all the catalysts. It could be related to the large particle sizes of the resins and underestimation of mixing rate in calculation of slip velocity. External (liquid-solid) and inter particle mass transfer control adsorption of the reactant to the catalyst surface.

In order to evaluate the catalytic activity of the developed catalysts, the effects of pH, Cl^-, initial concentration of the reactant and Pd content, and catalyst stability were examined. Similar adsorption and reduction kinetic were observed for hydrogenation of both 4-NP and 4-CP by the catalysts. That is, faster reduction and adsorption were observed for the catalysts supported on the neutral resins (MN200, MN100, and XAD4) at pH < pK_a, where the non-dissociated forms (i.e., protonated forms) of the target compounds have a higher adsorption affinity than the dissociated forms (i.e., anionic forms). For the catalysts supported on the anion exchange resins (i.e., IRA910 and IRA96), both reduction and adsorption were faster at pH > pK_a.

The initial reduction rates of 4-NP and 4-CP increased with increasing initial reactant concentration for all the catalysts, and it followed the trend of MN200 >= MN100 > IRA910 over the entire range of the tested concentrations. The desorption results at the end of each reaction showed that when the initial reactant concentration was low (< 1.5 mM), no detectable amount of the reactant was adsorbed. With increasing initial reactant concentration to beyond 1.5 mM, the amount of the reactant adsorbed on the catalysts during reactions also increased. Therefore, the rate determining step for hydrogenation by the catalysts changed from adsorption at low concentrations to surface reaction at high concentrations. The two kinetic models developed based on the Langmuir-Hinshelwood model for low and high concentration regions confirmed the above observation, and also indicated the importance of adsorption in the catalytic activity.

Cl^- had a poising effect on the catalysts supported on both neutral and ionic resins, however, this effect was more significant on the ionic resins. The decrease in the rate constant of hydrogenation of 4-CP and 4-NP by IRA910 when NaCl concentration was increased from 0 to 0.1 M was 70% and 52%, respectively, but it was only 20% for MN200. Sorption of Cl^- by the anion exchange resins and the subsequent formation of more $PdCl_3^-$ and $PdCl_4^{2-}$ species (non-reactive as opposed to Pd^{n+}) resulted in the lower resistance of the ionic resins to the poising effect of Cl^-.

The activity of MN200 catalysts with different Pd loadings was investigated to obtain the optimum Pd content. For this purpose, the catalysts with nominal loadings of 0.2, 0.5, and 1 wt% of Pd were prepared. Our results showed that 4-CP and 4-NP were adsorbed onto the 0.2 and 0.5 wt% Pd catalysts during hydrogenation reaction, with the adsorbed amount being higher for the 0.2 wt% Pd catalyst. However, the amount of 4-CP adsorbed onto the catalysts was much higher than that of 4-NP adsorbed. The observed rate constants for HDC of 4-CP by 0.2 and 0.5 wt% Pd catalysts were lower than those for 4-NP reduction. None of the reactants were adsorbed onto 1 wt% Pd catalyst during the reaction. Comparable rate constants were observed for reduction of both reactants by 1 wt% Pd catalyst. Therefore, it can be concluded that surface reaction is the RDS for hydrogenation of the reactants by 0.2 and 0.5 wt% Pd catalysts, and adsorption is the RDS for 1 wt% Pd catalyst. The apparent first order rate constants significantly increased with increasing Pd content from 0.2 to 0.5 wt%, and slightly from 0.5 to 1% Pd. Thus, the optimum Pd content is around 0.5 wt% when the RDS changes from surface reaction to adsorption.

The activity of the catalysts decreased over eight reaction cycles due to the adsorption of the reduction products, however, regeneration of the used catalysts largely restored the catalytic activity.

6.4 Environmental Significance

Understanding the molecular interactions between adsorbents and solutes is vital to select an appropriate adsorbent for a given organic contaminant. This is particularly the case for polymeric adsorbents that can be tailor-made by adjustment of resin structure during synthesis to selectively remove a specific organic compound. pp-LFER techniques enable us to identify the predominant interactions in sorption of a wide range of OCs by polymeric resins. We expect this method to be applicable to adsorption of various OCs by a variety of adsorbents, and to other chemical industries that involve separation processes. Also, the developed models provided a valuable tool to predict the adsorption behavior of other uninvestigated OCs on polymeric adsorbents based on their chemical parameters.

This study helps to develop sustainable treatment technologies for removal of toxic contaminants from water and wastewater effluents. The integration of catalytic processes and adsorption is advantageous because smaller environmental impacts, lower cost, and higher efficiency are expected compared to either adsorption or catalytic treatment alone. Regeneration of spent adsorbents that produces large amounts of secondary waste stream can be largely avoided by catalytic reduction of the adsorbed compounds and conversion to less toxic products. Furthermore, adsorption enhances catalytic activity and utilizes the use of metal nanoparticles.

6.5 Future Work

The current research can be extended further to advance and apply the findings of this study. More comprehensive predictive models can be constructed using an extensive set of contaminants that are representative of different classes of compounds, including emerging contaminants. This work has focused on the removal of cationic compounds by cation exchange resins. The predictive modeling and examination approach could further be applied to other resins and adsorbents to address a wider range of OCs with different chemical properties.

For Pd-based catalysis, our results indicated that further research is required to improve the developed kinetic models, enhance resistance of the resin-Pd catalysts to the poising effect of Cl^- and other co-solutes, and increase stability of the catalysts. Additionally, further work is required to investigate the application of the developed catalysts to catalytic reduction of other contaminants, examine the longevity of the catalysts in treating real wasteaters, optimize operating factors in column studies for large-scale applications, develop new Pd-based catalysts supported on resins with different structures, and improve catalytic reactivity of the catalysts.

When developing the kinetic models, adsorption of the reduction products at the beginning of the reaction and mass transfer limitation were ignored. Thus, a more realistic kinetic model is necessary to capture their impacts. pH plays a vital role in the catalytic reactivity and adsorption affinity of the resin-Pd catalysts. To provide a better understanding of catalytic hydrogenation, the kinetic models should be further examined for the activity results at different pHs. Results from this study showed that resin structure can significantly control reactivity, stability and the poising effect of Cl^-. Thus, new Pd-based catalysts supported on resins with different matrix structures and functional groups should be examined for this purpose. It should be noted that in designing new Pd/resins for reduction of OCs, it is important to select a resin that has minimum adsorption affinity to the possible products in order to improve stability and reactivity of the catalysts.

REFERENCES CITED

1. Hoke, J. B.; Gramiccioni, G. A.; Balko, E. N., Catalytic hydrodechlorination of chlorophenols. *Appl Catal B: Environ* **1992,** *1*, (4), 285-296.

2. Calvo, L.; Gilarranz, M.; Casas, J.; Mohedano, A.; Rodríguez, J., Hydrodechlorination of 4-chlorophenol in water with formic acid using a Pd/activated carbon catalyst. *J. Hazard. Mater.* **2009,** *161*, (2), 842-847.

3. Gupta, V.; Ali, I.; Saini, V., Removal of chlorophenols from wastewater using red mud: an aluminum industry waste. *Environ. Sci. Technol.* **2004,** *38*, (14), 4012-4018.

4. Lan, Y.; Yang, L.; Zhang, M.; Zhang, W.; Wang, S., Microreactor of Pd nanoparticles immobilized hollow microspheres for catalytic hydrodechlorination of chlorophenols in water. *ACS Appl Mater Inter* **2009,** *2*, (1), 127-133.

5. Lipczynska-Kochany, E., Degradation of aqueous nitrophenols and nitrobenzene by means of the Fenton reaction. *Chemosphere* **1991,** *22*, (5), 529-536.

6. Tan, I.; Hameed, B.; Ahmad, A., Equilibrium and kinetic studies on basic dye adsorption by oil palm fibre activated carbon. *Chem. Eng. J.* **2007,** *127*, (1), 111-119.

7. Spadaro, J. T.; Gold, M. H.; Renganathan, V., Degradation of azo dyes by the lignin-degrading fungus Phanerochaete chrysosporium. *Appl. Environ. Microbiol.* **1992,** *58*, (8), 2397-2401.

8. Fernandez-Cornejo, J.; Nehring, R. F.; Osteen, C.; Wechsler, S.; Martin, A.; Vialou, A., Pesticide Use in US Agriculture: 21 Selected Crops, 1960-2008. *USDA-ERS Economic Information Bulletin* **2014**, (124).

9. Agency, E. E., Environmental Signals 2000: Chapter 6 Agriculture. **(2011)**

10. Pal, A.; Gin, K. Y.-H.; Lin, A. Y.-C.; Reinhard, M., Impacts of emerging organic contaminants on freshwater resources: review of recent occurrences, sources, fate and effects. *Sci. Total Environ.* **2010,** *408*, (24), 6062-6069.

11. Cai, Q.-Y.; Mo, C.-H.; Wu, Q.-T.; Zeng, Q.-Y.; Katsoyiannis, A., Occurrence of organic contaminants in sewage sludges from eleven wastewater treatment plants, China. *Chemosphere* **2007,** *68*, (9), 1751-1762.

12. Kolpin, D. W.; Furlong, E. T.; Meyer, M. T.; Thurman, E. M.; Zaugg, S. D.; Barber, L. B.; Buxton, H. T., Pharmaceuticals, hormones, and other organic wastewater contaminants in US streams, 1999-2000: A national reconnaissance. *Environ. Sci. Technol.* **2002,** *36*, (6), 1202-1211.

13. J.S. Tertuliani, D. A. A., E.T. Furlong, M.T. Meyer, S.D. Zaugg, and G.F. Koltun, Occurrence of organic wastewater compounds in the tinkers creek watershed and two other tributaries to the Cuyahoga river, northeast Ohio. *U.S. Geological Survey* **2008**.

14. Katz, A. L. F. a. B. G., Occurrence of organic compounds in source and finished samples from seven drinking-water treatment facilities in Miami-Dade county, Florida, 2008. *U.S. Geological Survey* **2008**.

15. Focazio, M. J.; Kolpin, D. W.; Barnes, K. K.; Furlong, E. T.; Meyer, M. T.; Zaugg, S. D.; Barber, L. B.; Thurman, M. E., A national reconnaissance for pharmaceuticals and other organic wastewater contaminants in the United States—II) Untreated drinking water sources. *Sci. Total Environ.* **2008,** *402*, (2), 201-216.

16. Bao, L.-J.; Maruya, K. A.; Snyder, S. A.; Zeng, E. Y., China's water pollution by persistent organic pollutants. *Environ. Pollut.* **2012,** *163*, 100-108.

17. Ashton, D.; Hilton, M.; Thomas, K., Investigating the environmental transport of human pharmaceuticals to streams in the United Kingdom. *Sci. Total Environ.* **2004,** *333*, (1), 167-184.

18. Matsushita, M.; Kuramitz, H.; Tanaka, S., Electrochemical oxidation for low concentration of aniline in neutral pH medium: application to the removal of aniline based on the electrochemical polymerization on a carbon fiber. *Environ. Sci. Technol.* **2005,** *39*, (10), 3805-3810.

19. Hameed, B.; Chin, L.; Rengaraj, S., Adsorption of 4-chlorophenol onto activated carbon prepared from rattan sawdust. *Desalination* **2008,** *225*, (1), 185-198.

20. Huang, C.; Dong, C.; Tang, Z., Advanced chemical oxidation: its present role and potential future in hazardous waste treatment. *Waste Manage. (Oxford)* **1993,** *13*, (5), 361-377.

21. Kormann, C.; Bahnemann, D.; Hoffmann, M. R., Photolysis of chloroform and other organic molecules in aqueous titanium dioxide suspensions. *Environ. Sci. Technol.* **1991,** *25*, (3), 494-500.

22. Czaplicka, M., Sources and transformations of chlorophenols in the natural environment. *Sci. Total Environ.* **2004,** *322*, (1), 21-39.

23. Yoon, Y.; Westerhoff, P.; Snyder, S.; Song, R.; Levine, B. In *A review on removal of endocrine-disrupting compounds and pharmaceuticals by drinking water treatment processes*, Water Quality Technology Conference, 2002; 2002.

24. Bolong, N.; Ismail, A.; Salim, M. R.; Matsuura, T., A review of the effects of emerging contaminants in wastewater and options for their removal. *Desalination* **2009,** *239*, (1), 229-246.

25. Walker, G.; Weatherley, L., Adsorption of acid dyes on to granular activated carbon in fixed beds. *Water Res.* **1997,** *31*, (8), 2093-2101.

26. Dutta, M.; Baruah, R.; Dutta, N., Adsorption of 6-aminopenicillanic acid on activated carbon. *Sep. Purif. Technol.* **1997,** *12*, (2), 99-108.

27. Mitch, W. A.; Sharp, J. O.; Trussell, R. R.; Valentine, R. L.; Alvarez-Cohen, L.; Sedlak, D. L., N-nitrosodimethylamine (NDMA) as a drinking water contaminant: a review. *J Environ Eng Sci* **2003,** *20*, (5), 389-404.

28. Matatov-Meytal, Y. I.; Sheintuch, M., Catalytic abatement of water pollutants. *Ind. Eng. Chem. Res.* **1998,** *37*, (2), 309-326.

29. Sadiq, R.; Rodriguez, M. J., Disinfection by-products (DBPs) in drinking water and predictive models for their occurrence: a review. *Sci. Total Environ.* **2004,** *321*, (1), 21-46.

30. Kunin, R., The use of macroreticular polymeric adsorbents for the treatment of waste effluents. *Pure Appl. Chem.* **1976,** *46*, (2-4), 205-211.

31. Kennedy, D. C., Treatment of effluent from manufacture of chlorinated pesticides with a synthetic, polymeric adsorbent, Amberlite XAD-4. *Environ. Sci. Technol.* **1973,** *7*, (2), 138-141.

32. Hurley, K. D.; Shapley, J. R., Efficient heterogeneous catalytic reduction of perchlorate in water. *Environ. Sci. Technol.* **2007,** *41*, (6), 2044-2049.

33. Shuai, D.; Chaplin, B. P.; Shapley, J. R.; Menendez, N. P.; McCalman, D. C.; Schneider, W. F.; Werth, C. J., Enhancement of oxyanion and diatrizoate reduction kinetics using selected azo dyes on Pd-based catalysts. *Environ. Sci. Technol.* **2010,** *44*, (5), 1773-1779.

34. Schreier, C. G.; Reinhard, M., Catalytic hydrodehalogenation of chlorinated ethylenes using palladium and hydrogen for the treatment of contaminated water. *Chemosphere* **1995,** *31*, (6), 3475-3487.

35. Chaplin, B. P.; Reinhard, M.; Schneider, W. F.; Schüth, C.; Shapley, J. R.; Strathmann, T. J.; Werth, C. J., Critical review of Pd-based catalytic treatment of priority contaminants in water. *Environ. Sci. Technol.* **2012,** *46*, (7), 3655-3670.

36. Munakata, N.; Reinhard, M., Palladium-catalyzed aqueous hydrodehalogenation in column reactors: Modeling of deactivation kinetics with sulfide and comparison of regenerants. *Appl Catal B: Environ* **2007,** *75*, (1), 1-10.

37. Lowry, G. V.; Reinhard, M., Pd-catalyzed TCE dechlorination in groundwater: Solute effects, biological control, and oxidative catalyst regeneration. *Environ. Sci. Technol.* **2000,** *34*, (15), 3217-3223.

38. Low, G. K.; McEvoy, S. R.; Matthews, R. W., Formation of nitrate and ammonium ions in titanium dioxide mediated photocatalytic degradation of organic compounds containing nitrogen atoms. *Environ. Sci. Technol.* **1991,** *25*, (3), 460-467.

39. Cheng, H.; Xu, W.; Liu, J.; Wang, H.; He, Y.; Chen, G., Pretreatment of wastewater from triazine manufacturing by coagulation, electrolysis, and internal microelectrolysis. *J. Hazard. Mater.* **2007,** *146*, (1), 385-392.

40. Guo, L.; Li, G.; Liu, J.; Yin, P.; Li, Q., Adsorption of aniline on cross-linked starch sulfate from aqueous solution. *Ind. Eng. Chem. Res.* **2009,** *48*, (23), 10657-10663.

41. Georgi, A.; Kopinke, F.-D., Interaction of adsorption and catalytic reactions in water decontamination processes: Part I. Oxidation of organic contaminants with hydrogen peroxide catalyzed by activated carbon. *Appl Catal B: Environ* **2005,** *58*, (1), 9-18.

42. Thomas, J.; Ward, C., In situ biorestoration of organic contaminants in the subsurface. *Environ. Sci. Technol.* **1989,** *23*, (7), 760-766.

43. O'neill, F.; Bromley-Challenor, K.; Greenwood, R.; Knapp, J., Bacterial growth on aniline: implications for the biotreatment of industrial wastewater. *Water Res.* **2000,** *34*, (18), 4397-4409.

44. Ferreira, F. C.; Han, S.; Boam, A.; Zhang, S.; Livingston, A. G., Membrane aromatic recovery system (MARS): lab bench to industrial pilot scale. *Desalination* **2002,** *148*, (1), 267-273.

45. Faria, P.; Órfão, J.; Pereira, M., Ozonation of aniline promoted by activated carbon. *Chemosphere* **2007,** *67*, (4), 809-815.

46. Pan, B.; Zhang, Q.; Meng, F.; Li, X.; Zhang, X.; Zheng, J.; Zhang, W.; Pan, B.; Chen, J., Sorption enhancement of aromatic sulfonates onto an aminated hyper-cross-linked polymer. *Environ. Sci. Technol.* **2005,** *39*, (9), 3308-3313.

47. Hinrichs, R.; Snoeyink, V., Sorption of benzenesulfonates by weak base anion exchange resins. *Water Res.* **1976,** *10*, (1), 79-87.

48. Gregory, J.; Semmens, M., Sorption of carboxylate ions by strongly basic anion exchangers. *J. Chem. Soc. Faraday Trans1: Physical Chemistry in Condensed Phases* **1972,** *68*, 1045-1052.

49. Xu, Z. Y.; Zhang, Q. X.; Fang, H. H. P., Applications of porous resin sorbents in industrial wastewater treatment and resource recovery. *Crit. Rev. Env. Sci. Technol.* **2003,** *33*, (4), 363-389.

50. Tao, W.; Li, A.; Long, C.; Qian, H.; Xu, D.; Chen, J., Adsorption of 5-sodiosulfoisophthalic acids from aqueous solution onto poly(2-vinylpyridine) resin. *J. Hazard. Mater.* **2010,** *175*, (1-3), 111-116.

51. Aramendıa, M.; Borau, V.; Garcıa, I.; Jimenez, C.; Lafont, F.; Marinas, A.; Marinas, J.; Urbano, F., Liquid-phase hydrodechlorination of chlorobenzene over palladium-supported catalysts: Influence of HCl formation and NaOH addition. *J. Mol. Catal. A: Chem.* **2002,** *184*, (1), 237-245.

52. Yin, L.; Liebscher, J., Carbon-carbon coupling reactions catalyzed by heterogeneous palladium catalysts. *Chem. Rev.* **2007,** *107*, (1), 133-173.

53. Diaz, E.; Mohedano, A. F.; Casas, J. A.; Calvo, L.; Gilarranz, M. A.; Rodriguez, J. J., Comparison of activated carbon-supported Pd and Rh catalysts for aqueous-phase hydrodechlorination. *Appl Catal B: Environ* **2011,** *106*, (3), 469-475.

54. Centi, G.; Ciambelli, P.; Perathoner, S.; Russo, P., Environmental catalysis: trends and outlook. *Catal. Today* **2002,** *75*, (1), 3-15.

55. Keane, M. A., A review of catalytic approaches to waste minimization: case study— liquid ‐ phase catalytic treatment of chlorophenols. *J. Chem. Technol. Biotechnol.* **2005,** *80*, (11), 1211-1222.

56. Zhang, M.; Jiang, M.; Liang, C., Palladium supported on an ion exchange resin for the Suzuki-Miyaura reaction. *Chinese J Catal* **2013,** *34*, (12), 2161-2166.

57. Chaplin, B. P.; Roundy, E.; Guy, K. A.; Shapley, J. R.; Werth, C. J., Effects of natural water ions and humic acid on catalytic nitrate reduction kinetics using an alumina supported Pd-Cu catalyst. *Environ. Sci. Technol.* **2006,** *40*, (9), 3075-3081.

58. Chaplin, B. P.; Shapley, J. R.; Werth, C. J., Regeneration of sulfur-fouled bimetallic Pd-based catalysts. *Environ. Sci. Technol.* **2007,** *41*, (15), 5491-5497.

59. Corain, B.; Centomo, P.; Lora, S.; Kralik, M., Functional resins as innovative supports for catalytically active metal nanoclusters. *J. Mol. Catal. A: Chem.* **2003,** *204*, 755-762.

60. Dodouche, I.; Barbosa, D. P.; Rangel, M. d. C.; Epron, F., Palladium–tin catalysts on conducting polymers for nitrate removal. *Appl Catal B: Environ* **2009,** *93*, (1), 50-55.

61. Rollet, P.; Kleist, W.; Dufaud, V.; Djakovitch, L., Copper-free heterogeneous catalysts for the Sonogashira cross-coupling reaction: Preparation, characterisation, activity and applications for organic synthesis. *J. Mol. Catal. A: Chem.* **2005,** *241*, (1), 39-51.

62. Wang, Y.; Liu, J.; Wang, P.; Werth, C. J.; Strathmann, T. J., Palladium Nanoparticles Encapsulated in Core–Shell Silica: A Structured Hydrogenation Catalyst with Enhanced Activity for Reduction of Oxyanion Water Pollutants. *ACS Catal* **2014,** *4*, (10), 3551-3559.

63. Pera-Titus, M.; Garcıa-Molina, V.; Baños, M. A.; Giménez, J.; Esplugas, S., Degradation of chlorophenols by means of advanced oxidation processes: a general review. *Appl Catal B: Environ* **2004,** *47*, (4), 219-256.

64. Valderrama, C.; Poch, J.; Barios, J. I.; Farran, A.; Luis Cortina, J., Binary fixed bed modeling of phenol/aniline removal from aqueous solutions onto hyper-cross-linked resin (Macronet MN200). *J. Chem. Eng. Data* **2012,** *57*, (5), 1502-1508.

65. Zhou, Y., Removal of aniline from aqueous solution using pine sawdust modified with citric acid and β-Cyclodextrin. *Ind. Eng. Chem. Res.* **2014,** *53*, (2), 887 - 894.

66. Ersoz, G.; Atalay, S., Low-pressure catalytic wet air oxidation of aniline over Co_3O_4/CeO_2. *Ind. Eng. Chem. Res.* **2010,** *49*, (4), 1625-1630.

67. Shuai, D.; Choe, J. K.; Shapley, J. R.; Werth, C. J., Enhanced Activity and Selectivity of Carbon Nanofiber Supported Pd Catalysts for Nitrite Reduction. *Environ. Sci. Technol.* **2012,** *46*, (5), 2847-2855.

68. Zhou, Y.; Gu, X.; Zhang, R.; Lu, J., Removal of aniline from aqueous solution using pine sawdust modified with citric acid and β-cyclodextrin. *Ind. Eng. Chem. Res.* **2014,** *53*, (2), 887-894.

69. Gosetti, F.; Chiuminatto, U.; Zampieri, D.; Mazzucco, E.; Marengo, E.; Gennaro, M. C., A new on-line solid phase extraction high performance liquid chromatography tandem mass spectrometry method to study the sun light photodegradation of mono-chloroanilines in river water. *J. Chromatogr. A* **2010,** *1217*, (20), 3427-3434.

70. Ferreira, F. C.; Han, S.; Livingston, A. G., Recovery of aniline from aqueous solution using the membrane aromatic recovery system (MARS). *Ind. Eng. Chem. Res.* **2002,** *41*, (11), 2766-2774.

71. McBain, A. J.; Ledder, R. G.; Moore, L. E.; Catrenich, C. E.; Gilbert, P., Effects of quaternary-ammonium-based formulations on bacterial community dynamics and antimicrobial susceptibility. *Appl. Environ. Microbiol.* **2004,** *70*, (6), 3449-3456.

72. Garcıa, M.; Ribosa, I.; Guindulain, T.; Sánchez-Leal, J.; Vives-Rego, J., Fate and effect of monoalkyl quaternary ammonium surfactants in the aquatic environment. *Environ. Pollut.* **2001,** *111*, (1), 169-175.

73. Boethling, R. S., Environmental fate and toxicity in wastewater treatment of quaternary ammonium surfactants. *Water Res.* **1984,** *18*, (9), 1061-1076.

74. Cooper, J. C., Review of the environmental toxicity of quaternary ammonium halides. *Ecotoxicol. Environ. Saf.* **1988,** *16*, (1), 65-71.

75. Ismail, Z. Z.; Tezel, U.; Pavlostathis, S. G., Sorption of quaternary ammonium compounds to municipal sludge. *Water Res.* **2010,** *44*, (7), 2303-2313.

76. Martínez-Carballo, E.; Sitka, A.; González-Barreiro, C.; Kreuzinger, N.; Fürhacker, M.; Scharf, S.; Gans, O., Determination of selected quaternary ammonium compounds by liquid chromatography with mass spectrometry. Part I. Application to surface, waste and indirect discharge water samples in Austria. *Environ. Pollut.* **2007,** *145*, (2), 489-496.

77. Grillitsch, B.; Gans, O.; Kreuzinger, N.; Scharf, S.; Uhl, M.; Fürhacker, M., Environmental risk assessment for quaternary ammonium compounds: a case study from Austria. *Water Sci. Technol.* **2006,** *54*, (11-12), 111-118.

78. Toxicological Profile for Chlorophenols. *U.S. Department of Health and Human Services, Agency for Toxic Substances and Disease Registry* **1999**.

79. Kiwi, J.; Pulgarin, C.; Peringer, P., Effect of Fenton and photo-Fenton reactions on the degradation and biodegradability of 2 and 4-nitrophenols in water treatment. *Appl Catal B: Environ* **1994,** *3*, (4), 335-350.

80. Podeh, M. R. H.; Bhattacharya, S. K.; Qu, M., Effects of nitrophenols on acetate utilizing methanogenic systems. *Water Res.* **1995,** *29*, (2), 391-399.

81. Goi, A.; Trapido, M., Hydrogen peroxide photolysis, Fenton reagent and photo-Fenton for the degradation of nitrophenols: a comparative study. *Chemosphere* **2002,** *46*, (6), 913-922.

82. Chauhan, A.; Pandey, G.; Sharma, N. K.; Paul, D.; Pandey, J.; Jain, R. K., p-Nitrophenol degradation via 4-nitrocatechol in Burkholderia sp. SJ98 and cloning of some of the lower pathway genes. *Environ. Sci. Technol.* **2010,** *44*, (9), 3435-3441.

83. Vincent, T.; Guibal, E., Chitosan-supported palladium catalyst. 5. Nitrophenol degradation using palladium supported on hollow chitosan fibers. *Environ. Sci. Technol.* **2004,** *38*, (15), 4233-4240.

84. Toxicological profile for nitrophenols: 2-nitrophenol 4-nitrophenol. *Agency for Toxic Substances and Disease Registry, U.S. Public Health Service*

1992.

85. Chiron, S.; Minero, C.; Vione, D., Occurrence of 2, 4-dichlorophenol and of 2, 4-dichloro-6-nitrophenol in the Rhône river delta (Southern France). *Environ. Sci. Technol.* **2007,** *41*, (9), 3127-3133.

86. Shen, S.; Chang, Z.; Liu, H., Three-liquid-phase extraction systems for separation of phenol and p-nitrophenol from wastewater. *Sep. Purif. Technol.* **2006,** *49*, (3), 217-222.

87. Oturan, M. A.; Peiroten, J.; Chartrin, P.; Acher, A. J., Complete destruction of p-nitrophenol in aqueous medium by electro-Fenton method. *Environ. Sci. Technol.* **2000,** *34*, (16), 3474-3479.

88. Yi, S.; Zhuang, W.-Q.; Wu, B.; Tay, S. T.-L.; Tay, J.-H., Biodegradation of p-nitrophenol by aerobic granules in a sequencing batch reactor. *Environ. Sci. Technol.* **2006,** *40*, (7), 2396-2401.

89. Chong, M. N.; Jin, B.; Chow, C. W.; Saint, C., Recent developments in photocatalytic water treatment technology: a review. *Water Res.* **2010,** *44*, (10), 2997-3027.

90. Alexander, H. J.; McClanahan, M. A., Kinetics of calcium carbonate precipitation in lime-soda ash softening. *J. Am. Water. Works. Ass.* **1975**, 618-621.

91. Bilgili, M. S., Adsorption of 4-chlorophenol from aqueous solutions by xad-4 resin: isotherm, kinetic, and thermodynamic analysis. *J. Hazard. Mater.* **2006,** *137*, (1), 157-164.

92. Malik, R.; Ramteke, D.; Wate, S., Adsorption of malachite green on groundnut shell waste based powdered activated carbon. *Waste Manage. (Oxford)* **2007,** *27*, (9), 1129-1138.

93. Westerhoff, P.; Yoon, Y.; Snyder, S.; Wert, E., Fate of endocrine-disruptor, pharmaceutical, and personal care product chemicals during simulated drinking water treatment processes. *Environ. Sci. Technol.* **2005,** *39*, (17), 6649-6663.

94. Zhang, H.; Shields, A. J.; Jadbabaei, N.; Nelson, M.; Pan, B.; Suri, R. P., Understanding and modeling removal of anionic organic contaminants (AOCs) by anion exchange resins. *Environ. Sci. Technol.* **2014,** *48*, (13), 7494-7502.

95. Radjenović, J.; Petrović, M.; Ventura, F.; Barceló, D., Rejection of pharmaceuticals in nanofiltration and reverse osmosis membrane drinking water treatment. *Water Res.* **2008,** *42*, (14), 3601-3610.

96. Adams, C.; Wang, Y.; Loftin, K.; Meyer, M., Removal of antibiotics from surface and distilled water in conventional water treatment processes. *J. Environ. Eng.* **2002,** *128*, (3), 253-260.

97. Legrini, O.; Oliveros, E.; Braun, A., Photochemical processes for water treatment. *Chem. Rev.* **1993,** *93*, (2), 671-698.

98. Vincent, T.; Guibal, E., Chitosan-supported palladium catalyst. 3. Influence of experimental parameters on nitrophenol degradation. *Langmuir* **2003,** *19*, (20), 8475-8483.

99. Kawabata, N.; Ohira, K., Removal and recovery of organic pollutants from aquatic environment. 1. Vinylpyridine-divinylbenzene copolymer as a polymeric adsorbent for removal and recovery of phenol from aqueous solution. *Environ. Sci. Technol.* **1979,** *13*, (11), 1396-1402.

100. Xu, Z.; Zhang, Q.; Fang, H. H., Applications of porous resin sorbents in industrial wastewater treatment and resource recovery. *Crit. Rev. Env. Sci. Technol.* **2003,** *33*, (4), 363-389.

101. Zagorodni, A. A., *Ion exchange materials: properties and applications: properties and applications*. Elsevier: 2006.

102. Bae, B. U.; Jung, Y. H.; Han, W. W.; Shin, H. S., Improved brine recycling during nitrate removal using ion exchange. *Water Res.* **2002,** *36*, (13), 3330-3340.

103. Pan, B.; Zhang, H., A modified polanyi-based model for mechanistic understanding of adsorption of phenolic compounds onto polymeric adsorbents. *Environ. Sci. Technol.* **2012,** *46*, (12), 6806-6814.

104. Janauer, G., The selectivity of a polystyrenebenzyltrimethylammonium-type anion-exchange resin for alkanesulfonates. *J. Phys. Chem.* **1969,** *73*, (7), 560-565.

105. Li, P.; Sengupta, A. K., Genesis of selectivity and reversibility for sorption of synthetic aromatic anions onto polymeric sorbents. *Environ. Sci. Technol.* **1998,** *32*, (23), 3756-3766.

106. Boyd. G. E, L. Q. V., The binding of quaternary ammonium ions by polystyrenesulfonic acid type cation exchangers *J. Am. Chem. Soc.* **1967,** *89*, (24), 6038-6042.

107. Hale, D. K.; Packham, D. I.; Pepper, K. W., Properties of ion-exchange resins in relation to their structure .5. exchange of organic cations. *J. Chem. Soc.* **1953**, (MAR), 844-851.

108. Gustafson, R. L., Adsorption of organic ions by anion exchange resins. *Ind. Eng. Chem. Res.* **1968,** *7*, (2), 116-120.

109. Xiong, Z.; Zhao, D.; Harper, W. F., Jr., Sorption and desorption of perchlorate with various classes of ion exchangers: A comparative study. *Ind. Eng. Chem. Res.* **2007,** *46*, (26), 9213-9222.

110. Chu, B., On anion exchange resin selectivities. *J. Inorg. Nucl. Chem.* **1962,** *24*, (11), 1405 - 1415.

111. Uemiya, S.; Sato, N.; Ando, H.; Kude, Y.; Matsuda, T.; Kikuchi, E., Separation of hydrogen through palladium thin film supported on a porous glass tube. *J. Membr. Sci* **1991,** *56*, (3), 303-313.

112. Praharaj, S.; Nath, S.; Ghosh, S. K.; Kundu, S.; Pal, T., Immobilization and recovery of Au nanoparticles from anion exchange resin: resin-bound nanoparticle matrix as a catalyst for the reduction of 4-nitrophenol. *Langmuir* **2004,** *20*, (23), 9889-9892.

113. Chinthaginjala, J. K.; Bitter, J. H.; Lefferts, L., Thin layer of carbon-nano-fibers (CNFs) as catalyst support for fast mass transfer in hydrogenation of nitrite. *Appl Catal A Gen* **2010,** *383*, (1), 24-32.

114. Choe, J. K.; Shapley, J. R.; Strathmann, T. J.; Werth, C. J., Influence of rhenium speciation on the stability and activity of Re/Pd bimetal catalysts used for perchlorate reduction. *Environ. Sci. Technol.* **2010,** *44*, (12), 4716-4721.

115. Davie, M. G.; Reinhard, M.; Shapley, J. R., Metal-catalyzed reduction of N-nitrosodimethylamine with hydrogen in water. *Environ. Sci. Technol.* **2006,** *40*, (23), 7329-7335.

116. Davie, M. G.; Shih, K.; Pacheco, F. A.; Leckie, J. O.; Reinhard, M., Palladium− indium catalyzed reduction of N-nitrosodimethylamine: Indium as a promoter metal. *Environ. Sci. Technol.* **2008,** *42*, (8), 3040-3046.

117. Chaplin, B. P.; Shapley, J. R.; Werth, C. J., The Selectivity and Sustainability of a Pd–In/γ-Al_2O_3 Catalyst in a Packed-Bed Reactor: The Effect of Solution Composition. *Catal. Lett.* **2009,** *130*, (1-2), 56-62.

118. Zhang, F.; Miao, S.; Yang, Y.; Zhang, X.; Chen, J.; Guan, N., Size-dependent hydrogenation selectivity of nitrate on Pd− Cu/TiO_2 catalysts. *J. Phys. Chem. C* **2008,** *112*, (20), 7665-7671.

119. Pintar, A.; Batista, J.; Levec, J., Catalytic denitrification: direct and indirect removal of nitrates from potable water. *Catal. Today* **2001,** *66*, (2), 503-510.

120. Pintar, A.; Batista, J.; Levec, J., Integrated ion exchange/catalytic process for efficient removal of nitrates from drinking water. *Chem. Eng. Sci.* **2001,** *56*, (4), 1551-1559.

121. Liu, J.; Choe, J. K.; Sasnow, Z.; Werth, C. J.; Strathmann, T. J., Application of a Re–Pd bimetallic catalyst for treatment of perchlorate in waste ion-exchange regenerant brine. *Water Res.* **2013,** *47*, (1), 91-101.

122. Kim, Y.-N.; Choi, M., Synergistic Integration of Ion-Exchange and Catalytic Reduction for Complete Decomposition of Perchlorate in Waste Water. *Environ. Sci. Technol.* **2014,** *48*, (13), 7503-7510.

123. Gašparovičová, D.; Králik, M.; Hronec, M.; Vallušová, Z.; Vinek, H.; Corain, B., Supported Pd–Cu catalysts in the water phase reduction of nitrates: Functional resin versus alumina. *J. Mol. Catal. A: Chem.* **2007,** *264*, (1), 93-102.

124. Gašparovičová, D.; Králik, M.; Hronec, M., Pd-Cu supported on anionic polymers-promising catalysts for removal of nitrates from drinking water. *Collect. Czech. Chem. Commun.* **1999,** *64*, (3), 502-514.

125. Prüsse, U.; Daum, J.; Bock, C.; Vorlop, K.-D., Catalytic nitrate reduction: kinetic investigations. *Stud. Surf. Sci. Catal.* **2000,** *130*, 2237-2242.

126. D'Arino, M.; Pinna, F.; Strukul, G., Nitrate and nitrite hydrogenation with Pd and Pt/SnO_2 catalysts: the effect of the support porosity and the role of carbon dioxide in the control of selectivity. *Appl Catal B: Environ* **2004,** *53*, (3), 161-168.

127. Barbosa, D. P.; Tchiéta, P.; Rangel, M. d. C.; Epron, F., The use of a cation exchange resin for palladium–tin and palladium–indium catalysts for nitrate removal in water. *J. Mol. Catal. A: Chem.* **2013,** *366*, 294-302.

128. Gašparovičová, D.; Králik, M.; Hronec, M.; Biffis, A.; Zecca, M.; Corain, B., Reduction of nitrates dissolved in water over palladium-copper catalysts supported on a strong cationic resin. *J. Mol. Catal. A: Chem.* **2006,** *244*, (1), 258-266.

129. Yuan, G.; Keane, M. A., Liquid phase hydrodechlorination of chlorophenols over Pd/C and Pd/Al_2O_3: a consideration of HCl/catalyst interactions and solution pH effects. *Appl Catal B: Environ* **2004,** *52*, (4), 301-314.

130. Yuan, G.; Keane, M. A., Catalyst deactivation during the liquid phase hydrodechlorination of 2, 4-dichlorophenol over supported Pd: influence of the support. *Catal. Today* **2003,** *88*, (1), 27-36.

131. Da-Silva, J.; Bruns, R. E.; Cobo, A., Study of the reaction conditions for the hydrodechlorination of pentachlorophenol on palladium catalysts. *Chem. Eng. J.* **2007,** *131*, (1), 59-64.

132. Chu, C.; Su, Z., Facile Synthesis of AuPt Alloy Nanoparticles in Polyelectrolyte Multilayers with Enhanced Catalytic Activity for Reduction of 4-Nitrophenol. *Langmuir* **2014,** *30*, (50), 15345-15350.

133. Dauthal, P.; Mukhopadhyay, M., Prunus domestica fruit extract-mediated synthesis of gold nanoparticles and its catalytic activity for 4-nitrophenol reduction. *Ind. Eng. Chem. Res.* **2012,** *51*, (40), 13014-13020.

134. Choudhary, V. R.; Sane, M. G.; Tambe, S. S., Kinetics of hydrogenation of o-nitrophenol to o-aminophenol on Pd/carbon catalysts in a stirred three-phase slurry reactor. *Ind. Eng. Chem. Res.* **1998,** *37*, (10), 3879-3887.

135. Bingwa, N.; Meijboom, R., Kinetic evaluation of dendrimer-encapsulated palladium nanoparticles in the 4-nitrophenol reduction reaction. *J. Phys. Chem. C* **2014,** *118*, (34), 19849-19858.

136. Chen, R.; Jiang, Y.; Xing, W.; Jin, W., Preparation of palladium nanoparticles deposited on a silanized hollow fiber ceramic membrane support and their catalytic properties. *Ind. Eng. Chem. Res.* **2013,** *52*, (14), 5002-5008.

137. Mei, Y.; Sharma, G.; Lu, Y.; Ballauff, M.; Drechsler, M.; Irrgang, T.; Kempe, R., High catalytic activity of platinum nanoparticles immobilized on spherical polyelectrolyte brushes. *Langmuir* **2005,** *21*, (26), 12229-12234.

138. Gao, L.; Li, R.; Sui, X.; Li, R.; Chen, C.; Chen, Q., Conversion of Chicken Feather Waste to N-Doped Carbon Nanotubes for the Catalytic Reduction of 4-Nitrophenol. *Environ. Sci. Technol.* **2014,** *48*, (17), 10191-10197.

139. Wu, Y.-g.; Wen, M.; Wu, Q.-s.; Fang, H., Ni/graphene nanostructure and its electron-enhanced catalytic action for hydrogenation reaction of nitrophenol. *J. Phys. Chem. C* **2014,** *118*, (12), 6307-6313.

140. Chen, R.; Jiang, Y.; Xing, W.; Jin, W., Fabrication and catalytic properties of palladium nanoparticles deposited on a silanized asymmetric ceramic support. *Ind. Eng. Chem. Res.* **2011,** *50*, (8), 4405-4411.

141. Xi, X.; Liu, Y.; Shi, J.; Cao, S., Palladium complex of poly (4-vinylpyridine-co-acrylic acid) for homogeneous hydrogenation of aromatic nitro compounds. *J. Mol. Catal. A: Chem.* **2003,** *192*, (1), 1-7.

142. Xu, S.; Xi, X.; Shi, J.; Cao, S., A homogeneous catalyst made of poly (4-vinylpyridine-co-N-vinylpyrrolidone)-Pd (0) complex for hydrogenation of aromatic nitro compounds. *J. Mol. Catal. A: Chem.* **2000,** *160*, (2), 287-292.

143. Wunder, S.; Polzer, F.; Lu, Y.; Mei, Y.; Ballauff, M., Kinetic analysis of catalytic reduction of 4-nitrophenol by metallic nanoparticles immobilized in spherical polyelectrolyte brushes. *J. Phys. Chem. C* **2010,** *114*, (19), 8814-8820.

144. Zeng, J.; Zhang, Q.; Chen, J.; Xia, Y., A comparison study of the catalytic properties of Au-based nanocages, nanoboxes, and nanoparticles. *Nano Lett.* **2009,** *10*, (1), 30-35.

145. Esumi, K.; Isono, R.; Yoshimura, T., Preparation of PAMAM-and PPI-metal (silver, platinum, and palladium) nanocomposites and their catalytic activities for reduction of 4-nitrophenol. *Langmuir* **2004,** *20*, (1), 237-243.

146. Dutta, S.; Sarkar, S.; Ray, C.; Roy, A.; Sahoo, R.; Pal, T., Mesoporous Gold and Palladium Nanoleaves from Liquid–Liquid Interface: Enhanced Catalytic Activity of the

Palladium Analogue toward Hydrazine-Assisted Room-Temperature 4-Nitrophenol Reduction. *ACS Appl Mater Inter* **2014,** *6*, (12), 9134-9143.

147. Zheng, G.; Kaefer, K.; Mourdikoudis, S.; Polavarapu, L.; Vaz, B.; Cartmell, S. E.; Bouleghlimat, A.; Buurma, N. J.; Yate, L.; de Lera, Á. R., Palladium Nanoparticle-Loaded Cellulose Paper: A Highly Efficient, Robust, and Recyclable Self-Assembled Composite Catalytic System. *J. Phys. Chem. Lett.* **2014,** *6*, (2), 230-238.

148. Johnson, J. A.; Makis, J. J.; Marvin, K. A.; Rodenbusch, S. E.; Stevenson, K. J., Size-dependent hydrogenation of p-nitrophenol with Pd nanoparticles synthesized with poly (amido) amine dendrimer templates. *J. Phys. Chem. C* **2013,** *117*, (44), 22644-22651.

149. Pozun, Z. D.; Rodenbusch, S. E.; Keller, E.; Tran, K.; Tang, W.; Stevenson, K. J.; Henkelman, G., A systematic investigation of p-nitrophenol reduction by bimetallic dendrimer encapsulated nanoparticles. *J. Phys. Chem. C* **2013,** *117*, (15), 7598-7604.

150. Jadbabaei, N.; Zhang, H., Sorption Mechanism and Predictive Models for Removal of Cationic Organic Contaminants by Cation Exchange Resins. *Environ. Sci. Technol.* **2014,** *48*, (24), 14572-14581.

151. Vilensky, M. Y.; Berkowitz, B.; Warshawsky, A., In situ remediation of groundwater contaminated by heavy- and transition-metal ions by selective ion-exchange methods. *Environ. Sci. Technol.* **2002,** *36*, (8), 1851-1855.

152. Sprunger, L. M.; Achi, S. S.; Acree Jr, W. E.; Abraham, M. H.; Leo, A. J.; Hoekman, D., Correlation and prediction of solute transfer to chloroalkanes from both water and the gas phase. *Fluid Phase Equilib.* **2009,** *281*, (2), 144-162.

153. Abraham, M. H.; Acree, W. E., Jr., Equations for the transfer of neutral molecules and ionic species from water to organic phases. *J. Org. Chem.* **2010,** *75*, (4), 1006-1015.

154. Bronner, G.; Goss, K.-U., Predicting sorption of pesticides and other multifunctional organic chemicals to soil organic carbon. *Environ. Sci. Technol.* **2010,** *45*, (4), 1313-1319.

155. Zhu, D.; Pignatello, J. J., A concentration-dependent multi-term linear free energy relationship for sorption of organic compounds to soils based on the hexadecane dilute-solution reference state. *Environ. Sci. Technol.* **2005,** *39*, (22), 8817-8828.

156. Zissimos, A. M.; Abraham, M. H.; Du, C. M.; Valko, K.; Bevan, C.; Reynolds, D.; Wood, J.; Tam, K. Y., Calculation of Abraham descriptors from experimental data from seven HPLC systems; evaluation of five different methods of calculation. *J. Chem. Soc., Perkin Trans. 2* **2002**, (12), 2001-2010.

157. Zissimos, A. M.; Abraham, M. H.; Barker, M. C.; Box, K. J.; Tam, K. Y., Calculation of Abraham descriptors from solvent-water partition coeffcients in four different systems; evaluation of different methods of calculation. *J. Chem. Soc., Perkin Trans. 2* **2002**, (3), 470-477.

158. Sprunger, L. M.; Achi, S. S.; Acree, W. E., Jr.; Abraham, M. H.; Leo, A. J.; Hoekman, D., Correlation and prediction of solute transfer to chloroalkanes from both water and the gas phase. *Fluid Phase Equilib.* **2009,** *281*, (2), 144-162.

159. Abraham, M. H.; Ibrahim, A.; Zissimos, A. M., Determination of sets of solute descriptors from chromatographic measurements. *J. Chromatogr. A* **2004,** *1037*, (1-2), 29-47.

160. Shih, Y.-H.; Gschwend, P. M., Evaluating activated carbon-water sorption coefficients of organic compounds using a linear solvation energy relationship approach and sorbate chemical activities. *Environ. Sci. Technol.* **2009,** *43*, (3), 851-857.

161. Cheng, S. L.; Yan, H. S.; Zhao, C. Q., The synergistic effect between hydrophobic and electrostatic interactions in the uptake of amino acids by strongly acidic cation-exchange resins. *J. Chromatogr. A* **2006,** *1108*, (1), 43-49.

162. Yang, K.; Xing, B., Adsorption of organic compounds by carbon nanomaterials in aqueous phase: polanyi theory and its application. *Chem. Rev.* **2010,** *110*, (10), 5989-6008.

163. Abraham, M. H.; Zhao, Y. H., Determination of solvation descriptors for ionic species: Hydrogen bond acidity and basicity. *J. Org. Chem.* **2004,** *69*, (14), 4677-4685.

164. Abraham, M. H.; Acree, W. E., Jr., The transfer of neutral molecules, ions and ionic species from water to wet octanol. *Phys. Chem. Chem. Phys.* **2010,** *12*, (40), 13182-13188.

165. Abraham, M. H.; Acree, W. E., Jr., Solute descriptors for phenoxide anions and their use to establish correlations of rates of reaction of anions with iodomethane. *J. Org. Chem.* **2010,** *75*, (9), 3021-3026.

166. Pan, B.; Zhang, H., Interaction mechanisms and predictive model for the sorption of aromatic compounds onto nonionic resins. *J. Phys. Chem. C* **2013,** *117*, (34), 17707-17715.

167. Droge, S. T.; Goss, K.-U., Development and evaluation of a new sorption model for organic cations in soil: contributions from organic matter and clay minerals. *Environ. Sci. Technol.* **2013,** *47*, (24), 14233-14241.

168. Borisover, M.; Graber, E. R., Classifying NOM - Organic sorbate interactions using compound transfer from an inert solvent to the hydrated sorbent. *Environ. Sci. Technol.* **2003,** *37*, (24), 5657-5664.

169. Schwarzenbach, R. P.; Gschwend, P. M., Imboden, D. M., *Environmental organic chemistry* Wiley-Interscience: NewYork: 2003.

170. Crittenden, J. C.; Sanongraj, S.; Bulloch, J. L.; Hand, D. W.; Rogers, T. N.; Speth, T. F.; Ulmer, M., Correlation of aqueous-phase adsorption isotherms. *Environ. Sci. Technol.* **1999,** *33*, (17), 2926-2933.

171. Yang, K.; Wu, W.; Jing, Q.; Zhu, L., Aqueous adsorption of aniline, phenol, and their substitutes by multi-walled carbon nanotubes. *Environ. Sci. Technol.* **2008,** *42*, (21), 7931-7936.

172. Dobruskin, V. K., Micropore volume filling. A condensation approximation approach as a foundation to the Dubinin-Astakhov equation. *Langmuir* **1998,** *14*, (14), 3840-3846.

173. Zhu, D. Q.; Pignatello, J. J., A concentration-dependent multi-term linear free energy relationship for sorption of organic compounds to soils based on the hexadecane dilute-solution reference state. *Environ. Sci. Technol.* **2005,** *39*, (22), 8817-8828.

174. Chiou, C. T., *Partition and adsorption of organic contaminants in environmental systems*. John Wiley & Sons: 2003.

175. Pan, B.; Du, W.; Zhang, W.; Zhang, X.; Zhang, Q.; Pan, B.; Lv, L.; Zhang, Q.; Chen, J., Improved adsorption of 4-nitrophenol onto a novel hyper-cross-linked polymer. *Environ. Sci. Technol.* **2007,** *41*, (14), 5057-5062.

176. Chang, C.-F.; Chang, C.-Y.; Hsu, K.-E.; Lee, S.-C.; Hoell, W., Adsorptive removal of the pesticide methomyl using hypercrosslinked polymers. *J. Hazard. Mater.* **2008,** *155*, (1-2), 295-304.

177. Bohdana, C. M.; Cantea, D. S.; Dale, J. A.; Pincovschi, E.; Oancea, M. S., Polymeric Ion Exchangers Based on Styrene-Divinylbenzene Matrix. Textural and Structural Modifications after Grafting Different Functional Groups In Purolite, Ed. Cambridge, UK, **2008**.

178. Chen, J. H.; Chen, W. R.; Gau, Y. Y.; Lin, C. H., The preparation of di(2-ethylhexyl)phosphoric acid modified Amberlite 200 and its application in the separation of metal ions from sulfuric acid solution. *React. Funct. Polym.* **2003,** *56*, (3), 175-188.

179. Hickey, J. P.; Passinoreader, D. R., Linear solvation energy relationships - rules of thumb for estimation of variable values. *Environ. Sci. Technol.* **1991,** *25*, (10), 1753-1760.

180. Arp, H. P. H.; Droge, S. T.; Endo, S.; Giger, W.; Goss, K.-U.; Hawthorne, S. B.; Mabury, S. A.; Mayer, P.; Mclachlan, M. S.; Pankow, J. F., More of EPA's SPARC Online Calculator─The Need for High-Quality Predictions of Chemical Properties. *Environ. Sci. Technol.* **2010,** *44*, (12), 4400-4401.

181. Chan, K.; Jensen, N.; O'Brien, P. J., Structure-activity relationships for thiol reactivity and rat or human hepatocyte toxicity induced by substituted p-benzoquinone compounds. *J. Appl. Toxicol.* **2008,** *28*, (5), 608-620.

182. Meylan, W. M.; Howard, P. H., Bond contribution method for estimating henry's law constants. *Environ. Toxicol. Chem.* **1991,** *10*, (10), 1283-1293.

183. Dubinin, M. M., The potential theory of adsorption of gases and vapors for adsorbents with energetically nonuniform surfaces. *Chem. Rev.* **1960,** *60*, (2), 235-241.

184. Bucher, J.; Diamond, R.; Chu, B., Selectivity in heterovalent anion exchange. Ion pairing vs. ion hydration. *J. Phys. Chem* **1972,** *76*, (17), 2459-2462.

185. Helfferich, F. R., *Ion Exchanger*. McGraw-Hill: New York, **1962**.

186. Apul, O. G.; Wang, Q.; Shao, T.; Rieck, J. R.; Karanfil, T., Predictive model development for adsorption of aromatic contaminants by multi-walled carbon nanotubes. *Environ. Sci. Technol.* **2012,** *47*, (5), 2295-2303.

187. Lawrence, M. A.; Kukkadapu, R. K.; Boyd, S. A., Adsorption of phenol and chlorinated phenols from aqueous solution by tetramethylammonium-and tetramethylphosphonium-exchanged montmorillonite. *Appl. Clay. Sci.* **1998,** *13*, (1), 13-20.

188. Yoshinaga, Y.; Akita, T.; Mikami, I.; Okuhara, T., Hydrogenation of nitrate in water to nitrogen over Pd–Cu supported on active carbon. *J. Catal.* **2002,** *207*, (1), 37-45.

189. Davie, M. G.; Cheng, H.; Hopkins, G. D.; LeBron, C. A.; Reinhard, M., Implementing heterogeneous catalytic dechlorination technology for remediating TCE-contaminated groundwater. *Environ. Sci. Technol.* **2008,** *42*, (23), 8908-8915.

190. Keane, M. A., Supported transition metal catalysts for hydrodechlorination reactions. *ChemCatChem* **2011,** *3*, (5), 800-821.

191. Harriott, P., Mass transfer to particles: Part I. Suspended in agitated tanks. *AlChE J.* **1962,** *8*, (1), 93-101.

192. Weisz, P.; Prater, C., Interpretation of measurements in experimental catalysis. *Adv. Catal* **1954,** *6*, (143), 49.

193. Butt, J. B., *Reaction kinetics and reactor design*. CRC Press: 2000.

194. Shuai, D.; McCalman, D. C.; Choe, J. K.; Shapley, J. R.; Schneider, W. F.; Werth, C. J., Structure sensitivity study of waterborne contaminant hydrogenation using shape-and size-controlled Pd nanoparticles. *ACS Catal* **2013,** *3*, (3), 453-463.

195. Choi, M.; Wu, Z.; Iglesia, E., Mercaptosilane-assisted synthesis of metal clusters within zeolites and catalytic consequences of encapsulation. *J. Am. Chem. Soc.* **2010,** *132*, (26), 9129-9137.

196. Lin, S.-S.; Gurol, M. D., Catalytic decomposition of hydrogen peroxide on iron oxide: kinetics, mechanism, and implications. *Environ. Sci. Technol.* **1998,** *32*, (10), 1417-1423.

197. Wan, H.; Chaudhari, R. V.; Subramaniam, B., Catalytic hydroprocessing of p-Cresol: metal, solvent and mass-transfer effects. *Top. Catal.* **2012,** *55*, (3-4), 129-139.

198. Coq, B.; Ferrat, G.; Figueras, F., Conversion of chlorobenzene over palladium and rhodium catalysts of widely varying dispersion. *J. Catal.* **1986,** *101*, (2), 434-445.

199. Cheng, I. F.; Fernando, Q.; Korte, N., Electrochemical dechlorination of 4-chlorophenol to phenol. *Environ. Sci. Technol.* **1997,** *31*, (4), 1074-1078.

200. Zhu, X.; Castleberry, S. R.; Nanny, M. A.; Butler, E. C., Effects of pH and catalyst concentration on photocatalytic oxidation of aqueous ammonia and nitrite in titanium dioxide suspensions. *Environ. Sci. Technol.* **2005,** *39*, (10), 3784-3791.

201. Xu, T.; Cai, Y.; O'Shea, K. E., Adsorption and photocatalyzed oxidation of methylated arsenic species in TiO_2 suspensions. *Environ. Sci. Technol.* **2007,** *41*, (15), 5471-5477.

202. Branton, P.; Bradley, R. H., Effects of active carbon pore size distributions on adsorption of toxic organic compounds. *Adsorption-Journal of the International Adsorption Society* **2011,** *17*, (2).

203. Prüsse, U.; Hähnlein, M.; Daum, J.; Vorlop, K.-D., Improving the catalytic nitrate reduction. *Catal. Today* **2000,** *55*, (1), 79-90.

204. Prüsse, U.; Vorlop, K.-D., Supported bimetallic palladium catalysts for water-phase nitrate reduction. *J. Mol. Catal. A: Chem.* **2001,** *173*, (1), 313-328.

205. Gavagnin, R.; Biasetto, L.; Pinna, F.; Strukul, G., Nitrate removal in drinking waters: the effect of tin oxides in the catalytic hydrogenation of nitrate by Pd/SnO_2 catalysts. *Appl Catal B: Environ* **2002,** *38*, (2), 91-99.

206. Chen, H.; Xu, Z.; Wan, H.; Zheng, J.; Yin, D.; Zheng, S., Aqueous bromate reduction by catalytic hydrogenation over Pd/Al_2O_3 catalysts. *Appl Catal B: Environ* **2010,** *96*, (3), 307-313.

207. Kopinke, F.-D.; Angeles-Wedler, D.; Fritsch, D.; Mackenzie, K., Pd-catalyzed hydrodechlorination of chlorinated aromatics in contaminated waters—Effects of surfactants, organic matter and catalyst protection by silicone coating. *Applied Catalysis B: Environmental* **2010,** *96*, (3), 323-328.

208. Schüth, C.; Disser, S.; Schüth, F.; Reinhard, M., Tailoring catalysts for hydrodechlorinating chlorinated hydrocarbon contaminants in groundwater. *Appl Catal B: Environ* **2000,** *28*, (3), 147-152.

209. Ordóñez, S.; Sastre, H.; Díez, F. V., Hydrodechlorination of tetrachloroethene over Pd/Al_2O_3: Influence of process conditions on catalyst performance and stability. *Appl Catal B: Environ* **2003,** *40*, (2), 119-130.

APPENDIX

SUPPORTING INFORMATION OF CHAPTER 3

Table A-1: Regression coefficients e, s, a, v, j^+, and c of the multiple linear regressions between $\ln(\alpha_{A/Cl})$ and solute descriptors for MN500 (b=0). (Q_e μmol/g).

Q_e	*c*	*e*	*s*	*a*	*v*	*j^+*	R^2
1	-0.5±6.7	-0.0±2.0	4.2±1.1	-1.0±3.3	-0.4±1.0	-1.4±2.2	0.739
10	-0.9±4.7	0.4±1.4	2.9±0.8	0.1±2.3	0.2±0.7	-0.4±1.5	0.819
30	-1.3±3.8	0.6±1.1	2.3±0.6	0.6±1.9	0.4±0.5	0.1±1.2	0.881
50	-1.7±3.4	0.7±1.0	2.0±0.5	0.9±1.7	0.5±0.5	0.3±1.1	0.908
80	-2.0±3.2	0.9±0.9	1.7±0.5	1.2±1.6	0.6±0.5	0.6±1.0	0.929
100	-2.2±3.1	1.0±0.9	1.6±0.5	1.4±1.5	0.6±0.4	0.7±1.0	0.937
150	-2.7±3.1	1.1±0.9	1.3±0.5	1.9±1.5	0.6±0.4	1.0±1.0	0.946
200	-3.0±3.3	1.3±1.0	1.1±0.5	2.0±1.6	0.5±0.5	1.2±1.1	0.948
300	-3.7±4.9	1.6±1.5	0.7±0.8	2. 5±2.4	-0.1±0.7	1.9±1.6	0.929

Table A-2: The corresponding p-values for the regression coefficients in **Table A-1**. (Q_e μmol/g)

Q_e	c	E	S	A	V	J^+
1	0.946	0.988	0.008	0.77	0.712	0.55
10	0.856	0.801	0.008	0.985	0.771	0.792
30	0.734	0.604	0.009	0.752	0.439	0.947
50	0.645	0.488	0.011	0.608	0.314	0.77
80	0.548	0.378	0.016	0.468	0.239	0.585
100	0.501	0.331	0.02	0.405	0.222	0.497
150	0.425	0.265	0.04	0.312	0.244	0.359
200	0.396	0.246	0.086	0.275	0.359	0.291
300	0.48	0.326	0.412	0.332	0.9	0.276

Table A-3: Regression coefficients e, s, a, v, j^+, and c of the multiple linear regressions between $\ln(\alpha_{A/Cl})$ and solute descriptors for Amberlite 200 (b=0). (Q_e μmol/g)

Q_e	*c*	*e*	*s*	*a*	*v*	j^+	R^2
1	-2.7±4.0	1.1±1.2	0.3±0.6	1.3±2.0	0.2±0.6	1.3±1.3	0.869
2	-2.3±3.6	1.3±1.1	0.4±0.6	1.1±1.8	0.1±0.5	1.1±1.1	0.904
5	-2.0±3.2	1.6±1.0	0.5±0.5	1.0±1.6	0.1±0.5	0.8±1.0	0.932
10	-1.8±3.1	1.7±0.9	0.6±0.5	0.9±1.6	0.0±0.4	0.6±1.0	0.942
20	-1.9±3.3	1.8±1.0	0.7±0.5	1.0±1.6	-0.1±0.5	0.5±1.0	0.946
50	-2.3±3.6	1.8±1.1	0.7±0.6	1.2±1.8	-0.2±0.5	0.5±1.2	0.942
80	-2.7±3.9	1.7±1.2	0.7±0.6	1.4±1.9	-0.2±0.6	0.6±1.3	0.938
95	-2.9±4.0	1.6±1.2	0.7±0.6	1.6±2.0	-0.3±0.6	0.7±1.3	0.936

Table A-4: The corresponding p-values for the regression coefficients in **Table A-3**. (Q_e μmol/g)

Q_e	c	E	S	A	V	J^+
1	0.525	0.391	0.636	0.528	0.787	0.346
2	0.542	0.259	0.490	0.539	0.823	0.395
5	0.567	0.150	0.335	0.555	0.903	0.489
10	0.583	0.114	0.268	0.566	0.989	0.577
20	0.588	0.110	0.244	0.566	0.910	0.654
50	0.558	0.149	0.273	0.530	0.770	0.684
80	0.518	0.198	0.315	0.484	0.695	0.647
95	0.499	0.224	0.336	0.462	0.667	0.622

Table A-5: Three sets of regression coefficients for the multiple linear regressions between $\Delta G_{S\text{-}W,i}$ and solute descriptors for MN500 with the following compounds included in the regression: a) all solutes, b) all cations, and c) all neutral compounds. (Q_e μmol/g)

Set	Q_e	*c*	*e*	*s*	*a*	*b*	*V*	j^+	R^2
	1	5.7±9.3	2.1±3.6	6.7±3.4	-2.2±4.6	8.5±26.2	0.0±3.0	-4.4±3.5	0.623
	10	-1.8±6.4	1.3±2.5	5.2±2.3	2.0±3.2	9.4±18.0	1.5±2.1	-0.7±2.4	0.502
	30	-5.4±5.1	1.2±2.0	4.4±1.8	3.9±2.5	9.9±14.4	2.1±1.6	1.0±1.9	0.734
a) All	50	-7.1±4.6	1.3±1.8	4.0±1.6	4.7±2.2	10.2±12.8	2.3±1.5	1.7±1.7	0.825
Solutes	80	-8.7±4.1	1.5±1.6	3.7±1.5	5.5±2.0	10.5±11.5	2.4±1.3	2.4±1.5	0.882
	100	-9.4±3.9	1.6±1.5	3.5±1.4	5.9±1.9	10.6±10.9	2.4±1.2	2.7±1.4	0.901
	150	-10.7±3.6	1.9±1.4	3.1±1.3	6.5±1.8	10.9±10.0	2.2±1.1	3.3±1.3	0.927
	200	-11.5±3.4	2.3±1.3	2.8±1.2	6.9±1.7	11.1±9.6	1.9±1.1	3.8±1.3	0.939
	300	-11.9±3.6	3.5±1.4	2.3±1.3	7.4±1.8	11.2±10.2	0.3±1.2	4.7±1.3	0.939
	1	-1.2±16.6	-0.1±4.9	10.4±2.7	-2.5±8.2	_	-0.9±2.4	-3.4±5.4	0.739
	10	-2.2±11.6	0.9±3.4	7.3±1.9	0.1±5.7	_	0.5±1.7	-1.0±3.7	0.819
b)	30	-3.3±9.4	1.5±2.8	5.7±1.5	1.5±4.6	_	1.1±1.3	0.2±3.0	0.881
cations	50	-4.1±8.5	1.9±2.5	5.0±1.4	2.3±4.2	_	1.3±1.2	0.8±2.7	0.908
	80	-5.0±7.8	2.2±2.3	4.2±1.3	3.0±3.9	_	1.5±1.1	1.5±2.5	0.929
	100	-5.5±7.6	2.4±2.3	3.9±1.2	3.4±3.8	_	1.5±1.5	1.8±2.5	0.937
	150	-6.6±7.7	2.8±2.3	3.2±1.2	4.2±3.8	_	1.4±1.1	2.4±2.5	0.946
	200	-7.5±8.2	3.1±2.4	2.7±1.3	4.9±4.1	_	1.2±1.2	3.1±2.6	0.948
	300	-9.1±12.1	3.9±3.6	1.7±2.0	6.3±6.0	_	-0.2±1.7	4.7±3.9	0.929
	1	-15.5±9.8	54.3±9.3	-11.5±3.1	12.6±2.3	-25.7±10.7	-3.5±12.2	_	0.980
	10	-14.3±9.7	39.9±9.2	-7.1±3.1	11.9±2.3	-15.4±10.6	-5.7±12.1	_	0.973
	30	-13.7±10.2	33.0±9.7	-5.0±3.2	11.5±2.4	-10.5±11.2	-6.8±12.8	_	0.966
c) All	50	-13.4±10.6	29.8±10.0	-4.1±3.3	11.4±2.5	-8.2±11.6	-7.3±13.2	_	0.961
neutrals	80	-13.2±10.9	26.8±10.4	-3.2±3.4	11.2±2.6	-6.1±12.0	-7.7±13.7	_	0.956
	100	-13.1±11.1	25.4±10.6	-2.7±3.5	11.1±2.6	-5.1±12.2	-7.9±13.9	_	0.954
	150	-12.8±11.5	22.9±10.9	-2.0±3.6	11.0±2.7	-3.3±12.6	-8.3±14.4	_	0.948
	200	-12.7±11.8	21.1±11.2	-1.4±3.7	10.9±2.8	-2.0±12.9	-8.6±14.7	_	0.944
	300	-12.5±12.2	18.5±11.6	-0.7±3.9	10.8±2.9	-0.2±13.4	-9.0±15.3	_	0.938

Table A-6: The corresponding p-values for the regression coefficients in **Table A-5**. (Q_e μmol/g)

Set	Q_e	c	E	S	A	B	V	J^+
a) All Solutes	1	0.554	0.576	0.068	0.639	0.752	0.992	0.992
	10	0.786	0.616	0.041	0.54	0.611	0.469	0.469
	30	0.309	0.555	0.031	0.147	0.501	0.219	0.219
	50	0.143	0.48	0.028	0.055	0.439	0.138	0.138
	80	0.054	0.373	0.027	0.017	0.377	0.09	0.09
	100	0.031	0.309	0.027	0.009	0.347	0.076	0.076
	150	0.01	0.182	0.03	0.003	0.296	0.071	0.071
	200	0.005	0.099	0.037	0.001	0.268	0.103	0.103
	300	0.006	0.028	0.099	0.001	0.292	0.801	0.801
b) cations	1	0.946	0.988	0.008	0.77	_	0.712	0.55
	10	0.856	0.801	0.008	0.985	_	0.771	0.792
	30	0.734	0.604	0.009	0.752	_	0.439	0.947
	50	0.645	0.488	0.011	0.608	_	0.314	0.77
	80	0.548	0.378	0.016	0.468	_	0.239	0.585
	100	0.501	0.331	0.02	0.405	_	0.222	0.497
	150	0.425	0.265	0.04	0.312	_	0.244	0.359
	200	0.396	0.246	0.086	0.275	_	0.359	0.291
	300	0.48	0.326	0.412	0.332	_	0.9	0.276
c) All neutrals	1	0.253	0.028	0.065	0.031	0.138	0.804	_
	10	0.278	0.05	0.145	0.034	0.284	0.684	_
	30	0.312	0.077	0.258	0.04	0.448	0.649	_
	50	0.332	0.098	0.347	0.044	0.552	0.637	_
	80	0.352	0.123	0.455	0.048	0.662	0.629	_
	100	0.362	0.139	0.516	0.051	0.717	0.626	_
	150	0.381	0.172	0.641	0.055	0.819	0.621	_
	200	0.395	0.201	0.738	0.058	0.892	0.618	_
	300	0.415	0.252	0.88	0.064	0.99	0.615	_

Table A-7: Three sets of regression coefficients for the multiple linear regressions between $\Delta G_{S\text{-}W,i}$ and solute descriptors for Amberlite 200 with the following compounds included in the regression: a) all solutes, b) all cations, and c) all neutral compounds. (Q_e μmol/g)

Set	Q_e	*c*	*e*	*s*	*a*	*b*	*v*	j^+	R^2
	1	-13.0±6.6	1.7±2.8	3.9±2.9	4.9±4.3	13.4±25.2	1.5±2.1	1.8±3.2	0.678
	2	-12.3±5.6	2.1±2.4	3.9±2.5	4.7±3.7	7.7±21.6	1.3±1.8	1.6±2.7	0.774
	5	-11.7±4.6	2.5±2.0	3.8±2.0	4.5±3.0	1.4±17.8	1.1±1.5	1.5±2.2	0.865
a) All	10	-11.6±4.1	2.8±1.7	3.8±1.8	4.5±2.6	-2.3±15.6	0.9±1.3	1.4±2.0	0.908
Solutes	20	-11.6±3.7	2.9±1.5	3.7±1.6	4.7±2.4	-4.9±14.1	0.7±1.2	1.5±1.8	0.933
	50	-12.3±3.5	2.9±1.5	3.6±1.5	5.2±2.3	-5.6±13.4	0.3±1.1	1.7±1.7	0.946
	80	-13.1±3.7	2.6±1.6	3.5±1.6	5.7±2.4	-4.1±14.1	0.1±1.2	2.0±1.8	0.945
	95	-13.5±3.9	2.4±1.6	3.4±1.7	5.9±2.5	-3.3±14.9	0.0±1.2	2.1±1.9	0.941
	1	-6.6±9.8	2.7±2.9	0.8±1.6	3.2±4.8	_	0.4±1.4	3.2±3.2	0.869
	2	-5.7±8.8	3.3±2.6	1.0±1.4	2.8±4.3	_	0.3±1.2	2.6±2.8	0.904
b)	5	-4.8±8.8	3.9±2.6	1.4±1.4	2.5±4.3	_	0.1±1.2	1.9±2.8	0.932
cations	10	-4.5±7.8	4.3±2.3	1.5±1.3	2.3±3.8	_	0.0±1.1	1.5±2.5	0.942
	20	-4.6±8.1	4.5±2.4	1.7±1.3	2.4±4.0	_	-0.1±1.1	1.2±2.6	0.946
	50	-5.6±9.0	4.4±2.7	1.8±1.4	3.0±4.4	_	-0.4±1.3	1.2±2.9	0.942
	80	-6.6±9.6	4.2±2.9	1.7±1.6	3.5±4.8	_	-0.6±1.4	1.5±3.1	0.938
	95	-7.1±9.9	4.0±2.9	1.7±1.6	3.8±4.9	_	-0.6±1.4	1.7±3.2	0.936
	1	-4.2±10.5	-6.8±15.0	5.7±2.6	16.7±6.0	22.5±34.8	-7.9±12.2	_	0.984
	2	-4.5±8.8	-0.1±12.6	5.5±2.1	13.1±5.0	5.4±29.2	-8.9±10.2	_	0.987
	5	-4.3±8.4	6.3±12.0	5.3±2.0	9.3±4.8	-11.2±27.7	-10.4±9.7	_	0.986
c) All	10	-3.6±9.1	8.9±13.0	5.2±2.2	7.5±5.2	-18.2±30.1	-11.9±10.5	_	0.981
neutrals	20	-2.3±10.3	9.1±14.7	5.0±2.5	6.8±5.8	-19.0±34.2	-13.7±12.0	_	0.973
	50	1.0±12.8	3.9±18.3	4.7±3.1	8.4±7.3	-6.3±42.4	-17.1±14.8	_	0.956
	80	4.2±15.3	-3.1±21.9	4.4±3.7	11.2±8.7	11.4±50.7	-20.0±17.8	_	0.938
	95	6.5±17.2	-7.8±24.6	4.2±4.2	13.1±9.7	23.0±57.0	-22.0±20.0	_	0.925

Table A-8: The corresponding p-values for the regression coefficients in **Table A-7**. (Q_e μmol/g)

Set	Q_e	c	E	S	A	B	V	J^+
	1	0.070	0.558	0.196	0.272	0.605	0.479	0.582
	2	0.048	0.396	0.140	0.223	0.726	0.467	0.559
	5	0.025	0.215	0.080	0.156	0.938	0.469	0.519
a) All	10	0.014	0.125	0.052	0.109	0.883	0.500	0.480
Solutes	20	0.007	0.079	0.036	0.072	0.733	0.577	0.430
	50	0.004	0.076	0.036	0.041	0.683	0.790	0.341
	80	0.004	0.118	0.051	0.033	0.774	0.951	0.291
	95	0.004	0.159	0.065	0.035	0.826	0.984	0.285
	1	0.525	0.391	0.636	0.528	_	0.787	0.346
	2	0.542	0.259	0.490	0.539	_	0.823	0.395
b)	5	0.567	0.150	0.335	0.555	_	0.903	0.489
cations	10	0.583	0.114	0.268	0.566	_	0.989	0.577
	20	0.588	0.110	0.244	0.566	_	0.910	0.654
	50	0.558	0.149	0.273	0.530	_	0.770	0.684
	80	0.518	0.198	0.315	0.484	_	0.695	0.647
	95	0.499	0.224	0.336	0.462	_	0.667	0.622
	1	0.726	0.696	0.158	0.107	0.584	0.582	_
	2	0.660	0.995	0.124	0.121	0.870	0.476	_
	5	0.659	0.651	0.121	0.189	0.726	0.395	_
c) All	10	0.731	0.563	0.144	0.283	0.607	0.376	_
neutrals	20	0.845	0.600	0.184	0.365	0.633	0.370	_
	50	0.947	0.850	0.274	0.369	0.895	0.368	_
	80	0.811	0.901	0.364	0.328	0.843	0.376	_
	95	0.742	0.781	0.420	0.313	0.726	0.386	_

Table A-9: Three sets of regression coefficients for the multiple linear regressions between $\Delta G_{S\text{-}G,i}$ and solute descriptors for MN500 with the following compounds included in the regression: a) all solutes, b) all cations, and c) all neutral compounds. (Q_e μmol/g)

Set	**Q_e**	***c***	***e***	***s***	***a***	***b***	***v***	***j^+***	**R^2**
	1	-21.4±8.3	19.3±3.0	16.4±2.9	21.5±4.1	38.9±23.5	-13.7±2.6	33.4±3.1	0.988
	10	-24.6±6.4	19.9±2.3	15.5±2.2	23.7±3.1	26.8±18.0	-12.2±2.0	34.8±2.4	0.994
	30	-26.8±5.9	20.3±2.1	15.0±2.0	24.8±2.9	22.5±16.5	-11.7±1.9	35.6±2.2	0.995
a) All	50	-27.9±5.7	20.5±2.1	14.7±2.0	25.4±2.8	20.9±16.1	-11.5±1.8	36.0±2.1	0.996
Solutes	80	-29.1±5.6	20.8±2.1	14.4±2.0	26.0±2.8	19.7±15.9	-11.4±1.8	36.5±2.1	0.996
	100	-29.7±5.6	21.0±2.1	14.2±2.0	26.3±2.8	19.3±15.9	-11.4±1.8	36.7±2.1	0.996
	150	-30.8±5.6	21.4±2.1	13.9±2.0	26.8±2.8	18.8±15.9	-11.5±1.8	37.2±2.1	0.996
	200	-31.6±5.7	21.8±2.1	13.7±2.0	27.2±2.8	18.6±16.1	-11.8±1.8	37.6±2.1	0.996
	300	-32.8±6.0	22.9±2.2	13.2±2.1	27.8±2.9	18.8±16.9	-13.4±1.9	38.5±2.2	0.996
	1	-47.5±22.2	12.3±6.2	18.3±3.2	32.1±10.9	_	-12.0±2.9	41.4±7.7	0.992
	10	-47.7±21.3	13.1±5.9	15.1±3.1	34.6±10.5	_	-10.5±2.7	43.3±7.4	0.993
b)	30	-48.4±21.4	13.7±6.0	13.5±3.1	35.9±10.5	_	-9.8±2.8	44.3±7.5	0.993
cations	50	-49.0±21.7	14.0±6.0	12.7±3.2	36.6±10.7	_	-9.6±2.8	44.8±7.6	0.993
	80	-49.7±22.1	14.3±6.1	12.0±3.2	37.3±10.8	_	-9.4±2.8	45.3±7.7	0.992
	100	-50.1±22.3	14.5±6.2	11.6±3.2	37.7±10.9	_	-9.4±2.9	45.6±7.8	0.992
	150	-51.1±22.8	14.8±6.3	10.9±3.3	38.5±11.0	_	-9.5±2.9	46.2±8.0	0.992
	200	-52.0±23.3	15.1±6.5	10.4±3.4	39.3±11.5	_	-9.7±3.0	46.8±8.1	0.992
	300	-54.0±24.9	15.7±6.9	9.3±3.6	41.0±12.2	_	-11.0±3.2	48.6±8.7	0.992
	1	-31.3±11.5	62.4±11.0	4.9±3.6	30.8±2.7	-16.9±12.6	-17.1±14.4	_	0.996
	10	-30.0±10.6	47.9±10.0	9.3±3.3	30.1±2.5	-6.6±11.5	-19.4±13.2	_	0.996
	30	-29.4±10.6	41.0±10.0	11.4±3.3	29.7±2.5	-1.7±11.6	-20.4±13.2	_	0.996
c) All	50	-29.2±10.7	37.8±10.2	12.4±3.4	29.6±2.5	0.6±11.7	-20.9±13.4	_	0.996
neutrals	80	-28.9±10.9	34.9±10.4	13.3±3.4	29.4±2.5	2.7±11.9	-21.4±13.6	_	0.996
	100	-28.8±11.0	33.5±10.5	13.7±3.5	29.3±2.6	3.7±12.0	-21.6±13.7	_	0.996
	150	-28.6±11.2	31.0±10.7	14.5±3.5	29.2±2.6	5.5±12.3	-22.0±14.0	_	0.996
	200	-28.4±11.4	29.1±10.8	15.0±3.6	29.1±2.7	6.8±12.5	-22.3±14.2	_	0.995
	300	-28.2±11.7	26.6±11.1	15.8±3.7	29.0±2.7	8.6±12.8	-22.7±14.6	_	0.995

Table A-10: The corresponding p-values for the regression coefficients in **Table A-9**. (Q_e μmol/g)

Set	Q_e	c	E	S	A	B	V	J^+
a) All Solutes	1	0.024	0	0	0	0.122	0	0
	10	0.002	0	0	0	0.161	0	0
	30	0.001	0	0	0	0.197	0	0
	50	0	0	0	0	0.218	0	0
	80	0	0	0	0	0.237	0	0
	100	0	0	0	0	0.245	0	0
	150	0	0	0	0	0.259	0	0
	200	0	0	0	0	0.267	0	0
	300	0	0	0	0	0.285	0	0
b) cations	1	0.077	0.094	0.001	0.026	_	0.006	0.002
	10	0.066	0.068	0.003	0.016	_	0.009	0.001
	30	0.065	0.062	0.005	0.014	_	0.012	0.001
	50	0.065	0.06	0.007	0.014	_	0.014	0.001
	80	0.065	0.058	0.01	0.014	_	0.016	0.001
	100	0.066	0.058	0.012	0.014	_	0.017	0.001
	150	0.066	0.058	0.017	0.014	_	0.018	0.001
	200	0.067	0.058	0.022	0.014	_	0.018	0.001
	300	0.073	0.064	0.043	0.015	_	0.014	0.001
c) All neutrals	1	0.114	0.03	0.307	0.008	0.313	0.357	_
	10	0.105	0.041	0.107	0.007	0.624	0.28	_
	30	0.109	0.055	0.076	0.007	0.896	0.262	_
	50	0.113	0.066	0.067	0.007	0.966	0.258	_
	80	0.118	0.078	0.061	0.007	0.844	0.257	_
	100	0.12	0.085	0.058	0.008	0.789	0.257	_
	150	0.126	0.101	0.055	0.008	0.699	0.257	_
	200	0.13	0.115	0.053	0.008	0.642	0.258	_
	300	0.137	0.139	0.05	0.009	0.572	0.261	_

Table A-11: Three sets of regression coefficients for the multiple linear regressions between $\Delta G_{S\text{-}G,i}$ and solute descriptors for Amberlite 200 with the following compounds included in the regression: a) all solutes, b) all cations, and c) all neutral compounds. (Q_e μmol/g)

Set	Q_e	*c*	*e*	*s*	*a*	*b*	*v*	j^+	R^2
a) All Solutes	1	-32.7±7.3	17.7±3.1	15.3±3.2	26.7±4.8	21.0±28.1	-10.5±2.3	31.6±3.6	0.994
	2	-32.1±6.6	18.1±2.8	15.3±2.9	26.5±4.3	15.4±25.5	-10.7±2.1	31.5±3.2	0.995
	5	-31.5±6.0	18.6±2.5	15.2±2.6	26.3±3.9	9.1±23.1	-10.9±1.9	31.3±2.9	0.996
	10	-31.3±5.7	18.8±2.4	15.2±2.5	26.3±3.8	5.3±22.1	-11.1±1.8	31.3±2.8	0.996
	20	-31.4±5.6	19.0±2.4	15.1±2.5	26.5±3.7	2.8±21.8	-11.3±1.8	31.3±2.8	0.997
	50	-32.1±5.8	18.9±2.4	15.0±2.5	27.0±3.8	2.1±22.2	-11.7±1.8	31.5±2.8	0.997
	80	-32.9±6.0	18.6±2.5	14.8±2.6	27.5±3.9	3.5±22.9	-11.9±1.9	31.8±2.9	0.996
	95	-33.2±6.1	18.5±2.6	14.8±2.7	27.7±4.0	4.4±23.5	-12.0±1.9	31.9±3.0	0.996
b) cations	1	-42.2±12.8	14.1±3.8	10.8±2.1	33.7±6.3	_	-9.7±1.8	38.8±4.1	0.997
	2	-41.3±14.0	14.6±4.2	11.1±2.3	33.3±6.9	_	-9.8±2.0	38.2±4.5	0.996
	5	-40.4±15.9	15.3±4.7	11.4±2.6	32.9±7.8	_	-9.9±2.3	37.5±5.1	0.995
	10	-40.1±17.4	15.7±5.2	11.6±2.8	32.8±8.6	_	-10.1±2.5	37.1±5.6	0.995
	20	-40.2±19.0	15.9±5.7	11.7±3.1	32.8±9.4	_	-10.2±2.7	36.8±6.1	0.994
	50	-41.2±21.1	15.8±6.3	11.8±3.4	33.4±10.4	_	-10.5±3.0	36.8±6.8	0.992
	80	-42.2±22.1	15.5±6.6	11.8±3.6	34.0±11.0	_	-10.6±3.2	37.1±7.1	0.992
	95	-42.7±22.5	15.4±6.7	11.7±3.6	34.3±11.1	_	-10.7±3.2	37.2±7.2	0.991
c) All neutrals	1	-40.3±14.4	4.3±20.5	23.5±3.5	30.4±8.1	-2.4±47.4	7.2±16.6	_	0.996
	2	-40.6±12.4	11.0±17.7	23.3±3.0	26.8±7.0	-19.4±41.0	6.3±14.4	_	0.997
	5	-40.3±11.3	17.4±16.1	23.1±2.7	23.0±6.4	-36.0±37.2	4.7±13.0	_	0.998
	10	-39.6±11.4	20.0±16.2	23.0±2.8	21.2±6.4	-43.0±37.6	3.3±13.2	_	0.997
	20	-38.3±12.2	20.2±17.4	22.8±3.0	20.5±6.9	-43.9±40.4	1.4±14.2	_	0.997
	50	-35.1±14.6	15.0±20.9	22.5±3.6	22.1±8.3	-31.1±48.4	-2.0±17.0	_	0.995
	80	-31.9±17.3	8.0±24..6	22.2±4.2	24.9±9.8	-13.4±57.1	-4.9±20.0	_	0.994
	95	-29.5±19.2	3.3±27.4	22.0±4.7	26.8±10.9	-1.9±63.6	-6.8±22.3	_	0.992

Table A-12: The corresponding p-values for the regression coefficients in **Table A-11**. (Q_e μmol/g)

Set	Q_e	c	E	S	A	B	V	J^+
a) All Solutes	1	<0.001	<0.001	<0.001	<0.001	0.5	<0.001	<0.001
	2	<0.001	<0.001	<0.001	<0.001	0.6	<0.001	<0.001
	5	<0.001	<0.001	<0.001	<0.001	0.7	<0.001	<0.001
	10	<0.001	<0.001	<0.001	<0.001	0.8	<0.001	<0.001
	20	<0.001	<0.001	<0.001	<0.001	0.9	<0.001	<0.001
	50	<0.001	<0.001	<0.001	<0.001	0.9	<0.001	<0.001
	80	<0.001	<0.001	<0.001	<0.001	0.9	<0.001	<0.001
	95	<0.001	<0.001	<0.001	<0.001	0.9	<0.001	<0.001
b) cations	1	0.016	0.010	0.002	0.002	_	0.002	<0.001
	2	0.026	0.013	0.003	0.003	_	0.003	<0.001
	5	0.044	0.018	0.004	0.006	_	0.005	<0.001
	10	0.061	0.024	0.006	0.009	_	0.007	<0.001
	20	0.079	0.031	0.009	0.013	_	0.009	<0.001
	50	0.099	0.046	0.014	0.018	_	0.013	0.002
	80	0.105	0.056	0.017	0.021	_	0.015	0.002
	95	0.106	0.061	0.018	0.021	_	0.016	0.002
c) All neutrals	1	0.107	0.853	0.022	0.065	0.965	0.706	_
	2	0.082	0.598	0.016	0.063	0.682	0.705	_
	5	0.07	0.392	0.014	0.069	0.436	0.752	_
	10	0.074	0.343	0.014	0.081	0.372	0.828	_
	20	0.089	0.367	0.017	0.098	0.391	0.929	_
	50	0.139	0.547	0.024	0.117	0.586	0.918	_
	80	0.206	0.776	0.034	0.126	0.836	0.83	_
	95	0.265	0.916	0.042	0.133	0.979	0.789	_

Table A-13: Three sets of regression coefficients for the multiple linear regressions between $\Delta G_{S\text{-}G,i}$ and solute descriptors for MN500 with the following compounds included in the regression: a) all solutes, b) all cations, and c) all neutral compounds. (Q_e μmol/g)

Set	Q_e	*c*	*e*	*s*	*a*	*b*	*v*	j^+	R^2
	1	-21.4±8.3	19.3±3.0	16.4±2.9	21.5±4.1	38.9±23.5	-13.7±2.6	33.4±3.1	0.988
	10	-24.6±6.4	19.9±2.3	15.5±2.2	23.7±3.1	26.8±18.0	-12.2±2.0	34.8±2.4	0.994
	30	-26.8±5.9	20.3±2.1	15.0±2.0	24.8±2.9	22.5±16.5	-11.7±1.9	35.6±2.2	0.995
a) All	50	-27.9±5.7	20.5±2.1	14.7±2.0	25.4±2.8	20.9±16.1	-11.5±1.8	36.0±2.1	0.996
Solutes	80	-29.1±5.6	20.8±2.1	14.4±2.0	26.0±2.8	19.7±15.9	-11.4±1.8	36.5±2.1	0.996
	100	-29.7±5.6	21.0±2.1	14.2±2.0	26.3±2.8	19.3±15.9	-11.4±1.8	36.7±2.1	0.996
	150	-30.8±5.6	21.4±2.1	13.9±2.0	26.8±2.8	18.8±15.9	-11.5±1.8	37.2±2.1	0.996
	200	-31.6±5.7	21.8±2.1	13.7±2.0	27.2±2.8	18.6±16.1	-11.8±1.8	37.6±2.1	0.996
	300	-32.8±6.0	22.9±2.2	13.2±2.1	27.8±2.9	18.8±16.9	-13.4±1.9	38.5±2.2	0.996
	1	-47.5±22.2	12.3±6.2	18.3±3.2	32.1±10.9	_	-12.0±2.9	41.4±7.7	0.992
	10	-47.7±21.3	13.1±5.9	15.1±3.1	34.6±10.5	_	-10.5±2.7	43.3±7.4	0.993
b)	30	-48.4±21.4	13.7±6.0	13.5±3.1	35.9±10.5	_	-9.8±2.8	44.3±7.5	0.993
cations	50	-49.0±21.7	14.0±6.0	12.7±3.2	36.6±10.7	_	-9.6±2.8	44.8±7.6	0.993
	80	-49.7±22.1	14.3±6.1	12.0±3.2	37.3±10.8	_	-9.4±2.8	45.3±7.7	0.992
	100	-50.1±22.3	14.5±6.2	11.6±3.2	37.7±10.9	_	-9.4±2.9	45.6±7.8	0.992
	150	-51.1±22.8	14.8±6.3	10.9±3.3	38.5±11.0	_	-9.5±2.9	46.2±8.0	0.992
	200	-52.0±23.3	15.1±6.5	10.4±3.4	39.3±11.5	_	-9.7±3.0	46.8±8.1	0.992
	300	-54.0±24.9	15.7±6.9	9.3±3.6	41.0±12.2	_	-11.0±3.2	48.6±8.7	0.992
	1	-31.3±11.5	62.4±11.0	4.9±3.6	30.8±2.7	-16.9±12.6	-17.1±14.4	_	0.996
	10	-30.0±10.6	47.9±10.0	9.3±3.3	30.1±2.5	-6.6±11.5	-19.4±13.2	_	0.996
	30	-29.4±10.6	41.0±10.0	11.4±3.3	29.7±2.5	-1.7±11.6	-20.4±13.2	_	0.996
c) All	50	-29.2±10.7	37.8±10.2	12.4±3.4	29.6±2.5	0.6±11.7	-20.9±13.4	_	0.996
neutrals	80	-28.9±10.9	34.9±10.4	13.3±3.4	29.4±2.5	2.7±11.9	-21.4±13.6	_	0.996
	100	-28.8±11.0	33.5±10.5	13.7±3.5	29.3±2.6	3.7±12.0	-21.6±13.7	_	0.996
	150	-28.6±11.2	31.0±10.7	14.5±3.5	29.2±2.6	5.5±12.3	-22.0±14.0	_	0.996
	200	-28.4±11.4	29.1±10.8	15.0±3.6	29.1±2.7	6.8±12.5	-22.3±14.2	_	0.995
	300	-28.2±11.7	26.6±11.1	15.8±3.7	29.0±2.7	8.6±12.8	-22.7±14.6	_	0.995

Table A-14: The corresponding p-values for the regression coefficients in **Table A-13**. (Q_e μmol/g)

Set	Q_e	c	E	S	A	B	V	J^+
	1	0.024	0	0	0	0.122	0	0
	10	0.002	0	0	0	0.161	0	0
	30	0.001	0	0	0	0.197	0	0
a) All	50	0	0	0	0	0.218	0	0
Solutes	80	0	0	0	0	0.237	0	0
	100	0	0	0	0	0.245	0	0
	150	0	0	0	0	0.259	0	0
	200	0	0	0	0	0.267	0	0
	300	0	0	0	0	0.285	0	0
	1	0.077	0.094	0.001	0.026	_	0.006	0.002
	10	0.066	0.068	0.003	0.016	_	0.009	0.001
b)	30	0.065	0.062	0.005	0.014	_	0.012	0.001
cations	50	0.065	0.06	0.007	0.014	_	0.014	0.001
	80	0.065	0.058	0.01	0.014	_	0.016	0.001
	100	0.066	0.058	0.012	0.014	_	0.017	0.001
	150	0.066	0.058	0.017	0.014	_	0.018	0.001
	200	0.067	0.058	0.022	0.014	_	0.018	0.001
	300	0.073	0.064	0.043	0.015	_	0.014	0.001
	1	0.114	0.03	0.307	0.008	0.313	0.357	_
	10	0.105	0.041	0.107	0.007	0.624	0.28	_
	30	0.109	0.055	0.076	0.007	0.896	0.262	_
c) All	50	0.113	0.066	0.067	0.007	0.966	0.258	_
neutrals	80	0.118	0.078	0.061	0.007	0.844	0.257	_
	100	0.12	0.085	0.058	0.008	0.789	0.257	_
	150	0.126	0.101	0.055	0.008	0.699	0.257	_
	200	0.13	0.115	0.053	0.008	0.642	0.258	_
	300	0.137	0.139	0.05	0.009	0.572	0.261	_

Table A-15: Three sets of regression coefficients for the multiple linear regressions between $\Delta G_{S\text{-}G,i}$ and solute descriptors for Amberlite 200 with the following compounds included in the regression: a) all solutes, b) all cations, and c) all neutral compounds. (Q_e μmol/g)

Set	Q_e	*c*	*e*	*s*	*a*	*b*	*v*	j^+	R^2
a) All Solutes	1	-32.7±7.3	17.7±3.1	15.3±3.2	26.7±4.8	21.0±28.1	-10.5±2.3	31.6±3.6	0.994
	2	-32.1±6.6	18.1±2.8	15.3±2.9	26.5±4.3	15.4±25.5	-10.7±2.1	31.5±3.2	0.995
	5	-31.5±6.0	18.6±2.5	15.2±2.6	26.3±3.9	9.1±23.1	-10.9±1.9	31.3±2.9	0.996
	10	-31.3±5.7	18.8±2.4	15.2±2.5	26.3±3.8	5.3±22.1	-11.1±1.8	31.3±2.8	0.996
	20	-31.4±5.6	19.0±2.4	15.1±2.5	26.5±3.7	2.8±21.8	-11.3±1.8	31.3±2.8	0.997
	50	-32.1±5.8	18.9±2.4	15.0±2.5	27.0±3.8	2.1±22.2	-11.7±1.8	31.5±2.8	0.997
	80	-32.9±6.0	18.6±2.5	14.8±2.6	27.5±3.9	3.5±22.9	-11.9±1.9	31.8±2.9	0.996
	95	-33.2±6.1	18.5±2.6	14.8±2.7	27.7±4.0	4.4±23.5	-12.0±1.9	31.9±3.0	0.996
b) cations	1	-42.2±12.8	14.1±3.8	10.8±2.1	33.7±6.3	_	-9.7±1.8	38.8±4.1	0.997
	2	-41.3±14.0	14.6±4.2	11.1±2.3	33.3±6.9	_	-9.8±2.0	38.2±4.5	0.996
	5	-40.4±15.9	15.3±4.7	11.4±2.6	32.9±7.8	_	-9.9±2.3	37.5±5.1	0.995
	10	-40.1±17.4	15.7±5.2	11.6±2.8	32.8±8.6	_	-10.1±2.5	37.1±5.6	0.995
	20	-40.2±19.0	15.9±5.7	11.7±3.1	32.8±9.4	_	-10.2±2.7	36.8±6.1	0.994
	50	-41.2±21.1	15.8±6.3	11.8±3.4	33.4±10.4	_	-10.5±3.0	36.8±6.8	0.992
	80	-42.2±22.1	15.5±6.6	11.8±3.6	34.0±11.0	_	-10.6±3.2	37.1±7.1	0.992
	95	-42.7±22.5	15.4±6.7	11.7±3.6	34.3±11.1	_	-10.7±3.2	37.2±7.2	0.991
c) All neutrals	1	-40.3±14.4	4.3±20.5	23.5±3.5	30.4±8.1	-2.4±47.4	7.2±16.6	_	0.996
	2	-40.6±12.4	11.0±17.7	23.3±3.0	26.8±7.0	-19.4±41.0	6.3±14.4	_	0.997
	5	-40.3±11.3	17.4±16.1	23.1±2.7	23.0±6.4	-36.0±37.2	4.7±13.0	_	0.998
	10	-39.6±11.4	20.0±16.2	23.0±2.8	21.2±6.4	-43.0±37.6	3.3±13.2	_	0.997
	20	-38.3±12.2	20.2±17.4	22.8±3.0	20.5±6.9	-43.9±40.4	1.4±14.2	_	0.997
	50	-35.1±14.6	15.0±20.9	22.5±3.6	22.1±8.3	-31.1±48.4	-2.0±17.0	_	0.995
	80	-31.9±17.3	8.0±24..6	22.2±4.2	24.9±9.8	-13.4±57.1	-4.9±20.0	_	0.994
	95	-29.5±19.2	3.3±27.4	22.0±4.7	26.8±10.9	-1.9±63.6	-6.8±22.3	_	0.992

Table A-16: The corresponding p-values for the regression coefficients in **Table A-15**. (Q_e μmol/g)

Set	Q_e	c	E	S	A	B	V	J^+
a) All Solutes	1	<0.001	<0.001	<0.001	<0.001	0.5	<0.001	<0.001
	2	<0.001	<0.001	<0.001	<0.001	0.6	<0.001	<0.001
	5	<0.001	<0.001	<0.001	<0.001	0.7	<0.001	<0.001
	10	<0.001	<0.001	<0.001	<0.001	0.8	<0.001	<0.001
	20	<0.001	<0.001	<0.001	<0.001	0.9	<0.001	<0.001
	50	<0.001	<0.001	<0.001	<0.001	0.9	<0.001	<0.001
	80	<0.001	<0.001	<0.001	<0.001	0.9	<0.001	<0.001
	95	<0.001	<0.001	<0.001	<0.001	0.9	<0.001	<0.001
b) cations	1	0.016	0.010	0.002	0.002	_	0.002	<0.001
	2	0.026	0.013	0.003	0.003	_	0.003	<0.001
	5	0.044	0.018	0.004	0.006	_	0.005	<0.001
	10	0.061	0.024	0.006	0.009	_	0.007	<0.001
	20	0.079	0.031	0.009	0.013	_	0.009	<0.001
	50	0.099	0.046	0.014	0.018	_	0.013	0.002
	80	0.105	0.056	0.017	0.021	_	0.015	0.002
	95	0.106	0.061	0.018	0.021	_	0.016	0.002
c) All neutrals	1	0.107	0.853	0.022	0.065	0.965	0.706	_
	2	0.082	0.598	0.016	0.063	0.682	0.705	_
	5	0.07	0.392	0.014	0.069	0.436	0.752	_
	10	0.074	0.343	0.014	0.081	0.372	0.828	_
	20	0.089	0.367	0.017	0.098	0.391	0.929	_
	50	0.139	0.547	0.024	0.117	0.586	0.918	_
	80	0.206	0.776	0.034	0.126	0.836	0.83	_
	95	0.265	0.916	0.042	0.133	0.979	0.789	_

Text A1. $f^c(Q_e)$, $f^s(Q_e)$, etc. based on the training set of all solutes for (as shown in **Figures A-1a** and **A-2a**):

a) MN500

$$c = 0.052(\ln Q_e)^3 - 0.4(\ln Q_e)^2 - 2.53(\ln Q_e) + 5.661 \qquad R^2 = 0.999$$

$$e = 0.059(\ln Q_e)^3 - 0.323(\ln Q_e)^2 + 0.133(\ln Q_e) + 2.055 \qquad R^2 = 0.975$$

$$s = -0.01(\ln Q_e)^3 + 0.048(\ln Q_e)^2 - 0.704(\ln Q_e) + 6.675 \qquad R^2 = 1.00$$

$$a = -0.009(\ln Q_e)^3 + 0.031(\ln Q_e)^2 + 1.794(\ln Q_e) - 2.214 \qquad R^2 = 1.00$$

$$b = -0.008(\ln Q_e)^3 + 0.096(\ln Q_e)^2 + 0.199(\ln Q_e) + 8.482 \qquad R^2 = 1.00$$

$$v = -0.046(\ln Q_e)^3 + 0.26(\ln Q_e)^2 + 0.277(\ln Q_e) + 0.035 \qquad R^2 = 0.996$$

$$j^+ = 0.02(\ln Q_e)^3 - 0.174(\ln Q_e)^2 + 1.93(\ln Q_e) - 4.436 \qquad R^2 = 0.999$$

b) Amberlite 200

$$c = -0.046(\ln Q_e)^3 - 0.11(\ln Q_e)^2 + 0.892(\ln Q_e) - 12.957 \qquad R^2 = 0.999$$

$$e = -0.027(\ln Q_e)^3 + 0.042(\ln Q_e)^2 + 0.544(\ln Q_e) + 1.675 \qquad R^2 = 0.998$$

$$s = -0.008(\ln Q_e)^3 + 0.025(\ln Q_e)^2 - 0.061(\ln Q_e) + 3.912 \qquad R^2 = 1.00$$

$$a = 0.031(\ln Q_e)^3 - 0.041(\ln Q_e)^2 - 0.230(\ln Q_e) + 4.889 \qquad R^2 = 0.999$$

$$b = 0.211(\ln Q_e)^3 - 0.036(\ln Q_e)^2 - 7.867(\ln Q_e) + 13.284 \qquad R^2 = 1.00$$

$$v = -0.006(\ln Q_e)^3 + 0.014(\ln Q_e)^2 - 0.268(\ln Q_e) + 1.518 \qquad R^2 = 1.00$$

$$j^+ = 0.022(\ln Q_e)^3 - 0.051(\ln Q_e)^2 - 0.160(\ln Q_e) + 1.792 \qquad R^2 = 0.997$$

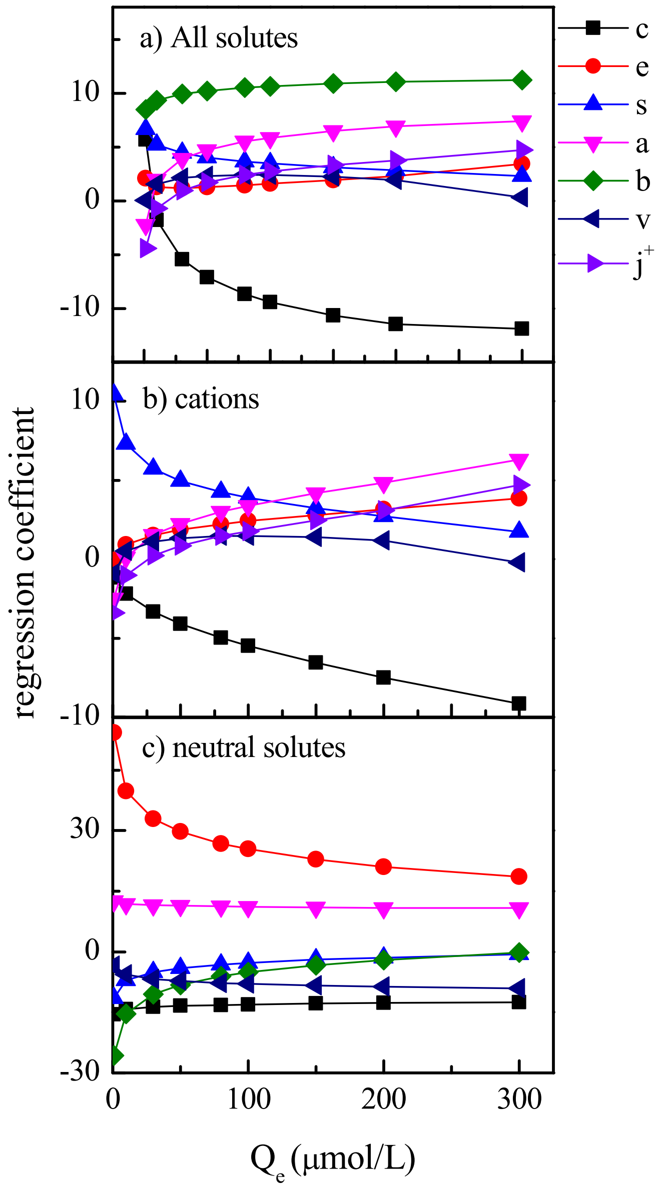

Figure A-1: Correlations of the regression coefficients for the multiple linear regressions between $\Delta G_{S\text{-}W,i}$ and solute descriptors with sorbed concentration for MN500 when a) all solutes; b) all cations; and c) all neutral solutes were included in the regression.

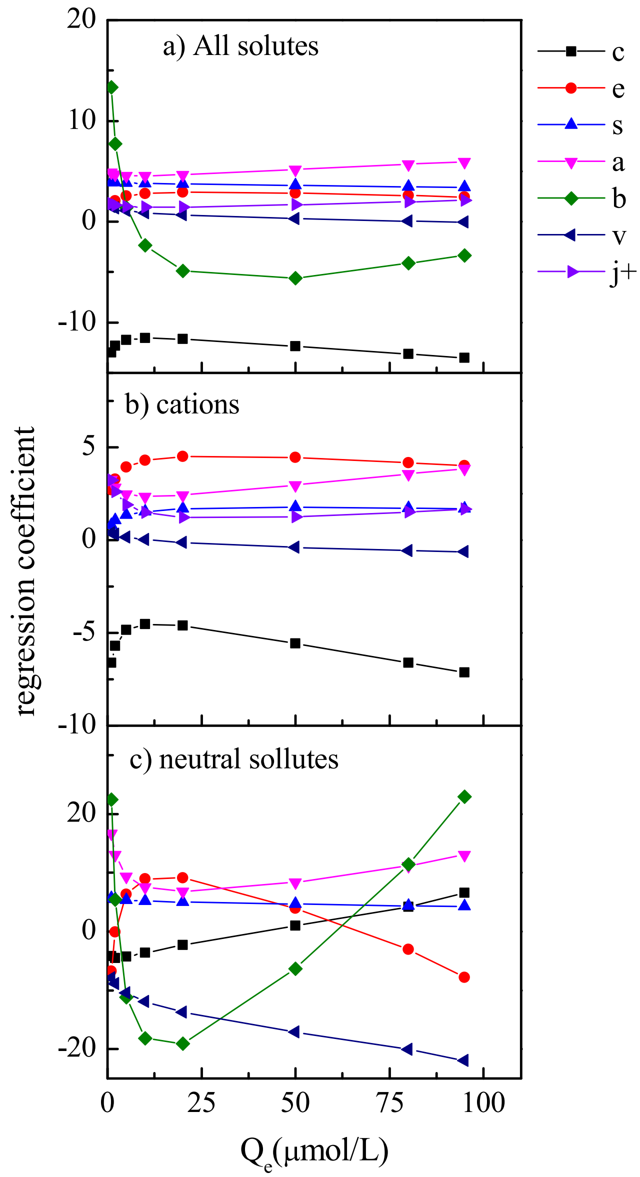

Figure A-2: Correlations of the regression coefficients for the multiple linear regressions between $\Delta G_{S\text{-}W,i}$ and solute descriptors with sorbed concentration for Amberlite 200 when a) all solutes; b) all cations; and c) all neutral solutes were included in the regression.

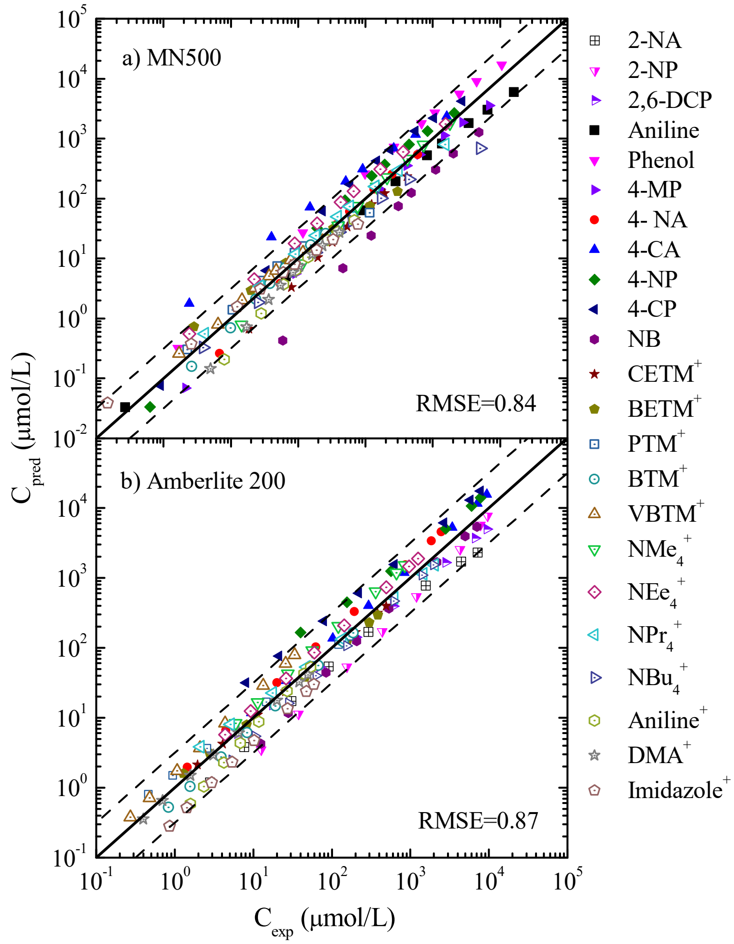

Figure A-3: Aqueous equilibrium concentrations calculated based on the predictive model (C_{pred} from eq 3.9) versus the experimental values (C_{exp}) for a training-set of 12 cations and 8 neutral aromatic solutes with a) 169 data points for MN500 and b) 161 data points for Amberlite 200. The solid lines show a perfect prediction, where the predicted values for C_e exactly equal the experimental values; the dashed lines are 0.5 log units above or below the solid lines.

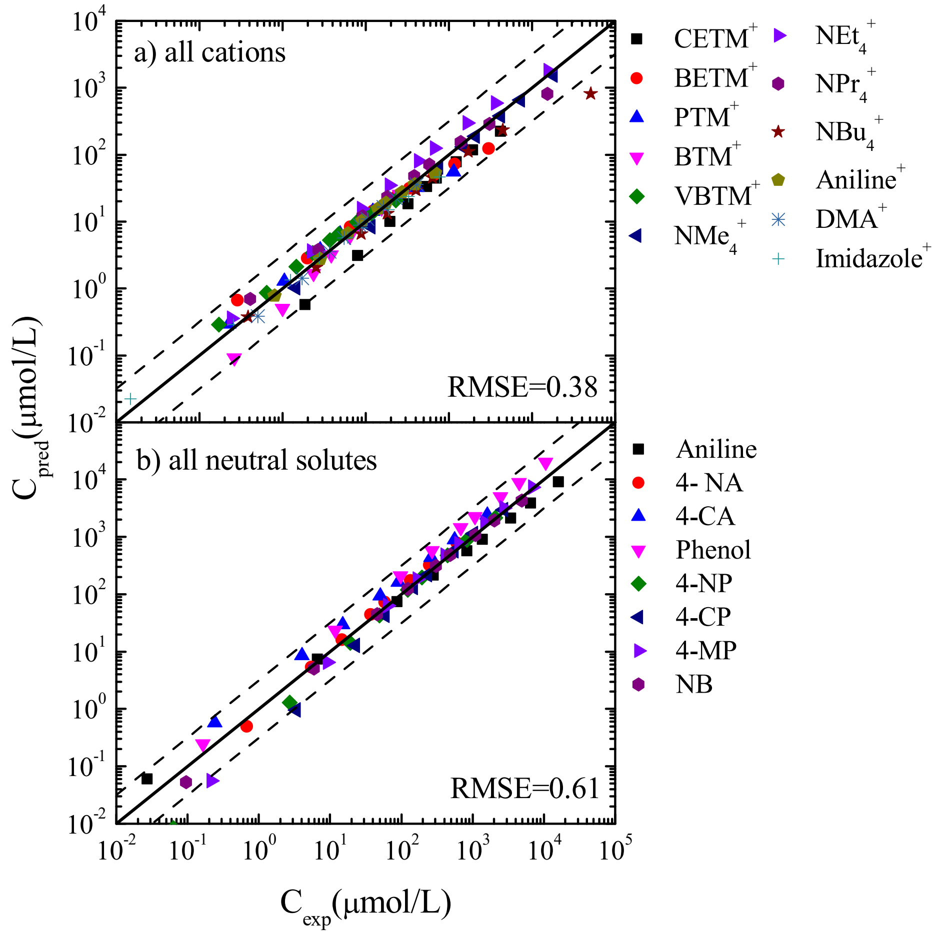

Figure A-4: Aqueous equilibrium concentrations calculated based on the predictive model (eq 3.9) versus the experimental values for a) a training-sets of 12 cations with 108 data points; and b) a training-set of 8 neutral solutes with 72 data points for MN500. The solid lines show a perfect prediction, where the predicted values for C_e exactly equal the experimental values; the dashed lines are 0.5 log units above or below the solid lines.

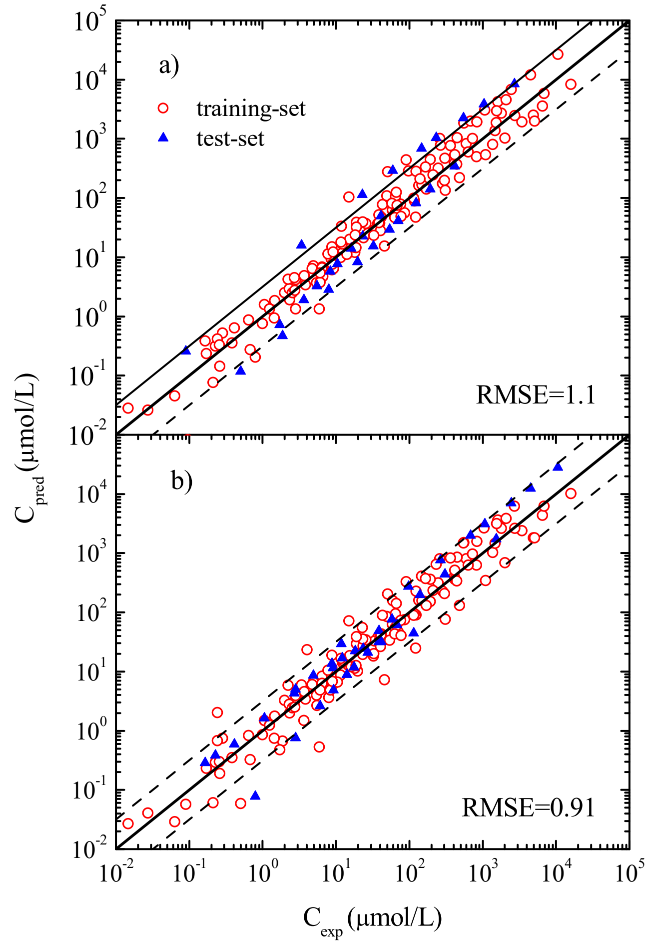

Figure A-5: Aqueous equilibrium concentrations calculated based on the predictive model (eq 3.9) versus the experimental values of MN500 for a) a training-set of 17 solutes with 153 data points and 3 test-set solutes (4-CP, $CETM^+$, DMA^+) with 36 data points b) a training-set of 17 solutes with 153 data points and 3 test-set solutes (Phenol, NPr_4^+, $Aniline^+$) with 36 data points. The solid lines show a perfect prediction, where the predicted values for C_e exactly equal the experimental values; the dashed lines are 0.5 log units above or below the solid lines.

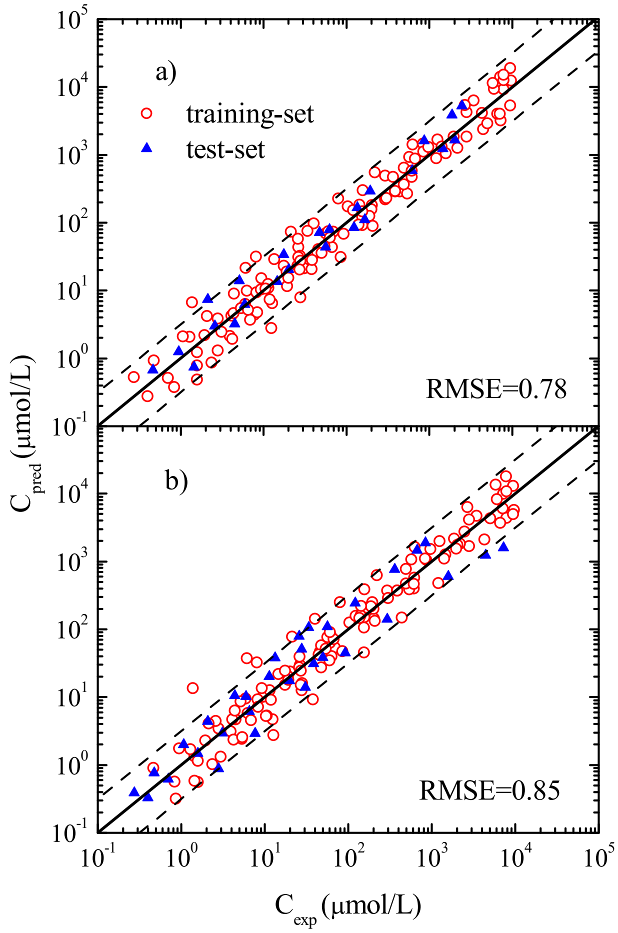

Figure A-6: Aqueous equilibrium concentrations calculated based on the predictive model (eq 3.9) versus the experimental values of Amberlite 200 for a) a training-set of 17 solutes with 134 data points and 3 test-set solutes (4-NA, PTM^+, and imidazole$^+$) with 24 data points b) a training-set of 16 solutes with 128 data points and 4 test-set solutes (2-NA, NMe_4^+, $VBTM^+$ and DMA^+) with 32 data points. The solid lines show a perfect prediction, where the predicted values for C_e exactly equal the experimental values; the dashed lines are 0.5 log units above or below the solid lines.

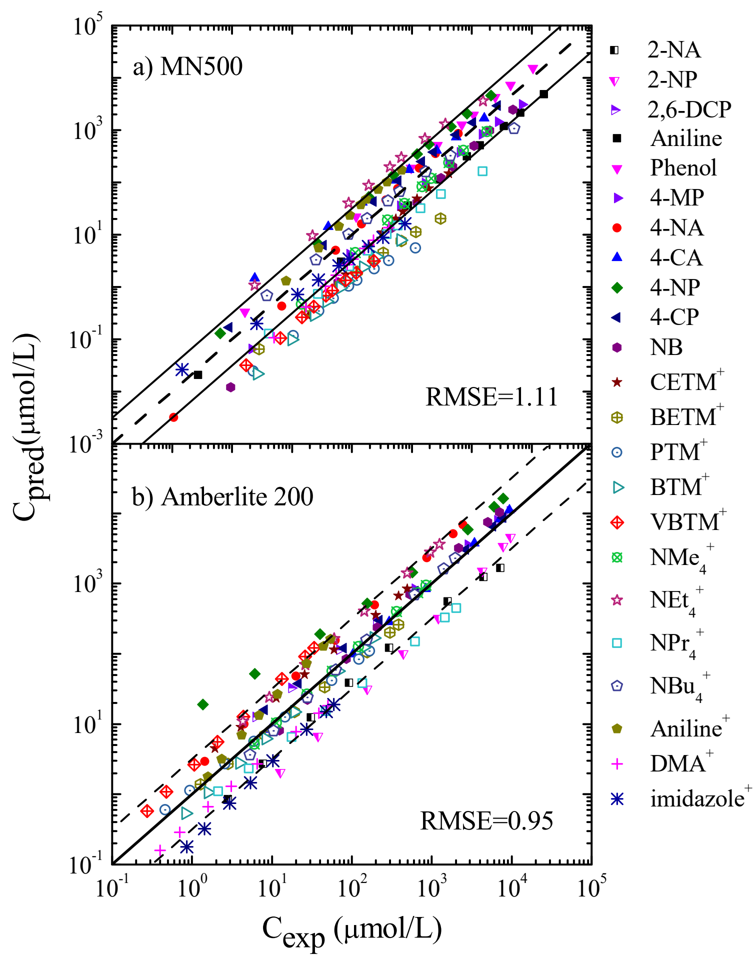

Figure A-7: Aqueous equilibrium concentrations calculated based on the predictive model (eqs 3.18 and 3.19) versus the experimental values for a) MN500 and b) Amberlite 200, the predictive model was constructed based on the correlations between $\Delta G_{S\text{-}G,i}$ and solute descriptors. The solid lines show a perfect prediction, where the predicted values for C_e exactly equal the experimental values; the dashed lines are 0.5 log units above or below the solid lines.

Flowchart A- 1: Development of the Predictive Models

For each solute, calculate C_e for any arbitrary value of Q_e based on the D-A model for fitting the experimental sorption isotherms (eqs 3.6 and 3.7). E, Q^0, and b are fitting parameters.

$$C_e = \frac{C_w^{sat}}{\exp\left(\frac{E \cdot (\log(\frac{Q^0}{Q_e}))^{1/b}}{RT}\right)}$$

Calculate $K_{S\text{-}W,i}$ of ionic solutes based on eq 3.4 for each pair of C_e and Q_e.

$$K_{S-W,i} = \frac{y_i x_{Na}}{y_{Na} x_i} = \frac{Q_e}{Q_c - Q_e} \cdot \frac{[Na^+]_0 + Q_e \frac{m}{V}}{C_e}$$

The empirical correlation between m/V and Q_e which can be developed based on the adsorption isotherm data is reported in **Table 3-1** for the studied resins and solutes.

For each C_e, calculate $\Delta G_{S\text{-}W,i}$ of ionic solutes based on eq 3.3

$$\Delta G_{S-W,i} = -RT \ln K_{S-W,i}$$

and $\Delta G_{S\text{-}W,i}$ of neutral solutes based on eq 3.10.

$$\Delta G_{S-W,i} = -RT \ln K_{S-W,i} + C_{ads}$$

For each Q_e, perform multiple linear regression between a set of $\Delta G_{S\text{-}W,i}$ values and the solute descriptors (which can be reported or estimated) based on eq 3.5 to determine regression coefficients e, s, a, b, v, j^+, and c.

Develop a relationship between each regression coefficient and Q_e i. e. $f^e(Q_e)$, $f^s(Q_e)$, $f^a(Q_e)$, $f^b(Q_e)$, $f^v(Q_e)$, $f^{j+}(Q_e)$, $f^c(Q_e)$.

Substitute regression coefficients $f^e(Q_e)$, $f^s(Q_e)$, $f^a(Q_e)$, $f^b(Q_e)$, $f^v(Q_e)$, $f^{j+}(Q_e)$, $f^c(Q_e)$, and eqs 3.8 and 3.3 into eq 3.5 to obtain eq 3.4.

Rearrange eq 3.8 to solve for C_e as predictive model (eq 3.9):

$$C_e = \frac{Q_e}{Q_c - Q_e} \cdot \left([Na^+]_0 + Q_e \frac{m}{V} \right) \cdot e^{\frac{f^{TOT}(Q_e)}{RT}}$$